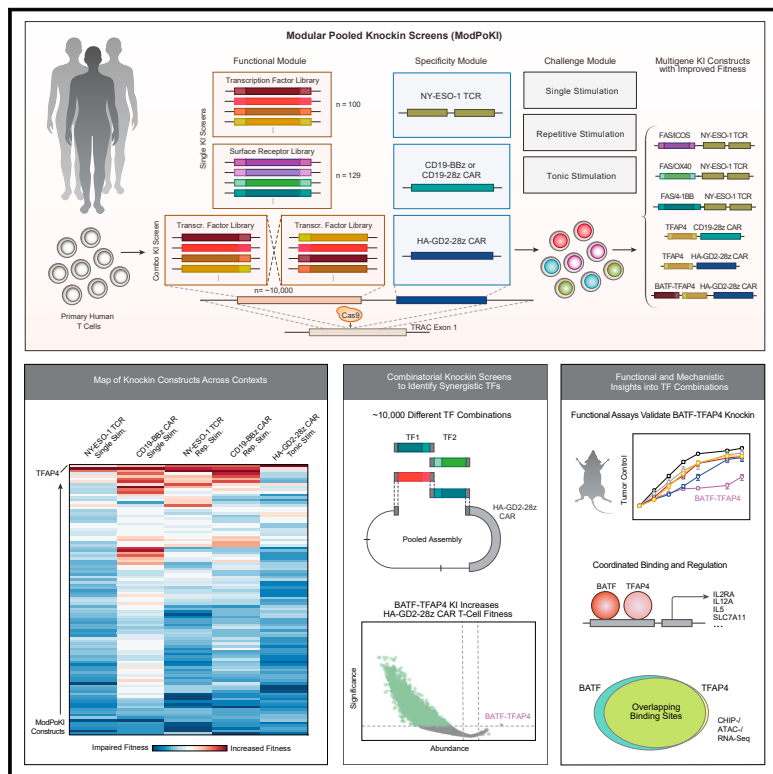


# Modular pooled discovery of synthetic knockin sequences to program durable cell therapies

## Graphical abstract



## Authors

Franziska Blaeschke, Yan Yi Chen,  
Ryan Apathy, ..., Eric Shifrut,  
Theodore L. Roth, Alexander Marson

## Correspondence

troth@stanford.edu (T.L.R.),  
alex.marson@gladstone.ucsf.edu (A.M.)

## In brief

Modular pooled knockin screening (ModPoKI) is an adaptable platform that enables the evaluation of hundreds to thousands of different T cell constructs for engineered cellular immunotherapies.

## Highlights

- Pooled knockin of hundreds of TFs/surface receptors combined with different TCRs/CARs
- Chronic stimulation screens discover programs to improve T cell persistence
- Combinatorial knockin screens with ~10,000 transcription factor combinations
- BATF-TFAP4 dual knockin construct improves CAR-T cell fitness and function



## Resource

# Modular pooled discovery of synthetic knockin sequences to program durable cell therapies

Franziska Blaesche,<sup>1,2</sup> Yan Yi Chen,<sup>1,2</sup> Ryan Apathy,<sup>1,2</sup> Bence Daniel,<sup>1,3,4</sup> Andy Y. Chen,<sup>1,3,5</sup> Peixin Amy Chen,<sup>1,2</sup> Katalin Sandor,<sup>1,3</sup> Wenxi Zhang,<sup>1,3</sup> Zhongmei Li,<sup>1,2</sup> Cody T. Mowery,<sup>1,2</sup> Tori N. Yamamoto,<sup>1,2</sup> William A. Nyberg,<sup>1,2</sup> Angela To,<sup>1,2</sup> Ruby Yu,<sup>1,2</sup> Raymund Bueno,<sup>6</sup> Min Cheol Kim,<sup>6</sup> Ralf Schmidt,<sup>1,2,20</sup> Daniel B. Goodman,<sup>1,2,7,8</sup> Tobias Feuchtinger,<sup>9,10,11</sup> Justin Eyquem,<sup>1,2,6,8,15,17</sup> Chun Jimmie Ye,<sup>1,2,6,8,12,13,14,15</sup> Julia Carnevale,<sup>1,2,8,17</sup> Ansuman T. Satpathy,<sup>1,3,8,18</sup> Eric Shifrut,<sup>1,2,21,22,23</sup> Theodore L. Roth,<sup>3,19,\*</sup> and Alexander Marson<sup>1,2,6,7,8,15,16,17,19,24,\*</sup>

<sup>1</sup>Gladstone-UCSF Institute of Genomic Immunology, San Francisco, CA 94158, USA

<sup>2</sup>Department of Medicine, University of California, San Francisco, San Francisco, CA 94143, USA

<sup>3</sup>Department of Pathology, Stanford University, Stanford, CA 94305, USA

<sup>4</sup>Center for Personal Dynamic Regulomes, Stanford University, Stanford, CA 94305, USA

<sup>5</sup>Department of Bioengineering, Stanford University, Stanford, CA 94305, USA

<sup>6</sup>Institute for Human Genetics (IHG), University of California, San Francisco, San Francisco, CA 94143, USA

<sup>7</sup>Diabetes Center, University of California, San Francisco, San Francisco, CA 94143, USA

<sup>8</sup>Parker Institute for Cancer Immunotherapy, University of California, San Francisco, San Francisco, CA 94129, USA

<sup>9</sup>Department of Pediatric Hematology, Oncology and Stem Cell Transplantation, Dr. von Hauner Children's Hospital, University Hospital, LMU Munich, Munich 80337, Germany

<sup>10</sup>German Cancer Consortium (DKTK), Partner Site Munich, Munich 80336, Germany

<sup>11</sup>National Center for Infection Research (DZIF), Munich 81377, Germany

<sup>12</sup>Institute for Computational Health Sciences, University of California, San Francisco, San Francisco, CA 94143, USA

<sup>13</sup>Department of Epidemiology and Biostatistics, University of California, San Francisco, San Francisco, CA 94143, USA

<sup>14</sup>Department of Bioengineering and Therapeutic Sciences, University of California, San Francisco, San Francisco, CA 94143, USA

<sup>15</sup>Department of Microbiology and Immunology, University of California, San Francisco, San Francisco, CA 94143, USA

<sup>16</sup>Innovative Genomics Institute, University of California Berkeley, Berkeley, CA 94720, USA

<sup>17</sup>UCSF Helen Diller Family Comprehensive Cancer Center, University of California, San Francisco, San Francisco, CA 94158, USA

<sup>18</sup>Program in Immunology, Stanford University, Stanford, CA 94305, USA

<sup>19</sup>Senior author

<sup>20</sup>Present address: Medical University of Vienna, Department of Laboratory Medicine, Vienna, Austria

<sup>21</sup>Present address: The School of Neurobiology, Biochemistry and Biophysics, The George S. Wise Faculty of Life Sciences, Tel Aviv University, Tel Aviv 6997801, Israel

<sup>22</sup>Present address: Department of Pathology, Faculty of Medicine, Tel Aviv University, Tel Aviv 6997801, Israel

<sup>23</sup>Present address: Dotan Center for Advanced Therapies, Tel Aviv Sourasky Medical Center, Tel Aviv 6423906, Israel

<sup>24</sup>Lead contact

\*Correspondence: troth@stanford.edu (T.L.R.), alex.marson@gladstone.ucsf.edu (A.M.)

<https://doi.org/10.1016/j.cell.2023.08.013>

## SUMMARY

Chronic stimulation can cause T cell dysfunction and limit the efficacy of cellular immunotherapies. Improved methods are required to compare large numbers of synthetic knockin (KI) sequences to reprogram cell functions. Here, we developed modular pooled KI screening (ModPoKI), an adaptable platform for modular construction of DNA KI libraries using barcoded multicistronic adaptors. We built two ModPoKI libraries of 100 transcription factors (TFs) and 129 natural and synthetic surface receptors (SRs). Over 30 ModPoKI screens across human TCR- and CAR-T cells in diverse conditions identified a transcription factor AP4 (TFAP4) construct that enhanced fitness of chronically stimulated CAR-T cells and anti-cancer function *in vitro* and *in vivo*. ModPoKI's modularity allowed us to generate an ~10,000-member library of TF combinations. Non-viral KI of a combined BATF-TFAP4 polycistronic construct enhanced fitness. Overexpressed BATF and TFAP4 co-occupy and regulate key gene targets to reprogram T cell function. ModPoKI facilitates the discovery of complex gene constructs to program cellular functions.

## INTRODUCTION

T cells expressing transgenic T cell receptors (TCRs) or chimeric antigen receptors (CARs) have emerged as powerful treatment

options for some malignancies.<sup>1–3</sup> However, T cell function can fail as a result of chronic stimulation.<sup>4,5</sup> Chronically stimulated T cells can differentiate into dysfunctional states characterized by the expression of inhibitory receptors (e.g., PD-1, LAG-3,



and TIM-3), reduced proliferation and cytokine production, and altered transcriptome and chromatin landscapes.<sup>6–11</sup> T cell dysfunction with hallmarks of exhaustion has been identified as a major contributor to poor treatment response.<sup>12</sup> Thus, engineering therapeutic T cells with improved fitness in contexts that otherwise predispose T cells to dysfunction—including chronic stimulation and tonic signaling—is a promising strategy to improve clinical responses.

Advances in genome engineering have offered numerous approaches to increase T cell fitness. One approach is to tune CAR regulation/signaling by targeted CAR integration under promoter regulation of the endogenous TCR alpha constant (*TRAC*) chain<sup>13</sup> or by screening co-stimulatory domains to identify favorable CAR designs.<sup>14–16</sup> A second approach uses CRISPR-Cas9 to ablate genes that restrict durable T cell function. CRISPR-Cas9-mediated knockout (KO) of inhibitory receptors—starting with PD-1—has been attempted in clinical trials.<sup>17</sup> Loss-of-function screens continue to nominate perturbations that increase T cell fitness, such as KO of *Regnase-1* and/or *Roquin*,<sup>18–20</sup> *Ptpn2*,<sup>21</sup> *SOCS1*,<sup>22</sup> or *RASA2*.<sup>23,24</sup> As a third approach, gain-of-function screens using CRISPR activation (CRISPRa)<sup>25</sup> or lentiviral libraries of open reading frames (ORFs) have revealed promising perturbations, such as overexpression of lymphotxin beta receptor (LTBR).<sup>26</sup> However, these gain-of-function screening approaches were not combined with antigen-specific TCRs or CARs in primary human T cells at scale, and CRISPRa screens cannot test synthetic gene products.

A promising approach is to engineer the state of TCR-/CAR-T cells by direct modulation of transcriptional regulators or through synthetic surface receptors (SRs) that alter cellular responses to external cues. For example, overexpression of AP-1/ATF transcription factors (TFs) c-Jun or BATF can improve CAR-T cell function.<sup>27,28</sup> Numerous groups have designed synthetic genes encoding “switch” receptors that convert inhibitory signals into activating signals by fusing domains of inhibitory receptors (e.g., PD-1) to activating domains (e.g., CD28).<sup>29–31</sup> An array of synthetic receptors including CD200R/CD28 and TIM-3/CD28 have been developed,<sup>32,33</sup> but systematic analysis is required to learn the rules that govern which domain pairings are most effective. More broadly, a modular screening approach is required to discover combinations of TFs or SRs that can be coupled with specific TCRs/CARs to improve functional performance.

Targeted CRISPR-mediated knockin (KI) screens not only allow for testing of constructs at specific loci but also overcome several limitations of pooled lenti-/retroviral screening approaches: viral recombination,<sup>34</sup> semi-random integration,<sup>35,36</sup> and variable integration numbers. We previously developed a non-viral pooled KI (PoKI) platform and screened a 36-member library in combination with an NY-ESO-1-specific TCR.<sup>37</sup> However, scaling of this approach was impeded by substantial barcode/construct misassignment due to template switching, which limited library size and adaptability.

Here, we developed modular pooled knockin (ModPoKI) to screen up to thousands of synthetic sequences combined with clinically relevant TCR/CAR genes at targeted genomic sites.<sup>38,39</sup> Barcoded adaptors facilitate pooled cloning, quantification by amplicon sequencing, and compatibility with single-

cell sequencing. We generated a 100-member TF library, a 129-member SR library, and an ~10,000-member combinatorial TFxTF library. Using bead stimulation, target-cell stimulation, repetitive stimulation, and tonic signaling assays, we performed >30 unique screens. The screens nominated multi-gene constructs that improved T cell fitness, including a transcription factor AP4 (TFAP4) and BATF multi-gene KI where TFAP4 and BATF overexpression work coordinately to shape gene expression and T cell function. Overall, these studies highlight large-scale ModPoKI screens as a powerful method to accelerate programming of cell states with enhanced durability and therapeutic functions.

## RESULTS

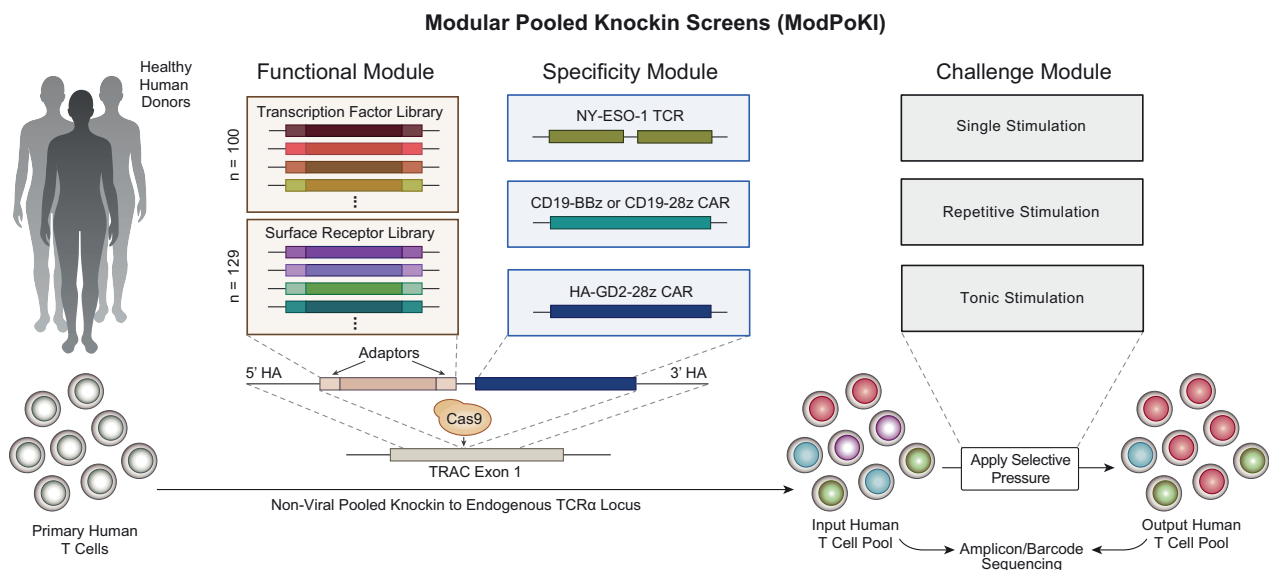
### ModPoKI enables pooled knockin of hundreds of multi-gene constructs

Recent studies have indicated that reprogramming T cell states by overexpressing TFs can enhance therapeutic function.<sup>27,28</sup> Here, we screened 100 TFs (and related proteins) and 129 SRs in the setting of different TCR/CAR specificities and diverse biological contexts (Figure 1A) to provide a systematic resource of gene constructs for improved T cell functionality.

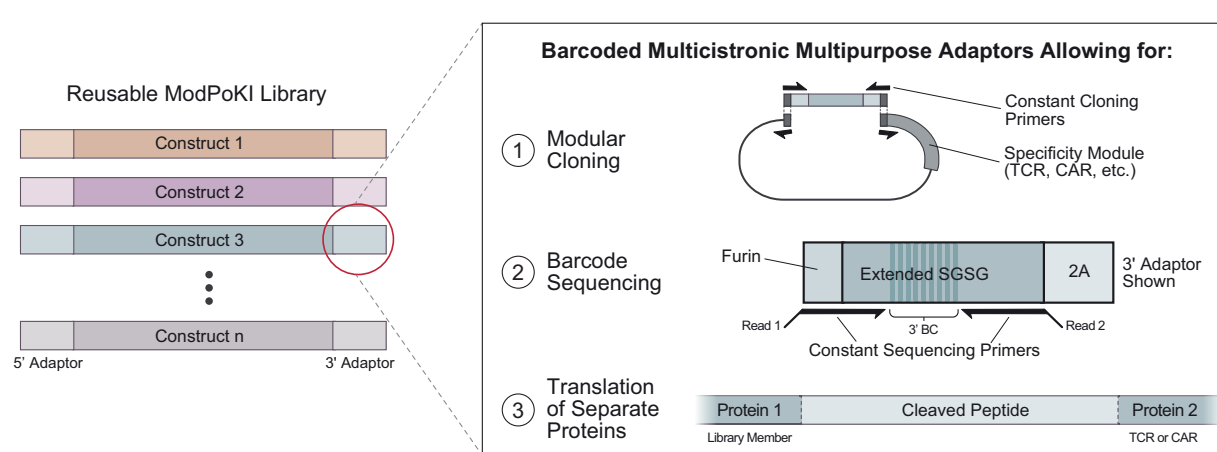
In our previously developed PoKI screening platform,<sup>37</sup> we had observed incorrect barcode/construct assignment due to template switching that prevented pooling at early stages and complicated scaling and adaptability. Template switching refers to a phenomenon where KI sequences are not correctly associated with their identifying barcode.<sup>42</sup> PoKI uses PCR to generate double-stranded DNA (dsDNA) templates from pooled plasmid libraries for homology-directed repair (HDR). During PCR amplification, the polymerase can terminate between the barcode and sequence of interest, resulting in an incomplete product that can serve as a primer in the next cycle to produce a chimera of the gene of interest with an unrelated barcode. In addition, the polymerase can jump between templates during elongation.<sup>42</sup> Because we now aimed to screen hundreds of T cell constructs in combination with various specificities (CAR/TCR), we developed ModPoKI (Figure 1A).

We generated constructs with multicistronic adaptors that were placed between the DNA sequences of the functional module (TF/SR) and the specificity module (CAR/TCR) and consisted of barcode-bearing linkers and cleavage sites (Figures 1B and S1A–S1C), including a furin sequence, to help remove 2A residues from the upstream gene product.<sup>40,41</sup> Each library member received two unique barcodes to determine construct identity at the genomic DNA or messenger RNA (mRNA)/complementary DNA (cDNA) level (STAR Methods), an approach that could enable >37 million possible combinatorial barcodes. Double-stranded HDR templates (HDRTs) were generated from the pooled plasmid libraries by PCR and then non-virally integrated into the human *TRAC* locus using CRISPR-Cas9 ribonucleoprotein (RNP) (Figure S1D).<sup>38</sup> 85% of the expressed insertions were calculated to be monoallelic (Figure S1E). The resulting ModPoKI system is barcoded (Figures 1C and S1F), reproducible across donors (Figures 1D and S1G), and adaptable between mRNA/cDNA and gDNA barcode sequencing (Figures 1E and S1H). It is highly sensitive (Figure 1F) and modular/scalable due to

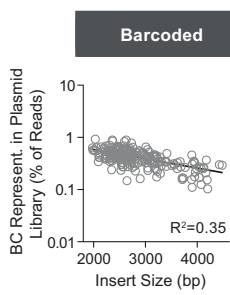
**A**



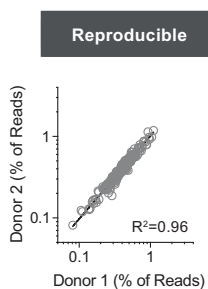
**B**



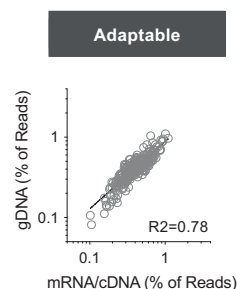
**C**



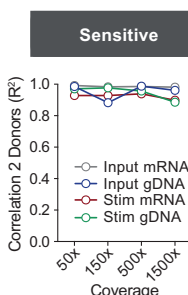
**D**



**E**



**F**



**G**

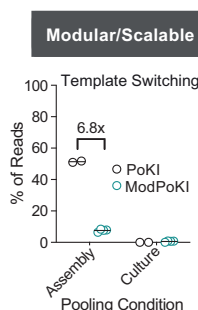


**Figure 1. ModPoKI screens to identify therapeutic candidates**

(A) Schematic illustration of the ModPoKI platform.

(B) Barcoded multicistronic adaptors allowed for modular cloning, barcode sequencing, and translation of separate proteins. A furin sequence was included to help remove 2A residues from the upstream gene product.<sup>40,41</sup>

(C) Barcode representation in the plasmid library (100 TFs, 129 SRs). n = 2 replicates. Indicated insert size does not include homology arms.

(D) Sequencing of the 5' barcode (BC) from genomic DNA (gDNA) after ModPoKI was reproducible across n = 2 human donors (7 days after electroporation).

(E) Correlation between gDNA and mRNA/cDNA barcode sequencing for one exemplary donor (7 days after electroporation). The second donor confirmed strong correlation ( $R^2 = 0.76$ ).

(legend continued on next page)

reduced template switching (<10%), likely due to reduced distance between the barcode and gene insert (Figures 1G and S1I). Pooled KI single-cell RNA sequencing (scRNA-seq) with barcode sequencing (ModPoKI-seq) at low coverage confirmed strong correlation between barcode and gene expression (Figure S2A). In summary, ModPoKI screens enable rapid evaluation of hundreds of T cell constructs for engineered immunotherapies.

#### Design of large synthetic libraries for ModPoKI screens

We designed two libraries to reprogram T cell function through TF overexpression or altered SR signaling. The TF library consisted of 100 members encompassing different TF families (Figure S2B), including known regulators of T cell proliferation, TFs that increase anti-tumor functions, and TFs with unknown functions in immunotherapy. We covered TFs predominantly expressed in CD4 and CD8 T cells, including TFs that are dynamically regulated upon T cell activation (Figure S2C; <https://dice-database.org/>). We also incorporated TFs that are predominantly expressed in monocytes, natural killer (NK) cells, and B cells to determine if subsets of these could be used to “synthetically” program improved T cell fitness (Figure S2C; Table S1A).

The SR library included mostly synthetic chimeric receptors (“switch receptors”) in which the extracellular domain of an inhibitory checkpoint, death, or other tumor necrosis factor (TNF) receptor superfamily member was fused to the intracellular domain of an activating receptor to convert inhibitory ligand-receptor interactions into activating signals (Figure S2B). We used a modular design in which a variety of different extracellular domains were combined with either 4-1BB, CD28, ICOS, or other intracellular activation domains. Taken together, the SR library comprises both published switch receptors and >80 fusion receptors alongside chemokine receptors, cytokine receptors, metabolic receptors (e.g., metabolite transporters), and stimulatory molecules (Table S1B).

#### Discovery of constructs to promote fitness of stimulated T cells

We first aimed to identify constructs that could be integrated into the endogenous *TRAC* locus to enhance T cell fitness following a single restimulation. The 1G4 95:LY variant of the NY-ESO-1 TCR (which functions independently of the CD4 or CD8 co-receptor<sup>43</sup>) was introduced into bulk T cells in combination with the TF or SR library. The KI T cell pool was subjected to various signals, including CD3-only stimulation, CD3/CD28 bead-based stimulation, excessive CD3/CD28 stimulation, or stimulation with NY-ESO-1+ target cells (A375 melanoma cells naturally expressing NY-ESO-1/HLA-A2 or Nalm-6 leukemia cells transduced

with HLA-A2/NY-ESO-1) (Figure 2A). RNA was isolated and transcribed into cDNA, and barcode amplicon sequencing was performed to compare the abundance of each construct in the input and output populations. KI of basic leucine zipper (bZIP) TFs (BATF and BATF3) or helix-loop-helix TFs (ID2 and ID3) had strong effects on T cell fitness (Figures 2B, 2C, and S2D). Among the top negative hits were EOMES, required for effector differentiation<sup>44</sup> and associated with exhaustion in anti-tumor T cells,<sup>45</sup> and NFATC1, which can promote exhaustion in CD8+ T cells (Figures 2B, 2C, and S2E).<sup>9</sup> Interestingly, BATF KI provided an advantage even in the absence of restimulation, suggesting potential stimulation-independent effects.

KI of SR library members could also modulate T cell fitness upon stimulation. Notably, upon excessive stimulation, a subset of receptor fusions (e.g., LTBR/OX40 and TNFRSF12/OX40) enhanced T cell fitness (Figures 2B, 2C, S2F, and S2G). Another hit was CTLA-4/CD28, the mouse version of which was shown to increase the efficacy of donor-lymphocyte infusions in preclinical models.<sup>46,47</sup> Fusion receptor FAS/OX40 strongly promoted T cell abundance across multiple screening conditions. Overall, FAS, LTBR, and CTLA-4 extracellular domains tended to perform best (Figure 2C). OX40 intracellular domains performed well with both FAS and LTBR extracellular domains (Figures 2D and 2E). Interestingly, CD28 was the only intracellular domain tested that increased abundance with the CTLA-4 extracellular domain (Figure 2F). Validation analyses revealed that FAS fusion proteins can increase the cytotoxic potential of NY-ESO-1 TCR-T cells during co-culture with Nalm-6 leukemia cells (Figures S3A–S3F). Interestingly, FAS fusion proteins seemed to perform better in co-culture with Nalm-6 cells compared with co-culture with A375 melanoma cells (Figure 2C), which could be explained by higher FASL levels on T cells after co-culture with Nalm-6 (Figure S3G). Arrayed validation across different synthetic FAS constructs revealed large differences in surface expression level, although all constructs shared the same extracellular and transmembrane FAS domains (Figure S3A). FAS constructs with higher surface expression tended to perform better in the ModPoKI screen (Figure S3B), which highlights the platform’s ability to test chimeric protein design and ensure proper expression, localization, and function. In summary, these highly parallelized functional assays have the potential to inform the design of fusion receptors that confer context-specific benefits to T cell therapies.

#### Repetitive stimulation screens discover that TFAP4 KI improves persistent T cell fitness

Therapeutic T cells must maintain persistent function through multiple rounds of target recognition if they are to clear large

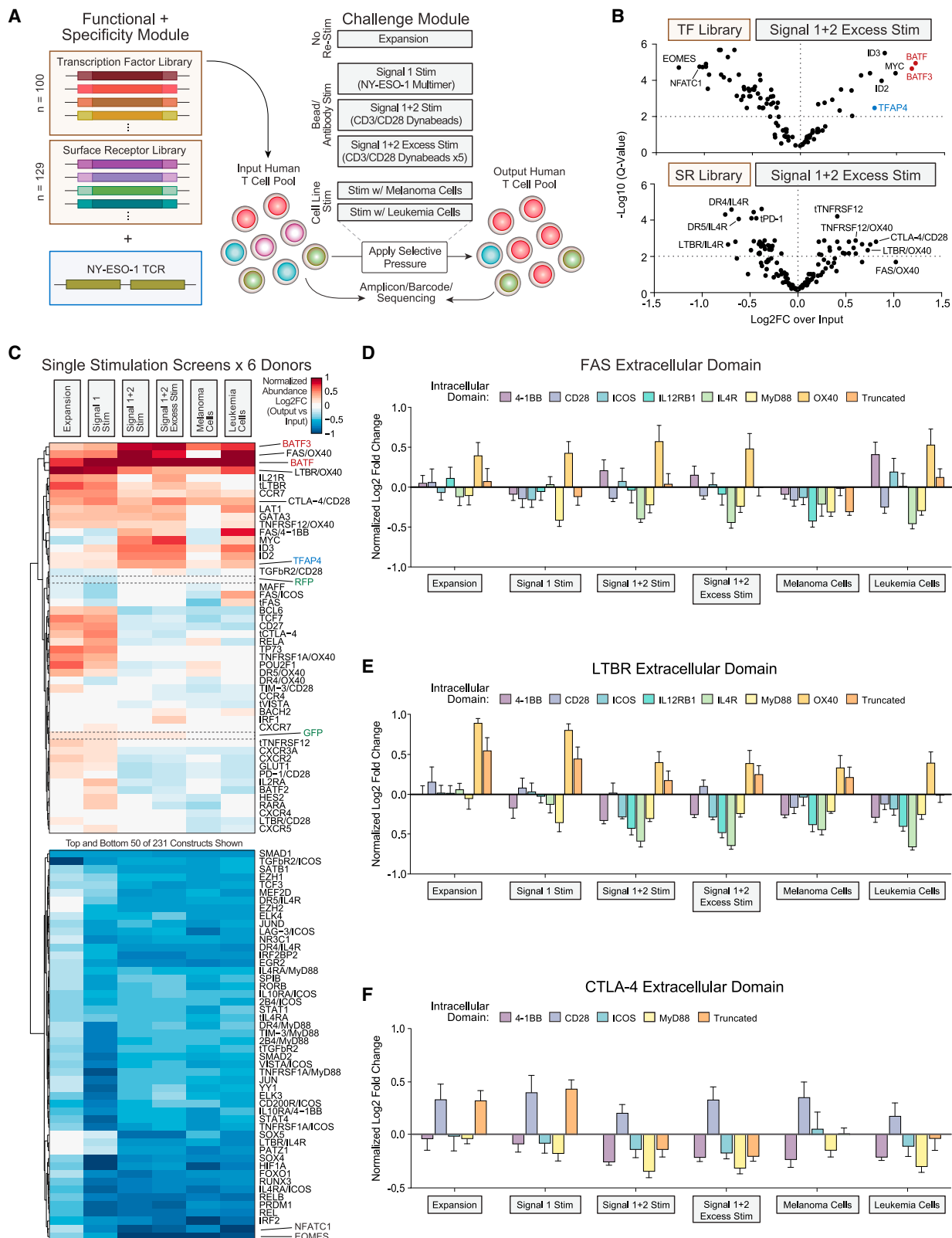
(F) Donors were highly correlated across cell coverage ranges, sequencing strategies, and experimental conditions (input cells [day 7 after electroporation] vs. cells after 4 days of CD3/CD28 bead stimulation [day 11]).

(G) A pilot two-member library of the NY-ESO-1 TCR plus GFP (green fluorescent protein) vs. RFP (red fluorescent protein) was pooled at the plasmid assembly stage or after separate electroporation (Figure S1I). T cells were sorted for TCR knockin and GFP or RFP positivity. Percentage of correctly assigned barcodes was determined by amplicon sequencing (3' barcode of mRNA/cDNA). The amount of template switching was calculated, extrapolated for an n > 200-member library<sup>37</sup> and compared with the previous PoKI version.<sup>37</sup> Bars represent mean. n = 2 donors.

(C)–(F) include data from NY-ESO-1 TCR TF and SR libraries.

R<sup>2</sup> was calculated using nonlinear regression (semilog, C or log-log line model, D–F; GraphPad Prism).

See also Figures S1 and S2.



(legend on next page)

tumor burdens. Unfortunately, repetitive stimulation can lead to T cell dysfunction. To discover constructs that can promote persistent T cell fitness, we performed a repetitive stimulation screen and transferred the T cell pool to fresh cancer cells every 48 h for five consecutive stimulations (Figure 3A). Pilot experiments with a control KI (NY-ESO-1 TCR plus tNGFR, truncated nerve growth factor receptor) confirmed that repetitive stimulations with cancer cells drive enrichment of NY-ESO-1 antigen-specific cells (Figure S3H) and increasingly differentiated T cell phenotypes (Figure 3B). PD-1 expression, which can be induced by T cell stimulation, increased after one stimulation and then decreased over time, similar to what was observed in related studies.<sup>23</sup> Notably, LAG-3 and TIM-3 (co-inhibitory receptors)<sup>48</sup> remained elevated through multiple rounds of stimulation, and CD39 and TOX (markers of exhaustion)<sup>49–52</sup> increased gradually (Figures 3C and S3I). RNA-seq confirmed increased TOX expression, along with decreases from peak levels in CD62L (SELL), granzyme B (GZMB), and interferon-gamma (IFN- $\gamma$ ) (IFNG) expression over time, consistent with cellular dysfunction (Figures S3J–S3L). This *in vitro* model with repetitive exposure to cancer cells provides opportunities to discover KI constructs that enhance persistent T cell fitness.

We introduced the SR or TF library in combination with the NY-ESO-1 TCR into primary human T cells via ModPoKI and monitored construct abundance throughout repetitive stimulation. Constructs in the SR library encoding the high-affinity interleukin (IL)-2R subunit (IL2RA) and the amino acid transporter LAT1 increased in abundance after five stimulations with target cells, highlighting that overexpression of natural SRs can induce durable fitness in T cells challenged by repetitive stimulation (Figures 3D, S3M, and S3N).

In the TF screen, BATF and BATF3 strongly promoted T cell fitness over multiple stimulations. In contrast, EOMES and NFATC1 constructs dropped out, suggesting that they limit persistent T cell fitness (Figures 3D, S3M, and S3N). KI of TFAP4 emerged as a new hit in the repetitive stimulation assay that had only mild effects in single stimulation screens. TFAP4 is a basic-helix-loop-helix (bHLH) TF that has been studied primarily in the context of murine viral infections, where it is crucial for sustained T cell activation and expansion.<sup>53</sup> In summary, these results nominate promising constructs and highlight the importance of testing candidate KIs in experimental contexts designed to assess persistent T cell fitness.

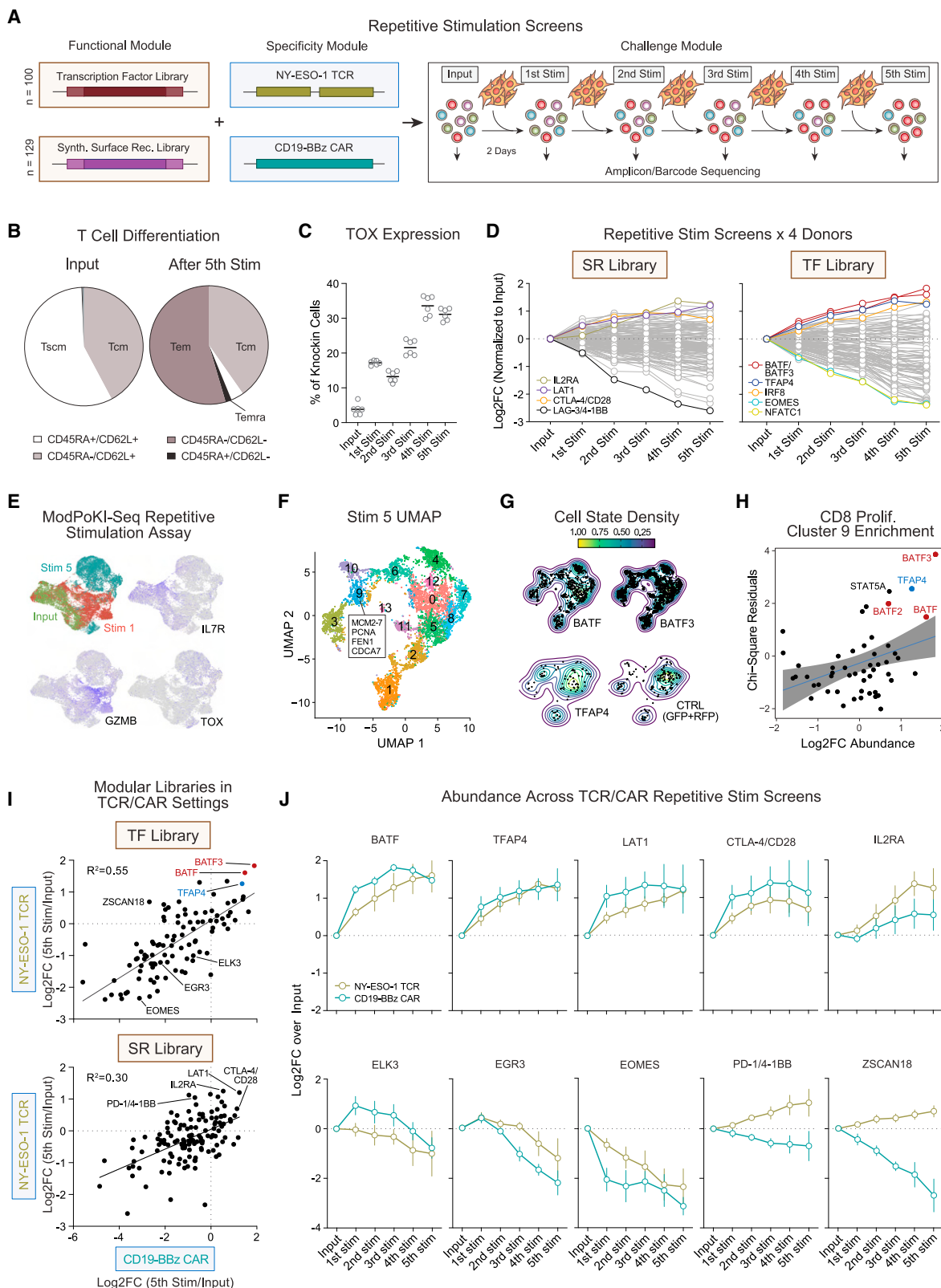
We next molecularly characterized the effects of TF KIs in the repetitive stimulation challenge. We coupled ModPoKI with scRNA-seq (ModPoKI-seq) to discover transcriptomic profiles

promoted by 100 TF KIs. We performed ModPoKI-seq at the input stage, after one stimulation, and after five stimulations with targets. The input population, stim 1, and stim 5 populations clustered separately with expected expression of hallmark genes (Figure 3E). The best-performing KIs in the fitness screens promoted relatively modest transcriptional changes relative to controls (GFP/RFP), whereas worse-performing constructs often caused a higher variance in gene expression (Figures S4A and S4B). To examine the more subtle beneficial transcriptional changes, we performed semi-supervised clustering of transcriptomes after five stimulations with target cells. This revealed a cluster of CD8 cells characterized by high expression of genes associated with proliferation (cluster 9), where cells were most strongly enriched for the KIs of top hits in our repetitive stimulation screen, including BATF3 and TFAP4 (Figures 3F–3H, S4C, and S4D). Key TF hits did not appear to influence fitness by consistently altering TRAC transcript levels, although TFAP4 KI modestly increased TCR protein levels (Figures S4E–S4I). ModPoKI-seq during repetitive stimulation can offer mechanistic insights into gene programs—TFs and downstream target genes—that can be modulated to promote persistent T cell function.

ModPoKI pooled assembly allowed us to combine the same TF and SR libraries with a CD19-BBz CAR (Figure S5A). We observed good correlation of hits when comparing NY-ESO-1 TCR with CD19-BBz CAR screens (Figures 3I, 3J, and S5B). KI of BATF, BATF3, TFAP4, or a CTLA-4/CD28 chimeric receptor all promoted durable fitness of CD19-BBz CAR-T cells in the repetitive stimulation assays, as they had with NY-ESO-1 TCR-T cells (Figures 3I and 3J). EOMES KI again dropped out with repetitive stimulation (Figure 3J). Interestingly, we identified TFs that had increased abundance after a single stimulation but failed to maintain this advantage after repetitive stimulations (e.g., EGR3 and ELK3). Although many constructs overall performed similarly when combined with a CAR vs. a TCR, we observed some constructs (e.g., PD-1/4-1BB, ZSCAN18) that had different kinetics in the CAR vs. TCR screens (Figures 3J and S5C–S5E). We performed an additional repetitive stimulation screen using a CD19-28z CAR to assess if different constructs would enhance the fitness of a CAR with a different intracellular domain (CD28-zeta vs. 4-1BB-zeta) (Figures S5F–S5K). Chimeric receptors with 4-1BB intracellular domains tended to perform better in this context, suggesting combinatorial effects of 4-1BB and CD28 signals or disadvantageous effects of excessive 4-1BB signaling (Figure S5H). In summary, repetitive stimulation screens highlighted constructs that preferentially promote durable fitness through multiple

#### Figure 2. Single stimulation ModPoKI screens reveal known and previously undescribed candidates

- (A) ModPoKI screens were performed in primary human T cells using the NY-ESO-1 TCR TF and SR libraries. Signal 1 stim = anti-CD3 antibody, signal 1 + 2 stim = CD3/CD28 beads (1:1 bead:cell ratio), signal 1 + 2 excess stim = CD3/CD28 beads (5:1 bead:cell ratio), melanoma cells = A375s, leukemia cells = Nalm-6 (overexpressing HLA-A2/NY-ESO-1).
- (B) Amplicon/barcode sequencing was performed before and after excessive CD3/CD28 stimulation to determine log<sub>2</sub>FC in construct abundance (after vs. before stim). FDR was calculated using the Benjamini-Krieger-Yekutieli method.
- (C) Representation of T cell constructs was evaluated prior to and after different stimulation conditions.
- (D–F) Effect of the intracellular domains of FAS, LTBR, and CTLA-4 switch receptors was analyzed. n = 6 donors (B–F). Mean + SEM log<sub>2</sub>FC over input population is shown. Log<sub>2</sub>FC was normalized to abundance of RFP/GFP controls and to fit on a scale from -1 to +1 for comparability (C–F).
- See also Figures S2 and S3.



(legend on next page)

rounds of target-cell recognition. Differences in the performance of gene KIs paired with CD19-BBz vs. CD19-28z CARs vs. TCRs further underscore the importance of screening with the exact therapeutic construct that will later be used in the clinic.

### TFAP4 KI improves T cell fitness during chronic stimulation

In addition to facing repetitive stimulation, CAR-T cells are challenged by tonic signaling, which can also promote T cell dysfunction.<sup>54</sup> In order to discover synthetic constructs that promote T cell fitness during tonic signaling, we combined our libraries with the high-affinity GD2-28z CAR (HA-GD2-28z) demonstrated to drive an “exhaustion-like” state through tonic signaling.<sup>28</sup> Although the HA-GD2-28z CAR might drive a less dysfunctional phenotype when placed under *TRAC* promoter control compared with retroviral delivery, we did observe tonic activation, decreased memory markers (*CCR7* and *LEF1*), and increased levels of dysfunction markers (*TOX*, *LAG-3*, *HAVCR2* [TIM-3], and *ENTPD1* [CD39]) on HA-GD2-28z CARs (Figures S6A–S6C). We performed ModPoKI of the HA-GD2-28z CAR with the SR (Figures S6D and S6E) or the TF library (Figure 4A). In the TF library, TFAP4 was distinctive in its strong enrichment trajectory in the HA-GD2-28z CAR screen (Figure 4B). While constructs containing BATF and BATF3 showed increased abundance across multiple screens, TFAP4-overexpressing constructs were more clearly enriched in chronic stimulation settings that promote dysfunction, especially with the tonic-signaling HA-GD2-28z CAR.

We next performed arrayed KIs of CARs in combination with TFAP4 or a control (tNGFR) for deeper characterization and validation of potential benefits. First, we confirmed that TFAP4 HA-GD2-28z CARs expand more than co-cultured control T cells over time (Figures S6F–S6H). We next co-cultured GD2+ cancer cells with HA-GD2-28z CAR-T cells and observed that the TFAP4 KI constructs improved killing capacity across multiple effector:target (E:T) ratios (Figures 4C and S6I). The effects of non-viral KI of the TFAP4 and HA-GD2-28z CAR polycistron under *TRAC* promoter control differed from the effects of retroviral transduction. With retroviral transduction, TFAP4 still enhanced killing capacity *in vitro*, but we did not observe increased fitness

and cytokine release as we did with *TRAC*-targeted KI (Figures S7A–S7C). We also assessed effects on non-viral *TRAC* KI of a CD19-28z CAR. CD19-28z CAR-T cells demonstrated dysfunctional cancer-cell killing *in vitro* after multiple rounds of stimulation (Figure S7D), which was mitigated by TFAP4 KI (Figures 4C and S7E–S7G). Lastly, recognizing potential safety concerns, we confirmed that TFAP4 KI CD19-28z CARs spared CD19 negative targets (Figure S7H) and did not show antigen-independent proliferation (Figure S7I).

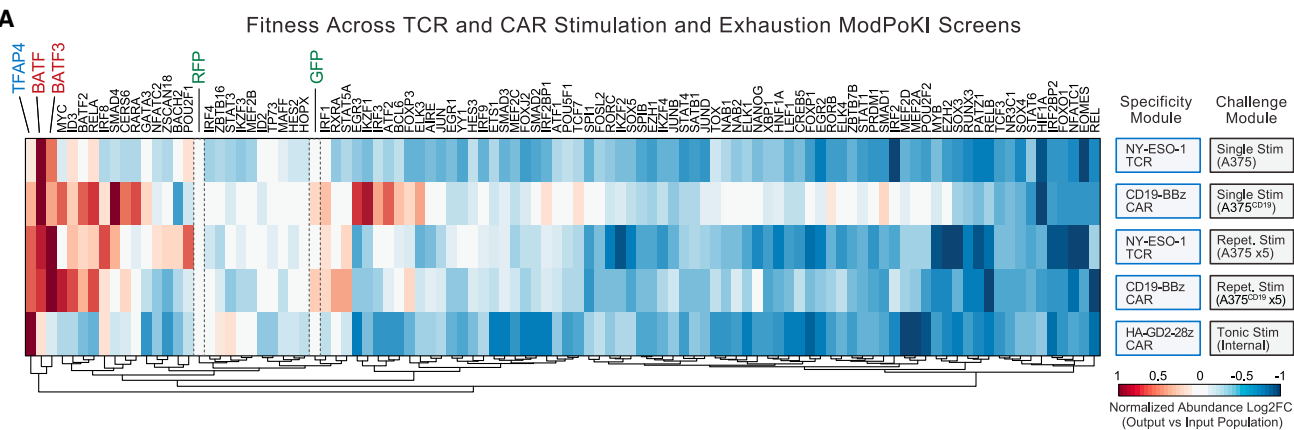
We next evaluated *in vivo* killing capacity conferred by TFAP4 KI in NOD/SCID/IL2Rg-null (NSG) mice that were challenged with Nalm-6/GFP/Luc/GD2 leukemia (Figure 4D). TFAP4 KI CAR-T cells enhanced leukemia control and survival in experiments using T cells from two human donors compared with controls (Figures 4D and 4E). In summary, TFAP4 KI promotes persistent and antigen-dependent anti-cancer T cell function.

We next evaluated the phenotypic changes induced by TFAP4 KI in human T cells. First, we confirmed that non-viral TFAP4 KI can increase TFAP4 expression beyond physiologic levels at transcript (Figures S8A and S8B) and protein levels (Figures S8C and S8D). TFAP4 is a direct target of MYC expressed after T cell activation (Figure 4F).<sup>55</sup> TFAP4 expression is regulated by TCR and IL-2R signals and mediates sustained T cell proliferation.<sup>53</sup> We observed that synthetic TFAP4 KI resulted in increased levels of IL-2RA (CD25) and promoted a gene signature enriched in the IL-2/STAT5 signaling pathway (Figures 4G, 4H, S8E, and S8F). TFAP4's potential to increase surface expression of IL-2RA was confirmed in an independent ModPoKI screen, in which HA-GD2-28z CAR-T cells with the TF library were sorted for IL-2RA high/low expression, and TFAP4 was the most enriched TF KI in the IL-2RA high bin (Figures S8G and S8H). RNA-seq also revealed increased levels of MYC target genes, IFN- $\gamma$ , and effector cytokine production, whereas it showed decreased IFN- $\gamma$  response genes (Figure 4H). Crucially, increases in IFN- $\gamma$  and IL-2 secretion were dependent on the presence of antigen-positive targets (Figures S8I and S8J). These results suggest that TFAP4 KI mediates increased proliferation and antigen-dependent cytokine production, and it can promote T cell states with enhanced fitness in the context of chronic stimulation.

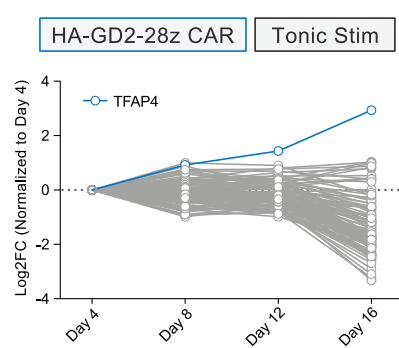
**Figure 3. ModPoKI screens identify highly functional T cell constructs after repetitive stimulation**

- (A) Schematic illustration of the repetitive stimulation screens.
  - (B) Control T cells (tNGFR NY-ESO-1 TCR) were generated and subjected to repetitive stimulation to evaluate T cell phenotype.
  - (C) Intracellular expression of TOX was measured by flow cytometry (tNGFR NY-ESO-1 TCR). Bars represent mean.
  - (D) ModPoKI T cells were generated using the NY-ESO-1 TCR SR and TF libraries. Average log<sub>2</sub>FC of construct abundance compared with input population is shown.
  - (E) The TF library (with NY-ESO-1 TCR) was knocked into T cells and scRNA-seq with barcode sequencing (ModPoKI-seq) was performed. Uniform manifold approximation and projection (UMAP) shows overexpression of hallmark genes at the input stage, after one and five stimulations with targets.
  - (F) Semi-supervised clustering of single cells based on gene expression after five stimulations. Cluster 9 cells expressed hallmarks of proliferating CD8 cells. Highlighted hallmark genes were derived from top 30 differentially expressed genes.
  - (G) Density plot of top candidates compared with control knockins (GFP, RFP) after five stimulations.
  - (H) Chi-square residuals for cluster 9 enrichment (proliferating CD8 cells, threshold >30 cells/knockin after 5 stimulations) were compared with abundance log<sub>2</sub>FC in bulk screens. n= 2 donors for ModPoKI-seq screen, n = 4 donors for bulk screens. Enrichment of KIs in other clusters is depicted in Figure S4D.
  - (I) CD19-BBz CAR TF and SR libraries were generated by pooled assembly. Repetitive stimulation CAR screening hits were compared with TCR screening hits. Nonlinear regression (line model, GraphPad Prism) was used to determine R<sup>2</sup>.
  - (J) Abundance log<sub>2</sub>FC (output vs. input) was compared between CAR vs. TCR repetitive stimulation screens. Mean + SEM shown.
- n = 2 donors in technical triplicates (B and C), n = 4 donors (D), n = 2 donors (E–G), n = 4 donors for TCR screens and n = 3 donors for CAR screens (I and J). See also Figures S3, S4, and S5.

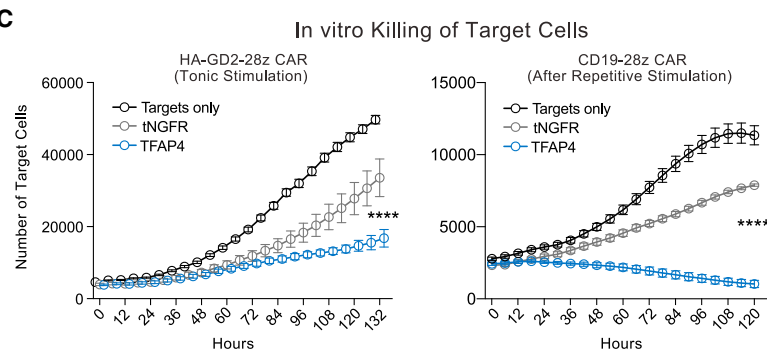
**A**



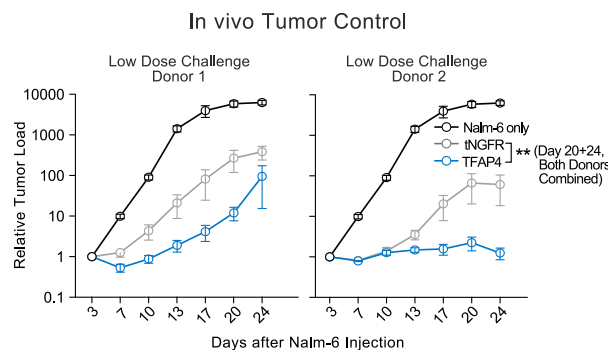
**B**



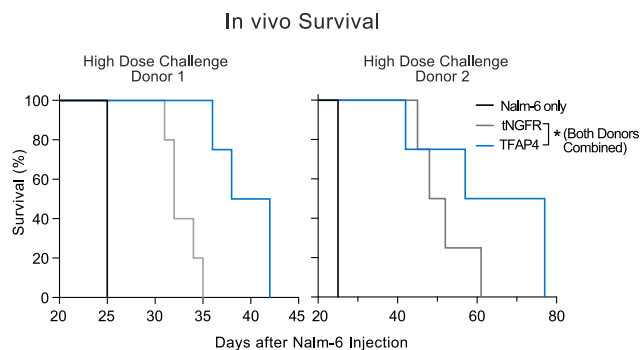
**C**



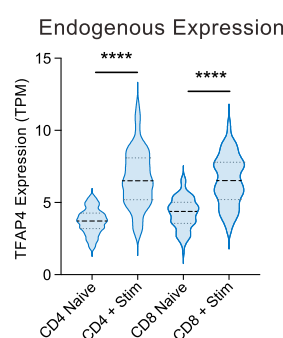
**D**



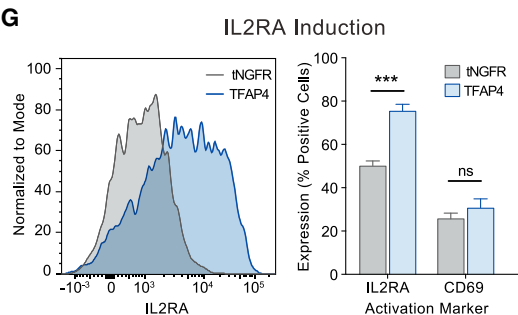
**E**



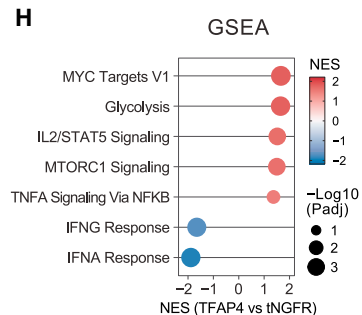
**F**



**G**



**H**



(legend on next page)

### Combinatorial ModPoKI screens to uncover synergistic TF combinations

TFs can act in combination to reprogram cells to desirable cell states.<sup>56</sup> We wondered if we could discover combinations of TFs that enhance T cell fitness during tonic signaling. Analyzing pairwise combinations of 100 different TFs requires (1) library sizes (~10,000 members) that have not been tested before in this setting and (2) KI of large constructs, especially when combined with a CAR (average construct size ~5.5 kb plus HAs), and thus cannot be performed readily with AAV (adeno-associated virus) HDRTs due to packaging limitations. We thus adapted our ModPoKI platform for large-scale combinatorial KI screens (Figures 5A, S9A, and S9B; STAR Methods). We created an ~10,000-member library (100 TFs plus two controls combined with 100 TFs plus two controls; Table S1C) cloned in constructs with the tonically signaling HA-GD2-28z CAR (STAR Methods). HDRTs were generated, and non-viral KI of the library into the *TRAC* locus of primary human T cells was performed. Notably, the constructs spanned a large size range from ~3.3 to ~8.2 kb. The fusion region between TF1 and TF2 served as a barcode to identify abundance and orientation (TF1 vs. TF2) (Figures S9C–S9E). Amplicon sequencing of the plasmid pool and the T cell pool confirmed the representation of >99% of the constructs, despite expected construct size-dependent effects (Figures 5B and 5C). Because dropout of constructs was an effect of insert size, large constructs could be spiked in to increase representation in future ModPoKI versions. Nonetheless, we were able to generate pooled libraries with thousands of different members and successfully achieve diverse KIs, including constructs as large as ~7.6 kb, based on barcode sequencing.

Because ModPoKI cells expanded in culture due to HA-GD2-28z CAR tonic signaling, we compared the abundance of each TF×TF combination after 16 days in culture with its baseline abundance on day 4 after electroporation. Most TF×TF combinations were depleted from the pool over time, consistent with previous evidence that major transcriptional changes can be detrimental to fitness (Figures S4A and S4B). Analysis of the constructs that increased the most in relative

abundance highlighted that several of the top-performing constructs included combinations of TFAP4 and BATF (or BATF3), suggesting that TFAP4 and BATF(3) are key TFs that can coordinately drive increased T cell fitness during repetitive simulations (Figures 5D and S9E). Analysis of biological replicate screens performed in cells from two human donors identified TFAP4 and BATF combination constructs (TFAP4-BATF and BATF-TFAP4) as the most significantly increased in abundance (Figure 5D). In summary, these data show that large-scale combinatorial KI screens are feasible using the ModPoKI platform and can help create an atlas of combinatorial KI constructs with potential to enhance therapeutic T cells.

### Combined BATF-TFAP4 KI induces favorable T cell states

To assess the benefit of KI constructs combining BATF and TFAP4, we next generated specific KI constructs with the HA-GD2-28z CAR and the following: (1) BATF-TFAP4 combination, (2) single TF + control (RFP-TFAP and BATF-RFP), or (3) control + control (RFP-tNGFR). We performed competitive fitness assays to assess if the combination outperformed the individual KIs. BATF-TFAP4 KI cells were co-cultured at an ~50:50 ratio with single TF (+ control) KI cells, and relative abundance was monitored (Figure 6A). KI cells with the BATF-TFAP4 combinatorial construct outcompeted both the RFP-TFAP4 and the BATF-RFP control KI cells. The relative benefit of the BATF-TFAP4 combination to BATF KI alone was more pronounced than the benefit compared with TFAP4 KI alone, hinting that the majority of fitness benefit (although not all of it) is conferred by TFAP4. Consistent with the effects of single TFAP4 KI constructs, we found increased levels of IL-2RA expression in TFAP4-containing combinatorial constructs (Figures 6B and S9F). When analyzing the phenotype of HA-GD2-28z CARs 14 days after electroporation, we observed that control (RFP-tNGFR) and BATF KI (BATF-RFP) T cells had high percentages of terminally differentiated effector memory (TEMRA) cells, whereas the phenotypes of TFAP4 KI cells (RFP-TFAP4 and BATF-TFAP4) were shifted toward memory states with

#### Figure 4. ModPoKI across dysfunction screens nominates candidate TFAP4

- (A) ModPoKI screens with the TF library were performed in NY-ESO-1 TCR and CD19-BBz CAR (single or repetitive stimulation) or HA-GD2-28z CAR (tonic stimulation) T cells. As the HA-GD2-28z CAR provides tonic stimulation, HA-GD2-28z CAR-T cells were cultured without addition of targets. Abundance log<sub>2</sub>FC is shown. Heatmap was normalized based on controls (RFP/GFP) and to fit on a scale from -1 to +1. N ≥ 3 donors/screen.
  - (B) Log<sub>2</sub>FC in the HA-GD2-28z CAR screen shows strong progressive enrichment of TFAP4 KI cells. Mean of n = 4 donors.
  - (C) Single knockin of the HA-GD2-28z or CD19-28z CAR with TFAP4 or control (tNGFR) was performed and cancer-cell killing was analyzed (Incucyte). CD19-28z CARs were pre-stimulated with targets 5 times. n = 2 donors/experiment in technical triplicates (HA-GD2-28z CAR) or quadruplicates (CD19-28z CAR). Two-way ANOVA was performed including Holm-Sidak's test as described in the STAR Methods. Significance at last time point (TFAP4 vs. tNGFR) is shown; E:T ratio 1:4 (left) and 1:1 (right panel).
  - (D) NSG mice were challenged with 0.5e6 Nalm-6/GFP/Luc/GD2 cells and treated with 1e6 HA-GD2-28z CAR+ T cells. Cancer growth was analyzed by bioluminescence imaging. Two T cell donors are shown (5 mice/donor/construct). Multiple unpaired t test (TFAP4 vs. tNGFR) with Holm-Sidak's test was performed (both donors combined).
  - (E) NSG mice were challenged with 1e6 Nalm-6/GFP/Luc/GD2 cells and treated with 3e6 HA-GD2-28z CAR+ T cells. Survival analysis for mice treated with CAR-T cells from two donors is shown (≥ 4 mice/donor/construct). COX regression was performed (TFAP4 vs. tNGFR, both donors combined).
  - (F) Expression of endogenous TFAP4 in naive vs. activated T cells in published RNA-seq data (<https://dice-database.org/>). Unpaired t test was performed.
  - (G) IL-2RA and CD69 expression on HA-GD2-28z CAR-T cells was analyzed on day 8 after electroporation. Multiple t test was performed including Holm-Sidak's test. n = 2 donors in technical duplicates.
  - (H) RNA sequencing of HA-GD2-28z CAR-T cells with TFAP4 or tNGFR KI was performed 7 days after electroporation. n = 2 donors.
- Mean + SEM shown (C, D, and G).  
See also Figures S6, S7, and S8.

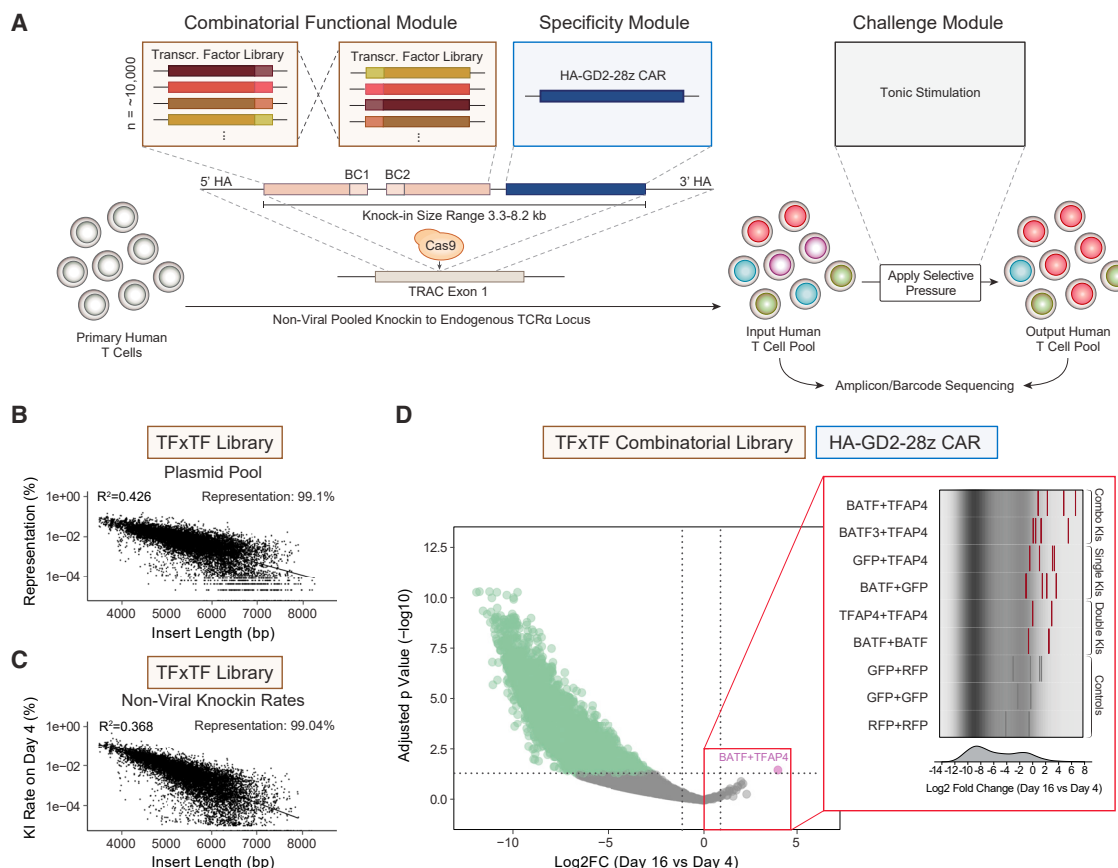


**Figure 5. Combinatorial ModPoKI screens uncover efficient TF combinations**

(A) Schematic illustration of combinatorial ModPoKI to screen ~10,000 TF combinations.  
(B) Barcode sequencing of the TF $\times$ TF plasmid library showed size-dependent representation but confirmed that >99% of constructs were represented after pooled assembly.  
(C) Knockin percentage of combinatorial constructs was analyzed in the cell pool on day 4 after electroporation by barcode sequencing and showed >99% representation of the ~10,000 constructs.  
(D) The TF $\times$ TF combinatorial library in combination with the HA-GD2-28z CAR was knocked into primary human T cells. Cells were sorted on days 4 and 16 after electroporation and log<sub>2</sub>FC in barcode abundance was assessed. Statistics were calculated using DESeq2. To create the volcano plot, the two possible construct orientations (e.g., BATF-TFAP4 and TFAP4-BATF) were combined. The right panel shows data for various KI combinations (barcodes for constructs with both orientations included as bars  $\times$  two donors).

n = 2 donors (C and D). Linear regression was performed (lm function, RStudio) (B and C).

See also Figure S9.

significantly reduced percentages of TEMRA cells (Figures 6C and 6D).

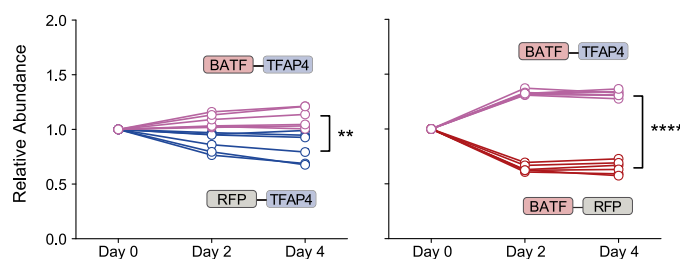
We next evaluated the transcriptional effects of the BATF-TFAP4 combination. Correlation analysis between the respective tested condition and control (RFP-tNGFR) showed that BATF-TFAP4 KI cells behaved more similarly to RFP-TFAP4 than to BATF-RFP KI cells (Figures S9G and S9H). BATF-TFAP4 KI cells had even less correlation with RFP-JUN KI cells, suggesting that the transcriptional program promoted by BATF-TFAP4 is divergent from the previously reported JUN-driven program.<sup>28</sup> Some genes, including *CCR3*, *CCR4*, and *CCR8*, were induced by BATF-TFAP4, BATF-RFP, and RFP-TFAP4 KI (relative to control cells). However, the combined BATF-TFAP4 KI also promoted differential expression of a variety of genes highlighted in yellow that were not differentially affected by either BATF or TFAP4 KI

alone (Figures 6E and S10A–S10C). Taken together, these results suggest that combinatorial KI of BATF and TFAP4 can drive both overlapping but also distinct transcriptional changes compared with single BATF or TFAP4 KIs to promote a fitness advantage in the HA-GD2-28z CAR model of tonic signaling.

The TFAP4 single KI construct had improved killing capacity of HA-GD2-28z CARs *in vitro* and *in vivo*. Next, we assessed if the BATF-TFAP4 combinatorial KI could further enhance the anti-cancer function of HA-GD2-28z CARs because this combination conferred an added fitness benefit. In both *in vitro* co-culture assays (Figures 6F, S10D, and S10E) and an *in vivo* NSG xenograft model (Figures 6G and S10F), BATF-TFAP4 KI CAR-T cells performed best to control leukemia growth (significantly better than control KI and with a trend toward better control than the TFAP4 single KI).

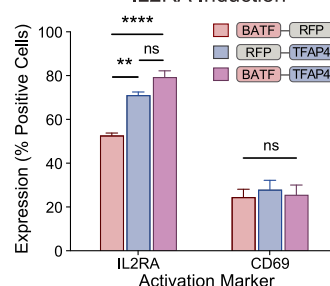
A

Competition/Abundance Validation



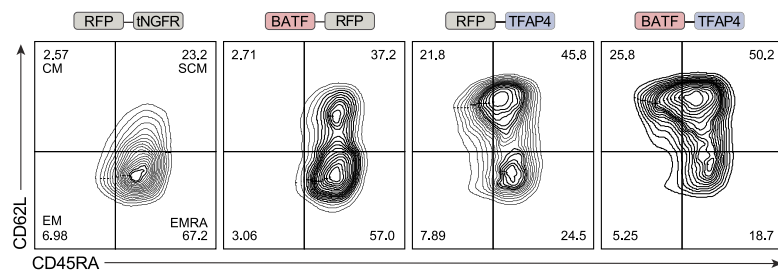
B

IL2RA Induction



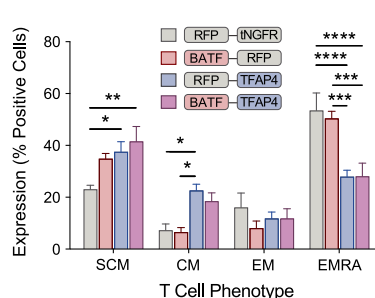
C

Exemplary Flow Plots: T Cell Phenotype



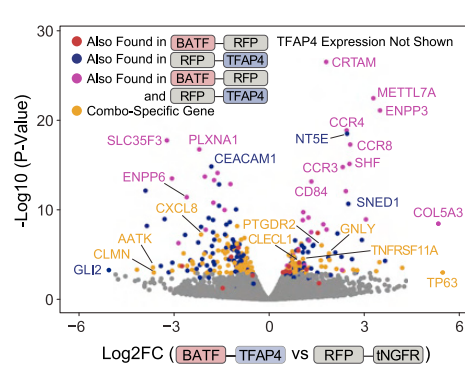
D

Reduction of Temra Cells



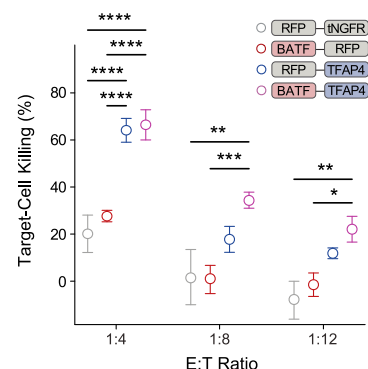
E

Differentially Expressed Genes



F

Killing Across E:T Ratios



G

In vivo Leukemia Control

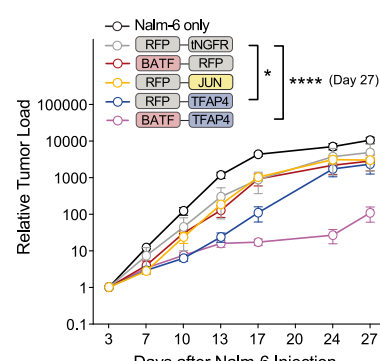
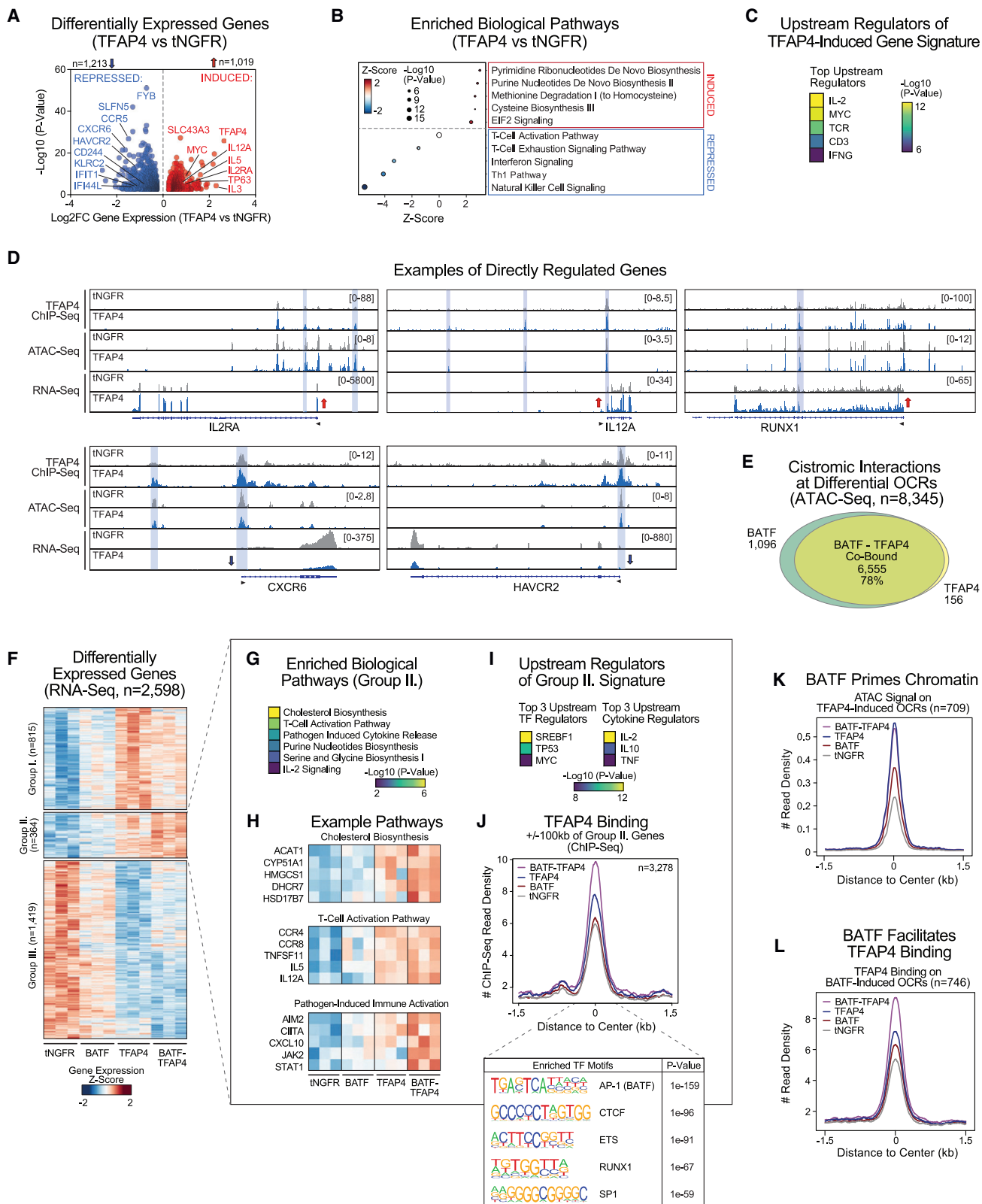


**Figure 6. Combinatorial BATF-TFAP4 knockin induces favorable T cell programs**

- (A) Competitive fitness assays with combinatorial knockin constructs (HA-GD2-28z CAR) were performed (data normalized to day 0, unpaired t test performed on day 4).
- (B) Activation marker expression was analyzed on HA-GD2-28z CARs 8 days after electroporation. 2-way ANOVA with Holm-Sidak's correction was performed.
- (C) Exemplary flow cytometry for phenotypic markers 14 days after electroporation.
- (D) Phenotypic analysis of combinatorial KI HA-GD2-28z CARs 14 days after electroporation. Two-way ANOVA with Holm-Sidak's correction was performed.
- (E) Differentially expressed genes in BATF-TFAP4 compared with RFP-tNGFR control KI HA-GD2-28z CARs were analyzed by RNA-seq 14 days after electroporation. The most differentially expressed gene was TFAP4 (not shown,  $\log_2FC$  5.0,  $p_{adj}$  6.03e-77). The color indicates if the respective gene was also found among the most differentially expressed genes when comparing TFAP4-RFP vs. control, BATF-RFP vs. control or in both of these comparisons. Highlighted in yellow are genes that were differentially expressed selectively in BATF-TFAP4 vs. RFP-tNGFR KI. n = 2 donors.
- (F) Combinatorial KI HA-GD2-28z CARs were co-cultured with Nalm-6/GFP/Luc/GD2 cells and target-cell killing was analyzed (Incucyte). Reduced number of replicates for RFP-tNGFR condition was due to low cell counts (Figures S10D and S10E). Two-way ANOVA with Holm-Sidak's correction was performed as described in the STAR Methods.
- (G) NSG mice were injected with 0.5e6 Nalm-6/GFP/Luc/GD2 cells and treated with 1e6 HA-GD2-28z CAR+ cells. Leukemic load was determined by bioluminescence imaging. n = 2 T cell donors, 2–5 mice/donor/group. Donors are shown separately in Figure S10F. Two-way ANOVA with Holm-Sidak's test was performed to compare all constructs against the control (RFP-tNGFR) (both donors combined).
- n = 2 donors in technical duplicates (B and D) or triplicates (A and F). Mean (+SEM) shown (A, B, D, F, and G). See also Figures S9 and S10.



(legend on next page)

### BATF facilitates TFAP4-mediated transcriptional rewiring

To understand how TFAP4 alone, or in combination with BATF, promotes T cell function, we performed an independent set of RNA-seq, chromatin immunoprecipitation (ChIP)-seq, and assay for transposase-accessible chromatin (ATAC)-seq experiments. For the first analysis, TFAP4 HA-GD2-28z CAR-T cells were compared with control tNGFR HA-GD2-28z CAR-T cells. We identified 2,232 TFAP4 KI-regulated genes (Figure 7A), for which we annotated TFAP4 KI-regulated open chromatin regions (OCRs) that bind TFAP4 (Figures S11A and S11B). T cell fitness genes such as *IL2RA*, *IL12A*, and *MYC* were upregulated in TFAP4 KI cells, whereas markers of dysfunctional cell states, such as *CD244* (2B4), *CXCR6*, and *HAVCR2* (TIM-3), were repressed (Figure 7A). Accordingly, pathway analysis showed enrichment in eIF2 signaling (which plays a critical role in translation initiation) and pathways involved in biosynthesis of substrates that are essential during cell division (Figure 7B). The prediction of the top upstream regulators of TFAP4 KI-regulated gene sets identified IL-2, MYC, and the TCR (Figure 7C). Taken together, TFAP4 facilitates T cell proliferation and, importantly, restrains overactivation and exhaustion of T cells (via repression of short-lived effector genes, e.g., *NFATC3*, *KLRC2*, and *KLRB1*; and markers of exhaustion, e.g., *CXCR6*, *HAVCR2*, and *CD244*). ChIP-/ATAC-seq indicated that TFAP4 binds to promoters and gene-proximal enhancers around regulated genes and exhibits chromatin-remodeling activity (Figure S11A). Directly regulated genes include *IL2RA*, *RUNX1*, *IL12A* (all upregulated), and *HAVCR2* (TIM-3, downregulated) (Figure 7D). *IL2RA* stood out as one of the primary drivers of the phenotypic effects of TFAP4 due to TFAP4's direct binding and chromatin-remodeling activity at the *IL2RA* locus (Figure 7D), which led to increased *IL2RA* expression on RNA (Figures 7A and 7D) and protein levels (Figures 4G and S8E–S8H). To evaluate whether increased *IL2RA* KI alone can phenocopy the effect of TFAP4 KI, we compared TFAP4 with *IL2RA* single KIs. Although *IL2RA*

KI increased cytotoxicity of HA-GD2-28z CARs, including increased release of some cytokines, TFAP4 KI had a much stronger effect on both cytokine levels and cytotoxicity (Figures S11C and S11D). In summary, TFAP4 is a TF with chromatin-remodeling activities that balances/optimizes T cell behavior by enhancing the proliferative capacity of T cells while restraining markers of exhaustion.

Evaluating potential coordinated effects of BATF and TFAP4, we observed that KI of these TFs has robust chromatin-remodeling activities affecting chromatin accessibility at 8,345 locations across the genome. Among these, they cooperatively open 2,256 genomic regions (group II), where we found strong enrichment for the TFAP4 DNA binding motif (ATAC-seq; Figure S11E). ChIP-seq revealed remarkable co-occupancy by BATF and TFAP4 at chromatin sites where accessibility was altered by BATF and/or TFAP4 KI (78% of regions filtered for differential OCRs, Figure S11E) (Figures 7E and S11F). Analysis of the two TFs' effects on gene expression also revealed their cooperative—either additive or synergistic—role in regulating 364 genes (Figure 7F, group II). Pathway analysis showed that these genes are constituents of T cell activation and cholesterol biosynthesis pathways (Figures 7G and 7H). Consistent with this, upstream regulator analysis predicted SREBF1 as the top TF regulator of group II genes, a key activator of cholesterol metabolism (Figure 7I). Cholesterol biosynthesis is important for membrane regeneration during cell proliferation. Moreover, an increase in cell membrane cholesterol can lead to more efficient formation of the immunological synapse.<sup>57</sup> Next, we annotated TFAP4-bound genomic regions to group II genes and found that BATF KI greatly facilitated the binding of TFAP4 (Figure 7J). BATF can open chromatin regions at TFAP4-bound sites and thus prime the chromatin for TFAP4 (Figures 7K, 7L, S11G, and S11H). This cooperation via BATF-mediated chromatin priming and facilitated TFAP4 binding was also observed in loci that solely get induced by TFAP4 KI, including *IL12A*, *IL5*, and *SLC7A11* (cystine/glutamate antiporter) (Figure S11I). Taken together, our results suggest that BATF

**Figure 7. BATF facilitates TFAP4-mediated epigenomic reprogramming**

- (A) Differentially expressed genes in RNA-seq of TFAP4 vs. tNGFR HA-GD2-28z CAR-T cells 14 days after electroporation.
- (B) Pathway analysis of the differentially expressed genes by QIAGEN Ingenuity Pathway Analysis (IPA). Top 5 enriched pathways are shown for induced/repressed genes.
- (C) Upstream regulator analysis of the TFAP4 KI-regulated gene signature by QIAGEN IPA. Top 5 hits are shown.
- (D) Examples of ChIP-/ATAC-/RNA-seq tracks at genomic loci regulated by TFAP4 KI.
- (E) Venn diagram depicts genome occupancy of BATF and/or TFAP4 (ChIP-seq) at differential open chromatin regions (OCRs).
- (F) Heatmap depicts the differentially expressed genes across indicated conditions. Gene groups were defined by k-means clustering and describe distinct expression patterns: group I. Induced by TFAP4 KI and damped by BATF KI; group II. Induced by TFAP4 KI and potentiated by BATF-TFAP4 KI; group III. Repressed by both TFAP4 and BATF.
- (G) Pathway analysis of group II genes by QIAGEN IPA. Top 5 enriched pathways are shown.
- (H) Gene expression heatmaps depict example genes from the top 3 biological pathways (G).
- (I) Upstream regulator analysis of the group II gene signature by QIAGEN IPA. Top 3 TF and cytokine hits are shown.
- (J) Metagene plot of normalized TFAP4 ChIP-seq signal at TFAP4 peaks  $\pm$ 100 kb around transcription start sites of group II genes with corresponding motif analysis.
- (K) Metagene plot of normalized ATAC-seq signal at TFAP4 KI-induced OCRs.
- (L) Metagene plot of normalized TFAP4 ChIP-seq signal at BATF KI-induced OCRs.
- (A, E, and F) FDR < 0.05,  $\log_2FC \geq 0.5$ . (A)–(D) include TFAP4 vs. tNGFR single KI HA-GD2-28z CARs. (E) summarizes data from all ChIP-seq conditions (TFAP4, BATF, tNGFR single KI and BATF-TFAP4 combinatorial KI HA-GD2-28z CARs). (F)–(I) include RNA-seq from RFP-tNGFR (labeled as tNGFR), BATF-RFP (labeled as BATF), RFP-TFAP4 (labeled as TFAP4) and BATF-TFAP4 HA-GD2-28z CARs. (J) and (L) show ChIP-seq data from TFAP4, BATF, and tNGFR single KI and BATF-TFAP4 combinatorial KI HA-GD2-28z CARs. (K) shows ATAC-seq from RFP-tNGFR (labeled as tNGFR), BATF-RFP (labeled as BATF), RFP-TFAP4 (labeled as TFAP4), and BATF-TFAP4 HA-GD2-28z CARs. n = 3 donors.

See also Figure S11.

supports TFAP4 function through two non-exclusive mechanisms: (1) BATF-mediated chromatin priming at TFAP4 binding sites and (2) BATF-facilitated TFAP4 binding, which is likely at least partially the result of BATF's chromatin priming activities. Therefore, together, BATF and TFAP4 increase T cell fitness and reduce dysfunction in therapeutic T cells, especially in the context of tonic signaling or chronic antigen stimulation.

## DISCUSSION

T cell dysfunction resulting from chronic stimulation can limit long-term success of adoptive cell therapies.<sup>4,5</sup> To discover KI constructs that can improve T cell functions, we designed non-viral ModPoKI screening. ModPoKI uses targeted integration at defined genomic sites. We chose to target the *TRAC* locus because it is functionally monoallelic (~85% in this system, see Figure S1E), KI can replace the endogenous antigen specificity, the endogenous regulatory elements can drive expression of transgenic CARs/TCRs mimicking expression of endogenous TCRs, and integration of CAR sequences into the *TRAC* locus can reduce T cell exhaustion.<sup>13,45,58</sup> Although the efficiency of non-viral ModPoKI is currently lower than that of viral transduction, KI rates can be increased further, e.g., with single-stranded DNA templates and/or non-homologous end joining (NHEJ) inhibitors.<sup>59</sup> We observed different effects of TFs when retroviral vectors were used to introduce CAR and TF constructs into non-targeted sites with heterologous promoters vs. non-viral KI under *TRAC* promoter control. These results underscore the importance of testing genetic modifications in the same genomic context that will eventually be employed therapeutically in order to identify lead synthetic constructs with the greatest potential for cell therapies. As cell therapies increasingly rely on targeted modification,<sup>60,61</sup> ModPoKI is optimized uniquely to compare functional properties of synthetic KI designs at defined genomic loci.

In order to clear large tumor burdens, therapeutic T cells have to maintain persistent function throughout chronic stimulation from repetitive antigen encounters and/or tonic signaling. Previous efforts focusing on viral overexpression of bZIP TFs have shown enhanced function of GD2, HER2, or CD19 CAR-T cells with improved expansion potential, diminished terminal differentiation, or enrichment of tumor-infiltrating lymphocytes.<sup>27,28</sup> Other approaches have investigated how loss of function of either TFs (e.g., KO of NR4A TFs or IKZF3)<sup>11,35,62,63</sup> or epigenetic reprogramming (e.g., KO of DNMT3A or knockdown/KO of TET2)<sup>64,65</sup> can help increase CAR-T cell functionality. Using the ModPoKI platform in combination with repetitive CAR/TCR stimulation or tonic signaling, we found that KI of TFAP4 can promote proliferative, stem-cell-like, and central memory states. Studies in mice have reported that *Tfap4* is a Myc-induced TF that maintains Myc-initiated activation and expansion programs in T cells to control microbial infections.<sup>55</sup> In mice, *Tfap4* is regulated by TCR and IL-2 signals, and gene-deletion studies indicate that it fine tunes clonal T cell expansion.<sup>53</sup> *Tfap4* has been studied primarily in the context of murine viral infections, where it was not essential for short-term virus elimination but was crucial in situations where infection could only be controlled by sustained activity of antigen-specific T cells.<sup>53</sup> These findings align with our discovery that the beneficial effects of TFAP4 KI constructs are most pronounced

after repetitive stimulation or tonic activation. Although IL2RA appears to be one of the strongest phenotypic drivers of TFAP4 KI-induced effects, isolated IL2RA KI cannot phenocopy the distinct transcriptional program driven by TFAP4. Chromatin analyses indicated that BATF KI primes chromatin at TFAP4 binding sites and facilitates TFAP4's DNA binding capacity. Taken together, BATF KI facilitates TFAP4 KI-augmented T cell fitness during chronic stimulation to maintain durable T cell functionality.

Safety profiles need to be assessed carefully for candidate genetic modifications to promote enhanced expansion and function of cellular therapies. Chromosomal abnormalities have been observed after double-strand break-inducing genetic engineering. Although T cells with chromosomal abnormalities often have a fitness disadvantage, strategies to decrease the frequency of cells with chromosomal abnormalities, such as sorting for certain surface markers, can be considered.<sup>66</sup> Another concern is uncontrolled proliferation, as recently observed in TET2 KO CAR-T cells characterized by sustained BATF3 expression.<sup>65</sup> Our screens did suggest a possible role for BATF in increasing T cell abundance in the absence of restimulation. Notably, we did not observe proliferation, cytokine release, or *in vitro* killing by TFAP4 KI CAR-T cells in the absence of the CAR antigen. Safety concerns may eventually warrant additional safety tests and perhaps the use of regulatable "kill" switches or synthetic circuits to control expression levels of the transgene.<sup>67-69</sup> Looking forward, ModPoKI could be useful to accelerate the design of these more complex logic-gated synthetic programs to enhance therapeutic safety profiles.

Unbiased genome-wide screens now serve as powerful tools to identify candidates for gene modification in T cells. We recently developed a platform for genome-wide CRISPRa screens in primary human T cells.<sup>25</sup> However, CRISPRa approaches cannot be immediately translated to the clinic because they require sustained expression of endonuclease-dead Cas9, which results in immunogenicity. Nevertheless, genome-wide CRISPRa screens can be used to nominate genes or pathways that can then be assessed with ModPoKI screens at the appropriate therapeutic locus. For example, both CRISPRa and ORF screens recently nominated overexpression of LTBR to enhance T cell function.<sup>25,26</sup> Here, ModPoKI screens revealed LTBR can be engineered into a chimeric receptor (e.g., an LTBR/OX40 fusion protein) that can be knocked into cells along with a TCR/CAR to improve fitness. In contrast to CRISPRa screens, ModPoKI allows for the screening of both natural and synthetic genes in multicistronic CAR/TCR constructs that can be readily moved toward clinical application without dependence on constant Cas9 expression.

Although we have focused on cell fitness as measured by abundance, ModPoKI can be adapted toward more complex phenotypes, such as cytokine production or T cell infiltration into a tumor *in vivo*. In the future, ModPoKI screens should be readily adaptable to different CARs or TCRs and even newer synthetic receptors, such as HITs (HLA-independent TCRs),<sup>70</sup> synthetic TCR and antigen receptors (STARs),<sup>71</sup> or synthetic intramembrane proteolysis receptors (SNIPRs), and SynNotch receptors.<sup>67,68</sup> Furthermore, future screens can be performed in regulatory T cells to facilitate the development of treatments for autoimmunity or inflammatory diseases, or in gamma-delta

T cells. The integration site could be modified to loci distinct from the *TRAC* locus, and we anticipate that ModPoKI will be powerful in designing novel gene programs for NK cell, B cell, and myeloid-cell therapies, iPS (induced pluripotent stem) cell-derived therapies, and beyond. Looking forward, ModPoKI will accelerate candidate selection and design optimization of synthetic constructs for basic biological discovery and a diverse array of cellular therapies.

### Limitations of the study

In this study, we achieved proof of concept for large-scale ModPoKI *in vitro*, focusing on melanoma and leukemia models. Future studies could utilize ModPoKI to perform *in vivo* screens in more challenging contexts, such as solid tumor xenografts. These studies will benefit from ongoing efforts to improve KI efficiencies, which will enable more complex ModPoKI screens.<sup>59</sup> Recent advances in murine T cell-specific AAV variants<sup>72</sup> could even enable ModPoKI screens in immunocompetent models with established tumor microenvironments. Technically, strict measures are required to minimize artifacts due to PCR contamination of barcodes; changing the barcodes used in arrayed validation experiments is one strategy that could be useful. Overall, future ModPoKI experiments will have opportunities to build on the lessons of these studies to explore larger sequence spaces—including more synthetic gene constructs—across disease models with more fidelity to human pathology.

### STAR★METHODS

Detailed methods are provided in the online version of this paper and include the following:

- KEY RESOURCES TABLE

- RESOURCE AVAILABILITY

- Lead contact
- Materials availability
- Data and code availability

- EXPERIMENTAL MODEL AND STUDY PARTICIPANT DETAILS

- Mouse strains
- Cell lines
- Primary cells

- METHOD DETAILS

- Isolation and culture of primary human T cells
- Generation of plasmid libraries for pooled KI
- Generation of combinatorial libraries for pooled KI
- Homology directed repair templates (HDRTs)
- Cas9 RNP electroporation
- Flow cytometry and FACS
- Single stimulation screens
- Repetitive and tonic stimulation screens
- FACS-based screen on IL2RA expression
- Barcode/amplicon sequencing
- Retrovirus generation and retroviral transduction
- Competition assay
- Activation marker and phenotype analysis
- Proliferation analysis
- RNA sequencing (bulk RNA-seq)

- ATAC sequencing
- ChIP sequencing
- Integrative analysis (RNA-, ATAC-, and ChIP-seq)
- Modular pooled knockin sequencing (ModPoKI-seq)
- Intracellular cytokine assay and Legendplex
- TOX stain
- *In vitro* killing assay
- *In vivo* mouse model

- QUANTIFICATION AND STATISTICAL ANALYSIS

### SUPPLEMENTAL INFORMATION

Supplemental information can be found online at <https://doi.org/10.1016/j.cell.2023.08.013>.

### ACKNOWLEDGMENTS

We thank all members of the Marson Lab; Chris Jeans (QB3 MacroLab); Vinh Nguyen; Camilia Azimi, Jacob W. Freimer, Maya Acre, Mineto Ota, Zachary Steinhart, Brian Shy, Vivasvan Vykunta, and Sebastian Blaeschke for helpful suggestions; Stacie Dodgson for critical input; Sarah Pyle for illustrations; Jennifer Okano, Jackie Sawin, Jon Woo, and Ron Manlapaz for generous assistance; UCSF Parnassus Flow CoLab (RRID:SCR\_018206, DRC Center grant NIH P30 DK063720, and NIH S10 1S10OD021822-01); Gladstone Flow Core (NIH S10 RR028962, James B. Pendleton Charitable Trust, DARPA); LARC, QB3 Genomics (UC Berkeley) RRID:SCR\_022170, UCSF CAT (UCSF PBBR, RRP IMIA, and NIH 1S10OD02851-01); Crystal Mackall and Robbie Majzner for HA-GD2-28Z sequences, Nalm-6/GFP/Luc/GD2, and retroviral plasmids; and Takeshi Egawa for providing TFAP4 antibody. T.L.R. was supported by the UCSF Medical Scientist Training Program (T32GM007618), the UCSF Endocrinology Training Grant (T32 DK007418), and the NIDDK (F30DK120213). T.N.Y. was supported by the NIH Institutional Research Service Award in Molecular and Cellular Mechanisms in Cancer under NCI Training Grant 5T32CA108462. J.C. was supported by NIH/NCI K08, 1K08CA252605-01, a Burroughs Wellcome Fund Career Award for Medical Scientists, and the Lydia Preisler Shorenstein Donor Advised Fund. C.J.Y. was supported by NIH grants R01HG011239 and R01AI136972 and by the Chan Zuckerberg Initiative, was an investigator at the Chan Zuckerberg Biohub, and is a member of the Parker Institute for Cancer Immunotherapy. F.B. was supported by the Care-for-Rare Foundation, the German Research Foundation (DFG), and the Emerging Investigators EHA-EBMT Joint Fellowship Award in the Field of Cell Therapy and Immunotherapy (EBMT, EHA, Gilead, and Kite). T.F. was supported by the German Research Foundation (DFG)—SFB-TRR338/1 2021–452881907. A.T.S. was supported by a Career Award for Medical Scientists (Burroughs Wellcome Fund), a Lloyd J. Old STAR Award (Cancer Research Institute), a Pew-Stewart Scholars in Cancer Research Award, and the Parker Institute for Cancer Immunotherapy. A.M. received funding from the Simons Foundation, Career Award for Medical Scientists, a Lloyd J. Old STAR Award (Cancer Research Institute), the Parker Institute for Cancer Immunotherapy, the Innovative Genomics Institute, and National Institutes of Health grants P30 DK063720 and S10 1S10OD021822-01 (both Parnassus Flow Cytometry Core, A.M.). A.M. was an investigator at Chan Zuckerberg Biohub and received gifts from the Byers family, Barbara Bakar, Karen Jordan, and Elena Radutzky. R.S. was supported by the Austrian Exchange Service, the Austrian Society of Laboratory Medicine, and the Max Kade Foundation. This work was supported by the National Institutes of Health grant S10 RR028962 and the NCI grant 1R01CA276368-01, the Parker Institute for Cancer Immunotherapy, the Cancer League, and the James B. Pendleton Charitable Trust.

### AUTHOR CONTRIBUTIONS

F.B., T.L.R., and A.M. designed the study. T.L.R. designed the ModPoKI system. F.B., T.L.R., R.A., R.Y., and Y.Y.C. designed constructs. F.B., Y.Y.C., R.A., P.A.C., and T.L.R. performed ModPoKI screens. Y.Y.C., R.A., T.L.R.,

F.B., and E.S. analyzed amplicon sequencing. F.B., C.T.M., and Y.Y.C. performed scRNA-seq experiments. B.D., A.Y.C., K.S., and W.Z. analyzed RNA-/ChIP-/ATAC-seq experiments. C.T.M., E.S., T.L.R., and F.B. analyzed ModPoKI-seq. C.J.Y., D.B.G., R.B., and M.C.K. advised on ModPoKI-seq analysis. F.B., Y.Y.C., R.A., R.S., W.A.N., A.T., T.N.Y., and Z.L. performed validation experiments. A.T.S., J.E., C.J.Y., E.S., J.C., and T.F. advised on the manuscript. F.B., T.L.R., and A.M. wrote the manuscript with input from all authors.

#### DECLARATION OF INTERESTS

F.B. received research awards (Gilead and Kite and Bristol Myers Squibb Foundation Immunonkologie). E.S. was an advisor for Arsenal Biosciences. J.E. is a compensated co-founder at Mnemo Therapeutics and compensated scientific advisor to Cytovia Therapeutics. J.E. owns stocks in Mnemo Therapeutics and Cytovia Therapeutics. J.E. has received a consulting fee from Castdin Capital. The Eyquem lab has received research support from Cytovia Therapeutics and Takeda. T.L.R. is a compensated co-founder, member of the scientific advisory board, and previously worked as the CSO of Arsenal Biosciences. A.T.S. is a founder of Immunai and Cartography Biosciences and receives research funding from Allogene Therapeutics and Merck Research Laboratories. C.T.M. is a compensated Bio+Health Venture Fellow at Andreessen Horowitz. C.J.Y. is founder for and holds equity in DropPrint Genomics (now ImmunAI) and Survey Genomics, a scientific advisory board member for and holds equity in Related Sciences and ImmunAI, a consultant for and holds equity in Maze Therapeutics, and a consultant for TRex Bio, HiBio, ImYoo, and Santa Ana. C.J.Y. has received research support from Chan Zuckerberg Initiative, Chan Zuckerberg Biohub, Genentech, BioLegend, ScaleBio, and Illumina. A.M. is a co-founder of Arsenal Biosciences, Spotlight Therapeutics, and Survey Genomics, serves on the boards of directors at Spotlight Therapeutics and Survey Genomics, is a board observer (and former member of the board of directors) at Arsenal Biosciences, is a member of the scientific advisory boards of Arsenal Biosciences, Spotlight Therapeutics, Survey Genomics, NewLimit, Amgen, Tenaya, and Lightcast, owns stock in Arsenal Biosciences, Spotlight Therapeutics, NewLimit, Survey Genomics, PACT Pharma, Tenaya, and Lightcast and has received fees from Arsenal Biosciences, Spotlight Therapeutics, Survey Genomics, NewLimit, 23andMe, PACT Pharma, Juno Therapeutics, Tenaya, Lightcast, GLG, Gilead, Trizell, Vertex, Merck, Amgen, Genentech, AlphaSights, Rupert Case Management, Bernstein, and ALDA. A.M. is an investor in and informal advisor to Offline Ventures and a client of EPIQ. The Marson laboratory received research support from Juno Therapeutics, Epinomics, Sanofi, GlaxoSmithKline, Gilead, and Anthen. T.L.R., F.B., A.M., R.A., Y.Y.C., C.T.M., and E.S. are listed on patent applications related to this work.

#### INCLUSION AND DIVERSITY

We support inclusive, diverse, and equitable conduct of research.

Received: June 25, 2022

Revised: April 22, 2023

Accepted: August 15, 2023

Published: September 14, 2023

#### REFERENCES

1. Esensten, J.H., Bluestone, J.A., and Lim, W.A. (2017). Engineering therapeutic T cells: from synthetic biology to clinical trials. *Annu. Rev. Pathol.* 12, 305–330. <https://doi.org/10.1146/annurev-pathol-052016-100304>.
2. Fesnak, A.D., June, C.H., and Levine, B.L. (2016). Engineered T cells: the promise and challenges of cancer immunotherapy. *Nat. Rev. Cancer* 16, 566–581. <https://doi.org/10.1038/nrc.2016.97>.
3. June, C.H., and Sadelain, M. (2018). Chimeric antigen receptor therapy. *N. Engl. J. Med.* 379, 64–73. <https://doi.org/10.1056/NEJMra1706169>.
4. Delgoffe, G.M., Xu, C., Mackall, C.L., Green, M.R., Gottschalk, S., Speiser, D.E., Zehn, D., and Beavis, P.A. (2021). The role of exhaustion in CAR T cell therapy. *Cancer Cell* 39, 885–888. <https://doi.org/10.1016/j.ccel.2021.06.012>.
5. Schietinger, A., Delrow, J.J., Basom, R.S., Blattman, J.N., and Greenberg, P.D. (2012). Rescued tolerant CD8 T cells are preprogrammed to reestablish the tolerant state. *Science* 335, 723–727. <https://doi.org/10.1126/science.1214277>.
6. Doering, T.A., Crawford, A., Angelosanto, J.M., Paley, M.A., Ziegler, C.G., and Wherry, E.J. (2012). Network analysis reveals centrally connected genes and pathways involved in CD8+ T cell exhaustion versus memory. *Immunity* 37, 1130–1144. <https://doi.org/10.1016/j.jimmuni.2012.08.021>.
7. Wherry, E.J., and Kurachi, M. (2015). Molecular and cellular insights into T cell exhaustion. *Nat. Rev. Immunol.* 15, 486–499. <https://doi.org/10.1038/nri3862>.
8. Man, K., Gabriel, S.S., Liao, Y., Glourey, R., Preston, S., Henstridge, D.C., Pellegrini, M., Zehn, D., Berberich-Siebelt, F., Febbraio, M.A., et al. (2017). Transcription factor IRF4 promotes CD8(+) T cell exhaustion and limits the development of memory-like T cells during chronic. *Immunity* 47, 1129–1141.e5. <https://doi.org/10.1016/j.jimmuni.2017.11.021>.
9. Martinez, G.J., Pereira, R.M., Äijö, T., Kim, E.Y., Marangoni, F., Pipkin, M.E., Togher, S., Heissmeyer, V., Zhang, Y.C., Crotty, S., et al. (2015). The transcription factor NFAT promotes exhaustion of activated CD8(+) T cells. *Immunity* 42, 265–278. <https://doi.org/10.1016/j.jimmuni.2015.01.006>.
10. Sen, D.R., Kaminski, J., Barnitz, R.A., Kurachi, M., Gerdemann, U., Yates, K.B., Tsao, H.W., Godec, J., LaFleur, M.W., Brown, F.D., et al. (2016). The epigenetic landscape of T cell exhaustion. *Science* 354, 1165–1169. <https://doi.org/10.1126/science.aae0491>.
11. Chen, J., López-Moyado, I.F., Seo, H., Lio, C.J., Hempleman, L.J., Sekiya, T., Yoshimura, A., Scott-Browne, J.P., and Rao, A. (2019). NR4A transcription factors limit CAR T cell function in solid tumours. *Nature* 567, 530–534. <https://doi.org/10.1038/s41586-019-0985-x>.
12. Fraietta, J.A., Lacey, S.F., Orlando, E.J., Pruteanu-Malinici, I., Gohil, M., Lundh, S., Boesteanu, A.C., Wang, Y., O'Connor, R.S., Hwang, W.T., et al. (2018). Determinants of response and resistance to CD19 chimeric antigen receptor (CAR) T cell therapy of chronic lymphocytic leukemia. *Nat. Med.* 24, 563–571. <https://doi.org/10.1038/s41591-018-0010-1>.
13. Eyquem, J., Mansilla-Soto, J., Giavridis, T., van der Stegen, S.J., Hamieh, M., Cunanan, K.M., Odak, A., Gönen, M., and Sadelain, M. (2017). Targeting a CAR to the TRAC locus with CRISPR/Cas9 enhances tumour rejection. *Nature* 543, 113–117. <https://doi.org/10.1038/nature21405>.
14. Di Roberto, R.B., Castellanos-Rueda, R., Schlatter, F.S., Palianina, D., Nguyen, O.T.P., Kapetanovic, E., Hierlemann, A., Khanna, N., and Reddy, S.T. (2021). speedingCARs: accelerating the engineering of CAR T cells by signaling domain shuffling and single-cell sequencing. <https://doi.org/10.1101/2021.08.23.457342>.
15. Goodman, D.B., Azimi, C.S., Kearns, K., Garakani, K., Garcia, J., Patel, N., Hwang, B., Lee, D., Park, E., Ye, C.J., et al. (2021). Pooled screening of CAR T cells identifies non-native signaling domains for next-generation immunotherapies. <https://doi.org/10.1101/2021.07.11.451980>.
16. Kyung, T., Gordon, K.S., Perez, C.R., Holec, P.V., Ramos, A., Zhang, A.Q., Liu, Y., Koch, C., Starchenko, A., Joughin, B., et al. (2021). CARPOOL: A library-based platform to rapidly identify next generation chimeric antigen receptors. <https://doi.org/10.1101/2021.07.09.450900>.
17. Stadtmauer, E.A., Fraietta, J.A., Davis, M.M., Cohen, A.D., Weber, K.L., Lancaster, E., Mangan, P.A., Kulikovskaya, I., Gupta, M., Chen, F., et al. (2020). CRISPR-engineered T cells in patients with refractory cancer. *Science* 367, eaba7365. <https://doi.org/10.1126/science.aba7365>.
18. Zhao, H., Liu, Y., Wang, L., Jin, G., Zhao, X., Xu, J., Zhang, G., Ma, Y., Yin, N., and Peng, M. (2021). Genome-wide fitness gene identification reveals Roquin as a potent suppressor of CD8 T cell expansion and anti-tumor immunity. *Cell Rep.* 37, 110083. <https://doi.org/10.1016/j.celrep.2021.110083>.

19. Wei, J., Long, L., Zheng, W., Dhungana, Y., Lim, S.A., Guy, C., Wang, Y., Wang, Y.D., Qian, C., Xu, B., et al. (2019). Targeting REGNASE-1 programs long-lived effector T cells for cancer therapy. *Nature* 576, 471–476. <https://doi.org/10.1038/s41586-019-1821-z>.
20. Mai, D., Johnson, O., Reff, J., Fan, T.J., Scholler, J., Sheppard, N.C., and June, C.H. (2023). Combined disruption of T cell inflammatory regulators Regnase-1 and Roquin-1 enhances antitumor activity of engineered human T cells. *Proc. Natl. Acad. Sci. USA* 120, e2218632120. <https://doi.org/10.1073/pnas.2218632120>.
21. LaFleur, M.W., Nguyen, T.H., Coxe, M.A., Yates, K.B., Trombley, J.D., Weiss, S.A., Brown, F.D., Gillis, J.E., Coxe, D.J., Doench, J.G., et al. (2019). A CRISPR-Cas9 delivery system for in vivo screening of genes in the immune system. *Nat. Commun.* 10, 1668. <https://doi.org/10.1038/s41467-019-09656-2>.
22. Sutra Del Galy, A., Menegatti, S., Fuentealba, J., Lucibello, F., Perrin, L., Heift, J., Darbois, A., Saitakis, M., Tosello, J., Rookhuizen, D., et al. (2021). In vivo genome-wide CRISPR screens identify SOCS1 as intrinsic checkpoint of CD4(+) TH1 cell response. *Sci. Immunol.* 6, eabe8219. <https://doi.org/10.1126/sciimmunol.abe8219>.
23. Carnevale, J., Shifrut, E., Kale, N., Nyberg, W.A., Blaeschke, F., Chen, Y.Y., Li, Z., Bapati, S.P., Diolaiti, M.E., O'Leary, P., et al. (2022). RASA2 ablation in T cells boosts antigen sensitivity and long-term function. *Nature* 609, 174–182. <https://doi.org/10.1038/s41586-022-05126-w>.
24. Shifrut, E., Carnevale, J., Tobin, V., Roth, T.L., Woo, J.M., Bui, C.T., Li, P.J., Diolaiti, M.E., Ashworth, A., and Marson, A. (2018). Genome-wide CRISPR screens in primary human T cells reveal key regulators of immune function. *Cell* 175, 1958–1971.e15. <https://doi.org/10.1016/j.cell.2018.10.024>.
25. Schmidt, R., Steinhart, Z., Layeghi, M., Freimer, J.W., Bueno, R., Nguyen, V.Q., Blaeschke, F., Ye, C.J., and Marson, A. (2022). CRISPR activation and interference screens decode stimulation responses in primary human T cells. *Science* 375, eabj4008. <https://doi.org/10.1126/science.abj4008>.
26. Legut, M., Gajic, Z., Guarino, M., Daniloski, Z., Rahman, J.A., Xue, X., Lu, C., Lu, L., Mimitou, E.P., Hao, S., et al. (2022). A genome-scale screen for synthetic drivers of T cell proliferation. *Nature* 603, 728–735. <https://doi.org/10.1038/s41586-022-04494-7>.
27. Seo, H., González-Avalos, E., Zhang, W., Ramchandani, P., Yang, C., Lio, C.J., Rao, A., and Hogan, P.G. (2021). BATF and IRF4 cooperate to counter exhaustion in tumor-infiltrating CAR T cells. *Nat. Immunol.* 22, 983–995. <https://doi.org/10.1038/s41590-021-00964-8>.
28. Lynn, R.C., Weber, E.W., Sotillo, E., Gennert, D., Xu, P., Good, Z., Arbuthnath, H., Lattin, J., Jones, R., Tieu, V., et al. (2019). C-Jun overexpression in CAR T cells induces exhaustion resistance. *Nature* 576, 293–300. <https://doi.org/10.1038/s41586-019-1805-z>.
29. Blaeschke, F., Stenger, D., Apfelbeck, A., Cadilha, B.L., Benmebarek, M.R., Mahdawi, J., Ortner, E., Lepenies, M., Habjan, N., Rataj, F., et al. (2021). Augmenting anti-CD19 and anti-CD22 CAR T-cell function using PD-1-CD28 checkpoint fusion proteins. *Blood Cancer J.* 11, 108. <https://doi.org/10.1038/s41408-021-00499-z>.
30. Liu, H., Lei, W., Zhang, C., Yang, C., Wei, J., Guo, Q., Guo, X., Chen, Z., Lu, Y., Young, K.H., et al. (2021). CD19-specific CART cells that express a PD-1/CD28 chimeric switch-receptor are effective in patients with PD-L1-positive B-cell lymphoma. *Clin. Cancer Res.* 27, 473–484. <https://doi.org/10.1158/1078-0432.CCR-20-1457>.
31. Liu, X., Ranganathan, R., Jiang, S., Fang, C., Sun, J., Kim, S., Newick, K., Lo, A., June, C.H., Zhao, Y., and Moon, E.K. (2016). A chimeric switch-receptor targeting PD1 augments the efficacy of second-generation CAR T cells in advanced solid tumors. *Cancer Res.* 76, 1578–1590. <https://doi.org/10.1158/0008-5472.CAN-15-2524>.
32. Oda, S.K., Daman, A.W., Garcia, N.M., Wagener, F., Schmitt, T.M., Tan, X., Chapuis, A.G., and Greenberg, P.D. (2017). A CD200R-CD28 fusion protein appropriates an inhibitory signal to enhance T-cell function and therapy of murine leukemia. *Blood* 130, 2410–2419. <https://doi.org/10.1182/blood-2017-04-777052>.
33. Zhao, S., Wang, C., Lu, P., Lou, Y., Liu, H., Wang, T., Yang, S., Bao, Z., Han, L., Liang, X., et al. (2021). Switch receptor T3/28 improves long-term persistence and antitumor efficacy of CAR-T cells. *J. Immunother. Cancer* 9, e003176. <https://doi.org/10.1136/jitc-2021-003176>.
34. Sack, L.M., Davoli, T., Xu, Q., Li, M.Z., and Elledge, S.J. (2016). Sources of error in mammalian genetic screens. *G3 (Bethesda)* 6, 2781–2790. <https://doi.org/10.1534/g3.116.030973>.
35. Fraietta, J.A., Nobles, C.L., Sammons, M.A., Lundh, S., Carty, S.A., Reich, T.J., Cogdill, A.P., Morrisette, J.J.D., DeNizio, J.E., Reddy, S., et al. (2018). Disruption of TET2 promotes the therapeutic efficacy of CD19-targeted T cells. *Nature* 558, 307–312. <https://doi.org/10.1038/s41586-018-0178-z>.
36. Cavazzana-Calvo, M., Payen, E., Negre, O., Wang, G., Hehir, K., Fusil, F., Down, J., Denaro, M., Brady, T., Westerman, K., et al. (2010). Transfusion independence and HMGA2 activation after gene therapy of human beta-thalassaemia. *Nature* 467, 318–322. <https://doi.org/10.1038/nature09328>.
37. Roth, T.L., Li, P.J., Blaeschke, F., Nies, J.F., Apathy, R., Mowery, C., Yu, R., Nguyen, M.L.T., Lee, Y., Truong, A., et al. (2020). Pooled knockin targeting for genome engineering of cellular immunotherapies. *Cell* 181, 728–744.e21. <https://doi.org/10.1016/j.cell.2020.03.039>.
38. Roth, T.L., Puig-Saus, C., Yu, R., Shifrut, E., Carnevale, J., Li, P.J., Hiatt, J., Saco, J., Krystofinski, P., Li, H., et al. (2018). Reprogramming human T cell function and specificity with non-viral genome targeting. *Nature* 559, 405–409. <https://doi.org/10.1038/s41586-018-0326-5>.
39. Nguyen, D.N., Roth, T.L., Li, P.J., Chen, P.A., Apathy, R., Mamedov, M.R., Vo, L.T., Tobin, V.R., Goodman, D., Shifrut, E., et al. (2020). Polymer-stabilized Cas9 nanoparticles and modified repair templates increase genome editing efficiency. *Nat. Biotechnol.* 38, 44–49. <https://doi.org/10.1038/s41587-019-0325-6>.
40. Fang, J., Qian, J.J., Yi, S., Harding, T.C., Tu, G.H., VanRoey, M., and Jooss, K. (2005). Stable antibody expression at therapeutic levels using the 2A peptide. *Nat. Biotechnol.* 23, 584–590. <https://doi.org/10.1038/nbt1087>.
41. Fang, J., Yi, S., Simmons, A., Tu, G.H., Nguyen, M., Harding, T.C., VanRoey, M., and Jooss, K. (2007). An antibody delivery system for regulated expression of therapeutic levels of monoclonal antibodies in vivo. *Mol. Ther.* 15, 1153–1159. <https://doi.org/10.1038/sj.mt.6300142>.
42. Hanna, R.E., and Doench, J.G. (2018). A case of mistaken identity. *Nat. Biotechnol.* 36, 802–804. <https://doi.org/10.1038/nbt.4208>.
43. Robbins, P.F., Li, Y.F., El-Gamil, M., Zhao, Y., Wargo, J.A., Zheng, Z., Xu, H., Morgan, R.A., Feldman, S.A., Johnson, L.A., et al. (2008). Single and dual amino acid substitutions in TCR CDRs can enhance antigen-specific T cell functions. *J. Immunol.* 180, 6116–6131. <https://doi.org/10.4049/jimmunol.180.9.6116>.
44. Pearce, E.L., Mullen, A.C., Martins, G.A., Krawczyk, C.M., Hutchins, A.S., Zediak, V.P., Banica, M., DiCioccio, C.B., Gross, D.A., Mao, C.A., et al. (2003). Control of effector CD8+ T cell function by the transcription factor eomesodermin. *Science* 302, 1041–1043. <https://doi.org/10.1126/science.1090148>.
45. Li, J., He, Y., Hao, J., Ni, L., and Dong, C. (2018). High levels of Eomes promote exhaustion of anti-tumor CD8(+) T cells. *Front. Immunol.* 9, 2981. <https://doi.org/10.3389/fimmu.2018.02981>.
46. Park, H.B., Lee, J.E., Oh, Y.M., Lee, S.J., Eom, H.S., and Choi, K. (2017). CTLA4-CD28 chimera gene modification of T cells enhances the therapeutic efficacy of donor lymphocyte infusion for hematological malignancy. *Exp. Mol. Med.* 49, e360. <https://doi.org/10.1038/emm.2017.104>.
47. Shin, J.H., Park, H.B., Oh, Y.M., Lim, D.P., Lee, J.E., Seo, H.H., Lee, S.J., Eom, H.S., Kim, I.H., Lee, S.H., and Choi, K. (2012). Positive conversion of negative signaling of CTLA4 potentiates antitumor efficacy of adoptive T-cell therapy in murine tumor models. *Blood* 119, 5678–5687. <https://doi.org/10.1182/blood-2011-09-380519>.
48. Anderson, A.C., Joller, N., and Kuchroo, V.K. (2016). Lag-3, Tim-3, and TIGIT: co-inhibitory receptors with specialized functions in immune

- regulation. *Immunity* 44, 989–1004. <https://doi.org/10.1016/j.jimmuni.2016.05.001>.
49. Gupta, P.K., Godec, J., Wolski, D., Adland, E., Yates, K., Pauken, K.E., Cosgrove, C., Ledderose, C., Junger, W.G., Robson, S.C., et al. (2015). CD39 expression identifies terminally exhausted CD8+ T cells. *PLoS Pathog.* 11, e1005177. <https://doi.org/10.1371/journal.ppat.1005177>.
  50. Khan, O., Giles, J.R., McDonald, S., Manne, S., Ngiow, S.F., Patel, K.P., Werner, M.T., Huang, A.C., Alexander, K.A., Wu, J.E., et al. (2019). TOX transcriptionally and epigenetically programs CD8(+) T cell exhaustion. *Nature* 571, 211–218. <https://doi.org/10.1038/s41586-019-1325-x>.
  51. Scott, A.C., Dündar, F., Zumbo, P., Chandran, S.S., Klebanoff, C.A., Shabib, M., Trivedi, P., Menocal, L., Appleby, H., Camara, S., et al. (2019). TOX is a critical regulator of tumour-specific T cell differentiation. *Nature* 571, 270–274. <https://doi.org/10.1038/s41586-019-1324-y>.
  52. Alfei, F., Kanev, K., Hofmann, M., Wu, M., Ghoneim, H.E., Roelli, P., Utzschneider, D.T., von Hoesslin, M., Cullen, J.G., Fan, Y., et al. (2019). TOX reinforces the phenotype and longevity of exhausted T cells in chronic viral infection. *Nature* 571, 265–269. <https://doi.org/10.1038/s41586-019-1326-9>.
  53. Chou, C., Pinto, A.K., Curtis, J.D., Persaud, S.P., Cella, M., Lin, C.C., Edelson, B.T., Allen, P.M., Colonna, M., Pearce, E.L., et al. (2014). c-Myc-induced transcription factor AP4 is required for host protection mediated by CD8+ T cells. *Nat. Immunol.* 15, 884–893. <https://doi.org/10.1038/ni.2943>.
  54. Long, A.H., Haso, W.M., Shern, J.F., Wanhainen, K.M., Murgai, M., Ingaramo, M., Smith, J.P., Walker, A.J., Kohler, M.E., Venkateshwara, V.R., et al. (2015). 4-1BB costimulation ameliorates T cell exhaustion induced by tonic signaling of chimeric antigen receptors. *Nat. Med.* 21, 581–590. <https://doi.org/10.1038/nm.3838>.
  55. Jung, P., Menssen, A., Mayr, D., and Hermeking, H. (2008). AP4 encodes a c-MYC-inducible repressor of p21. *Proc. Natl. Acad. Sci. USA* 105, 15046–15051. <https://doi.org/10.1073/pnas.0801773105>.
  56. Hosokawa, H., and Rothenberg, E.V. (2021). How transcription factors drive choice of the T cell fate. *Nat. Rev. Immunol.* 21, 162–176. <https://doi.org/10.1038/s41577-020-00426-6>.
  57. Yang, W., Bai, Y., Xiong, Y., Zhang, J., Chen, S., Zheng, X., Meng, X., Li, L., Wang, J., Xu, C., et al. (2016). Potentiating the antitumour response of CD8(+) T cells by modulating cholesterol metabolism. *Nature* 531, 651–655. <https://doi.org/10.1038/nature17412>.
  58. Schober, K., Müller, T.R., Gökmén, F., Grassmann, S., Effenberger, M., Poltorak, M., Stemberger, C., Schumann, K., Roth, T.L., Marson, A., and Busch, D.H. (2019). Orthotopic replacement of T-cell receptor alpha- and beta-chains with preservation of near-physiological T-cell function. *Nat. Biomed. Eng.* 3, 974–984. <https://doi.org/10.1038/s41551-019-0409-0>.
  59. Shy, B.R., Vykunta, V.S., Ha, A., Talbot, A., Roth, T.L., Nguyen, D.N., Pfeiffer, W.G., Chen, Y.Y., Blaeschke, F., Shifrut, E., et al. (2023). High-yield genome engineering in primary cells using a hybrid ssDNA repair template and small-molecule cocktails. *Nat. Biotechnol.* 41, 521–531.
  60. Foy, S.P., Jacoby, K., Bota, D.A., Hunter, T., Pan, Z., Stawiski, E., Ma, Y., Lu, W., Peng, S., Wang, C.L., et al. (2023). Non-viral precision T cell receptor replacement for personalized cell therapy. *Nature* 615, 687–696. <https://doi.org/10.1038/s41586-022-05531-1>.
  61. Zhang, J., Hu, Y., Yang, J., Li, W., Zhang, M., Wang, Q., Zhang, L., Wei, G., Tian, Y., Zhao, K., et al. (2022). Non-viral, specifically targeted CAR-T cells achieve high safety and efficacy in B-NHL. *Nature* 609, 369–374. <https://doi.org/10.1038/s41586-022-05140-y>.
  62. Zou, Y., Liu, B., Li, L., Yin, Q., Tang, J., Jing, Z., Huang, X., Zhu, X., and Chi, T. (2022). IKZF3 deficiency potentiates chimeric antigen receptor T cells targeting solid tumors. *Cancer Lett.* 524, 121–130. <https://doi.org/10.1016/j.canlet.2021.10.016>.
  63. Liu, X., Wang, Y., Lu, H., Li, J., Yan, X., Xiao, M., Hao, J., Alekseev, A., Khong, H., Chen, T., et al. (2019). Genome-wide analysis identifies NR4A1 as a key mediator of T cell dysfunction. *Nature* 567, 525–529. <https://doi.org/10.1038/s41586-019-0979-8>.
  64. Prinzing, B., Zebley, C.C., Petersen, C.T., Fan, Y., Anido, A.A., Yi, Z., Nguyen, P., Houke, H., Bell, M., Haydar, D., et al. (2021). Deleting DNMT3A in CAR T cells prevents exhaustion and enhances antitumor activity. *Sci. Transl. Med.* 13, eabh0272. <https://doi.org/10.1126/scitranslmed.abh0272>.
  65. Jain, N., Zhao, Z., Feucht, J., Koche, R., Iyer, A., Dobrin, A., Mansilla-Soto, J., Yang, J., Zhan, Y., Lopez, M., et al. (2023). TET2 guards against unchecked BATF3-induced CAR T cell expansion. *Nature* 615, 315–322. <https://doi.org/10.1038/s41586-022-05692-z>.
  66. Nahmad, A.D., Reuveni, E., Goldschmidt, E., Tenne, T., Liberman, M., Horovitz-Fried, M., Khosravi, R., Kobo, H., Reinstein, E., Madi, A., et al. (2022). Frequent aneuploidy in primary human T cells after CRISPR-Cas9 cleavage. *Nat. Biotechnol.* 40, 1807–1813. <https://doi.org/10.1038/s41587-022-01377-0>.
  67. Hyrenius-Wittsten, A., Su, Y., Park, M., Garcia, J.M., Alavi, J., Perry, N., Montgomery, G., Liu, B., and Roybal, K.T. (2021). SynNotch CAR circuits enhance solid tumor recognition and promote persistent antitumor activity in mouse models. *Sci. Transl. Med.* 13, eabd8836. <https://doi.org/10.1126/scitranslmed.abd8836>.
  68. Zhu, I., Liu, R., Garcia, J.M., Hyrenius-Wittsten, A., Piraner, D.I., Alavi, J., Israni, D.V., Liu, B., Khalil, A.S., and Roybal, K.T. (2022). Modular design of synthetic receptors for programmed gene regulation in cell therapies. *Cell* 185, 1431–1443.e16. <https://doi.org/10.1016/j.cell.2022.03.023>.
  69. Brandt, L.J.B., Barnkob, M.B., Michaels, Y.S., Heiselberg, J., and Barington, T. (2020). Emerging approaches for regulation and control of CAR T cells: A mini review. *Front. Immunol.* 11, 326. <https://doi.org/10.3389/fimmu.2020.00326>.
  70. Mansilla-Soto, J., Eyquem, J., Haubner, S., Hamieh, M., Feucht, J., Paillon, N., Zucchetti, A.E., Li, Z., Sjöstrand, M., Lindenberg, P.L., et al. (2022). HLA-independent T cell receptors for targeting tumors with low antigen density. *Nat. Med.* 28, 345–352. <https://doi.org/10.1038/s41591-021-01621-1>.
  71. Liu, Y., Liu, G., Wang, J., Zheng, Z.Y., Jia, L., Rui, W., Huang, D., Zhou, Z.X., Zhou, L., Wu, X., et al. (2021). Chimeric STAR receptors using TCR machinery mediate robust responses against solid tumors. *Sci. Transl. Med.* 13, eabb5191. <https://doi.org/10.1126/scitranslmed.eabb5191>.
  72. Nyberg, W.A., Ark, J., To, A., Clouden, S., Reeder, G., Muldoon, J.J., Chung, J.Y., Xie, W.H., Allain, V., Steinhart, Z., et al. (2023). An evolved AAV variant enables efficient genetic engineering of murine T cells. *Cell* 186, 446–460.e19. <https://doi.org/10.1016/j.cell.2022.12.022>.
  73. Watanabe, N., Bajgain, P., Sukumaran, S., Ansari, S., Heslop, H.E., Rooney, C.M., Brenner, M.K., Leen, A.M., and Vera, J.F. (2016). Fine-tuning the CAR spacer improves T-cell potency. *Oncoimmunology* 5, e1253656. <https://doi.org/10.1080/2162402X.2016.1253656>.
  74. Daniel, B., Balint, B.L., Nagy, Z.S., and Nagy, L. (2014). Mapping the genomic binding sites of the activated retinoid X receptor in murine bone marrow-derived macrophages using chromatin immunoprecipitation sequencing. *Methods Mol. Biol.* 1204, 15–24. [https://doi.org/10.1007/978-1-4939-1346-6\\_2](https://doi.org/10.1007/978-1-4939-1346-6_2).
  75. Egawa, T., and Littman, D.R. (2011). Transcription factor AP4 modulates reversible and epigenetic silencing of the Cd4 gene. *Proc. Natl. Acad. Sci. USA* 108, 14873–14878. <https://doi.org/10.1073/pnas.1112293108>.
  76. Butler, A., Hoffman, P., Smibert, P., Papalexi, E., and Satija, R. (2018). Integrating single-cell transcriptomic data across different conditions, technologies, and species. *Nat. Biotechnol.* 36, 411–420. <https://doi.org/10.1038/nbt.4096>.

## STAR★METHODS

### KEY RESOURCES TABLE

| REAGENT or RESOURCE  | SOURCE                    | IDENTIFIER                       |
|--|---------------------------|----------------------------------|
| <b>Antibodies</b>  |                           |                                  |
| Alexa Fluor 647 AffiniPure F(ab')2 Fragment Goat Anti-Mouse IgG, F(ab')2 fragment specific | Jackson ImmunoResearch    | Cat#115-606-072; RRID:AB_2338928 |
| APC anti-human CD271 (NGFR) Antibody   | Biolegend                 | Cat#345108; RRID:AB_10645515     |
| APC anti-human CD279 (PD-1) Antibody   | Biolegend                 | Cat#329908; RRID:AB_940475       |
| APC anti-human CD86 Antibody   | Biolegend                 | Cat#305412; RRID:AB_493231       |
| APC Mouse Anti-Human CD178   | BD                        | Cat#564262; RRID:AB_2738714      |
| APC Mouse IgG1, κ Isotype Control  | BD                        | Cat#555751; RRID:AB_398613       |
| BD Pharmingen PE Mouse anti-Human CD39   | BD                        | Cat#555464; RRID:AB_395856       |
| Brilliant Violet 421 anti-human CD25 Antibody  | Biolegend                 | Cat#302630; RRID:AB_11126749     |
| Brilliant Violet 421 anti-human CD366 (Tim-3) Antibody                                     | Biolegend                 | Cat#345008; RRID:AB_11218598     |
| Brilliant Violet 421 anti-human CD69 Antibody  | Biolegend                 | Cat#310930; RRID:AB_2561909      |
| Brilliant Violet 421 anti-human CD8a Antibody  | Biolegend                 | Cat#301036; RRID:AB_10960142     |
| Brilliant Violet 421 anti-human CD95 (Fas) Antibody  | Biolegend                 | Cat#305624; RRID:AB_2561830      |
| Brilliant Violet 421 anti-human TCRA/b Antibody  | Biolegend                 | Cat#306722; RRID:AB_2562805      |
| Brilliant Violet 421 Mouse IgG1, κ Isotype Ctrl Antibody                                   | Biolegend                 | Cat#400158; RRID:AB_11150232     |
| Brilliant Violet 711 anti-human CD137 (4-1BB) Antibody                                     | Biolegend                 | Cat#309832; RRID:AB_2650991      |
| Brilliant Violet 711 anti-human CD19 Antibody  | Biolegend                 | Cat#302246; RRID:AB_2562065      |
| Brilliant Violet 711 anti-human CD45RA Antibody  | Biolegend                 | Cat#304138; RRID:AB_2563815      |
| Brilliant Violet 711 anti-human CD80 Antibody  | Biolegend                 | Cat#305236; RRID:AB_2734270      |
| Brilliant Violet 711 anti-human CD86 Antibody  | Biolegend                 | Cat#305440; RRID:AB_2565835      |
| Brilliant Violet 711 anti-human TCR a/b Antibody   | Biolegend                 | Cat#306740; RRID:AB_2783169      |
| Brilliant Violet 711 Mouse IgG2b, κ Isotype Ctrl Antibody                                  | Biolegend                 | Cat#400354                       |
| BUV395 Mouse Anti-Human CD4  | BD                        | Cat#563550; RRID:AB_2738273      |
| BUV737 Mouse Anti-Human CD8  | BD                        | Cat#612754; RRID:AB_2870085      |
| BV421 Mouse IgG1, κ Isotype Control  | BD                        | Cat#562438; RRID:AB_11207319     |
| BV650 Mouse Anti-Human CD62L   | BD                        | Cat#563808; RRID:AB_2738433      |
| BV711 Mouse Anti-Human IL-2  | BD                        | Cat#563946; RRID:AB_2738501      |
| CD223 (LAG-3) Monoclonal Antibody (3DS223H), PerCP-eFluor 710, eBioscience                 | Thermo Fisher Scientific  | Cat#46-2239-42; RRID:AB_2573732  |
| eBioscience Fixable Viability Dye eFluor 780   | Thermo Fisher Scientific  | Cat#65-0865-18                   |
| FITC anti-human CD271 (NGFR) Antibody  | Biolegend                 | Cat#345104; RRID:AB_2282828      |
| FITC anti-human CD4 Antibody   | Biolegend                 | Cat#344604; RRID:AB_1937227      |
| FITC anti-human TCR a/b Antibody   | Biolegend                 | Cat#306706; RRID:AB_314644       |
| Myc-Tag (9B11) Mouse mAb (Alexa Fluor 647 Conjugate)                                       | Cell Signaling Technology | Cat#2233; RRID:AB_823474         |
| Pacific Blue anti-human TNF- $\alpha$ Antibody   | Biolegend                 | Cat#502920; RRID:AB_528965       |
| PE anti-HA.11 Epitope Tag Antibody   | Biolegend                 | Cat#901518; RRID:AB_2629623      |
| PE anti-human CD25 Antibody  | Biolegend                 | Cat#302606; RRID:AB_314276       |
| PE anti-human CD62L Antibody   | Biolegend                 | Cat#304806; RRID:AB_314466       |
| PE anti-human CD95 (Fas) Antibody  | Biolegend                 | Cat#305608; RRID:AB_314546       |

(Continued on next page)

**Continued**

| REAGENT or RESOURCE   | SOURCE                   | IDENTIFIER                        |
|---|--------------------------|-----------------------------------|
| PE Mouse Anti-Human IFN-γ   | BD                       | Cat#554701; RRID:AB_395518        |
| PE Mouse IgG1, κ Isotype Ctrl Antibody  | Biolegend                | Cat#400112; RRID:AB_2847829       |
| PE Streptavidin   | BD                       | Cat#349023                        |
| PE-Cy7 Mouse Anti-Human CD25  | BD                       | Cat#557741; RRID:AB_396847        |
| PE-Cy7 Mouse Anti-Human CD8   | BD                       | Cat#335787; RRID:AB_399966        |
| PE/Cyanine 7 anti-human CD258 (LIGHT) Antibody  | Biolegend                | Cat#318708; RRID:AB_2721660       |
| PE/Cyanine 7 anti-human CD271 (NGFR) Antibody   | Biolegend                | Cat#345110; RRID:AB_11203542      |
| PE/Cyanine 7 anti-human CD80 Antibody   | Biolegend                | Cat#305218; RRID:AB_2076148       |
| PE/Cyanine7 anti-human TCR α/β Antibody   | Biolegend                | Cat#306720; RRID:AB_10639947      |
| PE/Cyanine7 Mouse IgG2b, κ Isotype Ctrl Antibody                                      | Biolegend                | Cat#400326                        |
| PerCP anti-human CD69 Antibody  | Biolegend                | Cat#310928; RRID:AB_10679124      |
| PerCP Mouse IgG1, κ Isotype Ctrl Antibody   | Biolegend                | Cat#400148                        |
| PerCP/Cyanine5.5 anti-human CD4 Antibody  | Biolegend                | Cat#317428; RRID:AB_1186122       |
| TOX Antibody, anti-human/mouse, APC, REAfinity  | Miltenyi Biotec          | Cat#130-118-335; RRID:AB_2751485  |
| violetFluor 450 Anti-Human CD45RA (HI100)   | Tonbo                    | Cat#75-0458-T100; RRID:AB_2621951 |
| <b>Bacterial and virus strains</b>  |                          |                                   |
| Endura Competent Cells, Lucigen   | VWR                      | Cat#60242-2                       |
| NEB Stable Competent E.coli   | New England Biolabs      | Cat#C3040H                        |
| Stbl3 Competent Cells   | Berkeley MacroLab        | N/A                               |
| <b>Biological samples</b>   |                          |                                   |
| Human Peripheral Blood Leukopak, Fresh  | Stemcell                 | N/A                               |
| Trima Residual  | Vitalant                 | Cat#RE202                         |
| <b>Chemicals, peptides, and recombinant proteins</b>                                  |                          |                                   |
| AMPure XP Reagent, 5 mL   | Beckman Coulter          | Cat#A63880                        |
| BATF ChIP Antibody  | Brookwood Biomedical     | Cat#PAB4003                       |
| Biotinylated Human CD19 Protein, Fc Tag, ultra sensitivity                            | ACROBiosystems           | Cat#CD9-H8259                     |
| Cas9 protein  | Berkeley MacroLab        | N/A                               |
| crRNA TRAC 2 sequence AGAGTCTC TCAGCTGGTACA   | Dharmacon                | N/A                               |
| CTS (Cell Therapy Systems) Dynabeads  | Thermo Fisher Scientific | Cat#40203D                        |
| D-Luciferin, Potassium Salt   | Gold Biotechnology       | Cat#LUCK-10G                      |
| Dextramer- HLA-A*0201/SLLMWITQV-APC   | ImmuDex                  | Cat#WB3247-APC                    |
| Dextramer- HLA-A*0201/SLLMWITQV-PE  | ImmuDex                  | Cat#WB3247-PE                     |
| DSG Crosslinker 1 gram  | ProteoChem               | Cat#c1104-1gm                     |
| eBioscience Brefeldin A Solution (1000X)  | Thermo Fisher Scientific | Cat#00-4506-51                    |
| Gibson Assembly Master Mix - 50 rxns  | New England Biolabs      | Cat#E2611L                        |
| Glucose Solution  | Thermo Fisher Scientific | Cat#A2494001                      |
| GlycoBlue Coprecipitant (15 mg/mL)  | Thermo Fisher Scientific | Cat#AM9516                        |
| Invitrogen Recombinant Proteinase K Solution (20mg/mL)                                | Thermo Fisher Scientific | Cat#AM2548                        |
| KAPA HiFi HS RM   | Roche                    | Cat#07958935001                   |
| Lipofectamine 3000 Transfection Reagent   | Thermo Fisher Scientific | Cat#L3000150                      |
| Maxima H Minus Reverse Transcriptase  | Thermo Fisher Scientific | Cat#EP0753                        |
| NEBNext Ultra II Q5 Master Mix  | New England Biolabs      | Cat#M0544L                        |
| NEBuilder HiFi DNA Assembly Master Mix  | New England Biolabs      | Cat#E2621S                        |
| Opti-MEM I Reduced Serum Medium   | Thermo Fisher Scientific | Cat#31985088                      |
| Phenol:Chloroform:Isoamyl Alcohol 25:24:1, Saturated with 10mM Tris, pH 8.0, 1mM EDTA | MilliporeSigma           | Cat#P3803-400ML                   |

(Continued on next page)

**Continued**

| REAGENT or RESOURCE  | SOURCE   | IDENTIFIER  |
|--|--|---|
| Pierce 16% Formaldehyde (w/v), Methanol-free                             | Thermo Fisher Scientific   | Cat#28906   |
| Poly-L-glutamic acid   | Alamanda Polymers  | Cat#26247-79-0  |
| Poly-L-ornithine solution  | MilliporeSigma   | Cat#P4957-50ML  |
| Dynabeads Protein A for Immunoprecipitation                              | Invitrogen   | Cat#10002D  |
| Recombinant Human IL-15 GMP Protein, CF 25ug                             | R&D Systems  | Cat#247-GMP-025   |
| Recombinant Human IL-2 GMP Protein, CF                                   | R&D Systems  | Cat#202-GMP-01M   |
| Recombinant Human IL-7 GMP Protein, CF 25ug                              | R&D Systems  | Cat#BT-007-GMP025   |
| RetroNectin Recombinant Human Fibronectin Fragment                       | Takara Bio   | Cat#T100B   |
| RNAse A, Dnase and protease-free (10mg/mL)                               | Thermo Fisher Scientific   | Cat#EN0531  |
| Sera-Mag magnetic speedbeads   | Thermo Fisher Scientific   | Cat#09-981-123  |
| SPRIselect   | Beckman Coulter  | Cat#B23318  |
| tracrRNA   | Dharmacon  | Cat#U-002005-1000   |
| TRI Reagent  | MilliporeSigma   | Cat#93289-25ML  |
| TRIzol Reagent   | Thermo Fisher Scientific   | Cat#15596018  |
| X-Vivo 15  | Lonza  | Cat#BE02-060Q   |
| <b>Critical commercial assays</b>  |  |   |
| CellTrace Violet Cell Proliferation Kit, for flow cytometry              | Thermo Fisher Scientific   | Cat#C34557  |
| Chromium Single Cell 5' Reagent Kit, v1 chemistry                        | 10x Genomics   | Cat#PN-1000166  |
| EasySep Human T Cell Isolation Kit                                       | Stemcell   | Cat#100-0695  |
| EasySep Human TCR Alpha/Beta Depletion Kit                               | Stemcell   | Cat#17847   |
| eBioscience Foxp3 / Transcription Factor Staining Buffer Set             | Thermo Fisher Scientific   | Cat#00-5523-00  |
| FIX & PERM Cell Fixation & Cell Permeabilization Kit                     | Thermo Fisher Scientific   | Cat#GAS004  |
| LEGENDplex Human CD8/NK Panel (13-plex) with Filter Plate                | Biolegend  | Cat#740267  |
| MiniSeq High Output Reagent Kit (150-cycles)                             | Illumina   | Cat#FC-420-1002   |
| Nextera Chromium i7 Sample Indices N Set A                               | 10x Genomics   | Cat#PN-3000262  |
| Nextera XT DNA Library Preparation Kit                                   | Illumina   | Cat#FC-131-1096   |
| NextSeq 500/550 High Output Kit v2.5 (75 Cycles)                         | Illumina   | Cat#20024906  |
| NextSeq 500/550 Mid Output Kit v2.5 (150 Cycles)                         | Illumina   | Cat#20024904  |
| Ovation RNA-Seq System V2  | Tecan  | Cat#7102-32   |
| Ovation Ultralow V2 DNA-Seq Library Preparation Kit                      | Tecan  | Cat#0344NB-A01  |
| P3 Primary Cell 96-well Nucleofector Kit (960 RCT)                       | Lonza  | Cat#V4SP-3960   |
| Phusion High-Fidelity PCR Master Mix with HF Buffer                      | New England Biolabs  | Cat#M0531L  |
| Qubit 1X dsDNA HS Assay Kit  | Fisher Scientific  | Cat#Q33231  |
| <b>Deposited data</b>  |  |   |
| Bulk RNA-seq, combined ATAC-, ChIP- and RNA-seq and ModPoKI-Seq datasets | This paper   | GEO: GSE232824  |
| DICE dataset   | N/A  | <a href="https://dice-database.org/">https://dice-database.org/</a> |
| Bulk RNA-seq   | Carnevale et al. <sup>23</sup>                                     | GEO: GSE204862  |
| <b>Experimental models: Cell lines</b>                                   |  |   |
| A375   | ATCC   | CRL-1619; RRID:CVCL_0132  |
| A375/CD19  | ATCC, then modified to express CD19 Carnevale et al. <sup>23</sup> | N/A   |

(Continued on next page)

**Continued**

| REAGENT or RESOURCE                                   | SOURCE  | IDENTIFIER                         |
|---|---|------------------------------------|
| A375/RFP/CD19   | ATCC, then modified to express RFP and CD19<br>Carnevale et al. <sup>23</sup> ; Roth et al. <sup>37</sup> | N/A                                |
| GP2-293 cells from Retro-X Universal Packaging System | Takara Bio  | Cat#631530; RRID:CVCL_WI48         |
| Nalm-6/GFP/Luc  | Justin Eyquem   | N/A                                |
| Nalm-6/GFP/Luc/CD19KO                                 | Justin Eyquem   | N/A                                |
| Nalm-6/GFP/Luc/GD2                                    | Crystal Mackall and Robbie Majzner  | N/A                                |
| Nalm-6/GFP/Luc/HLA-A2/NY-ESO-1                        | Justin Eyquem   | N/A                                |
| <b>Experimental models: Organisms/strains</b>         |   |                                    |
| Mouse: NOD/SCID/IL2Rg-null (NSG)                      | The Jackson Laboratory  | Stock#005557; RRID:IMSR_JAX:005557 |
| <b>Oligonucleotides</b>                               |   |                                    |
| See Table S1D for oligonucleotides.                   | This paper  | N/A                                |
| <b>Recombinant DNA</b>                                |   |                                    |
| See Tables S1A–S1C for recombinant DNA (libraries).   | This paper  | N/A                                |
| <b>Software and algorithms</b>                        |   |                                    |
| Adobe Illustrator                                     | Adobe   | N/A                                |
| FlowJo  | BD  | N/A                                |
| GraphPad Prism  | GraphPad Software   | N/A                                |
| Incucyte Live Cell Analysis System                    | Sartorius   | N/A                                |
| Ingenuity Upstream Regulator Analysis in IPA          | Qiagen  | N/A                                |
| IVIS Spectrum In Vivo Imaging System                  | Perkin Elmer  | N/A                                |
| RStudio   | RStudio   | N/A                                |

## RESOURCE AVAILABILITY

### Lead contact

Further information and requests for resources and reagents should be directed to and will be fulfilled by the lead contact, Alexander Marson ([alex.marson@gladstone.ucsf.edu](mailto:alex.marson@gladstone.ucsf.edu)).

### Materials availability

Plasmids generated in this study have been deposited to Addgene or are available upon request.

### Data and code availability

Bulk RNA-seq, combined ATAC-, ChIP- and RNA-seq and ModPoKI-Seq datasets have been deposited at GEO and are publicly available as of the date of publication. Accession numbers are listed in the [key resources table](#). This paper also analyzes existing, publicly available data. Accession numbers are also listed in the [key resources table](#). Screening data and DNA sequences are shown in [Tables S1](#) and [S2](#). Original code has been deposited to Zenodo (<https://doi.org/10.5281/zenodo.8015657>). Additional information required to reanalyze the data reported in this paper is available from the [lead contact](#) upon request.

## EXPERIMENTAL MODEL AND STUDY PARTICIPANT DETAILS

### Mouse strains

NOD/SCID/IL2Rg-null (NSG) mice were purchased from Jackson Laboratory (#005557). 8–12-week-old female mice were used and mouse experiments were performed under an approved UCSF Institutional Animal Care and Use Committee protocol and according to regulatory standards. Mice were housed with a 12 h/12 h light/dark cycle and food/water available *ad libitum*.

### Cell lines

All cell lines were maintained in sterile conditions in a 5% CO<sub>2</sub> incubator at 37°C. Cell lines have been regularly tested for absence of mycoplasma and have been STR-typed. The Nalm-6 (ATCC CRL-3273) cell line used in the TCR single stimulation screens had been

previously modified to express the NY-ESO-1 antigen on HLA-A2 (in addition to GFP/Luc). In addition to these edited Nalm-6 cells, A375s (ATCC CRL-1619) with or without nuclear RFP expression and with CD19 (SFFV promoter knocked in upstream of endogenous CD19) or without CD19 expression (wild-type, WT) as well as Nalm-6 cells with and without CD19 expression were used. Nalm-6/GFP/Luc/GD2 were a kind gift from the Mackall lab (Stanford) and were reported to have an STR profile that was an ~60% match to Nalm-6, suggesting some degree of mutation/heterogeneity. GP2-293 cells were purchased from Takara Bio (#631458). Unless otherwise noted, A375s were cultured in complete RPMI (cRPMI) media consisting of Gibco RPMI 1640 media (Thermo Fisher Scientific) supplemented with 10% fetal bovine serum (FBS, Sigma-Aldrich, St. Louis, Missouri, USA), Penicillin-Streptomycin (Pen/Strep), L-Glutamine, MEM Non-Essential Amino Acids (NEAA), HEPES and Sodium Pyruvate (all Thermo Fisher Scientific). Unless otherwise noted, Nalm-6 cells were cultured in cRPMI media plus 2-Mercaptoethanol (beta-ME, Thermo Fisher Scientific). Unless otherwise noted, GP2-293 cells (Takara Bio) were cultured in complete DMEM (cDMEM) consisting of DMEM, high glucose (Thermo Fisher Scientific) supplemented with 10% FBS, Pen/Strep, L-Glutamine, HEPES, NEAA and Sodium Pyruvate.

### Primary cells

Human T cells were isolated from leukapheresis products (Leukopaks, Stemcell, samples collected with approved Stemcell IRB) or TRIMA Apheresis (Blood Centers of the Pacific, San Francisco) of male and female donors using EasySep Human T Cell Isolation Kit (Stemcell). For (sc)RNA-/ATAC-/ChIP-seq analyses, Leukopaks from Stemcell were used as starting material. T cells were cultured in X-VIVO 15 media (Lonza Bioscience) supplemented with 5% FBS, 50 µM beta-ME (Thermo Fisher Scientific), and 10 mM N-Acetyl-L-Cysteine (NAC, VWR) with different amounts of cytokines as indicated below.

### METHOD DETAILS

#### Isolation and culture of primary human T cells

T cell isolation was done as previously described.<sup>37</sup> Briefly, human T cells were isolated from leukapheresis products (Leukopaks, Stemcell, samples collected with approved Stemcell IRB) or TRIMA Apheresis (Blood Centers of the Pacific, San Francisco) using EasySep Human T Cell Isolation Kit (Stemcell). The use of human material is approved by the UCSF Committee on Human Research (CHR #13-11950). T cells were cultured in X-VIVO 15 media (Lonza Bioscience) supplemented with 5% FBS, 50 µM beta-ME (Thermo Fisher Scientific), and 10 mM NAC (VWR). Prior to electroporation, T cells were stimulated for 48 h at 1e6 cells per ml of media containing 500 U/ml IL-2 (R&D Systems), 5 ng/ml IL-7 (R&D Systems), 5 ng/ml IL-15 (R&D Systems), and CTS (Cell Therapy Systems) CD3/CD28 Dynabeads (Thermo Fisher Scientific, bead:cell ratio 1:1). After nucleofection, T cells were cultured in X-VIVO 15 media containing 500 U/ml IL-2 unless otherwise stated and split every 2 to 4 days.

#### Generation of plasmid libraries for pooled Ki

The 231 constructs included in the pooled knockin library (Tables S1A and S1B) were designed using the Twist Bioscience codon optimization tool and were commercially synthesized and cloned (Twist Bioscience) into a custom pUC19 plasmid containing the NY-ESO-1 TCR sequence (except for HIF1A, JUN and TCF7 constructs that were cloned individually using gBlocks Gene Fragments (Integrated DNA Technologies)). Twist Bioscience sequence-verified all 228 constructs after synthesis and cloning. However, we sequenced 96/228 constructs using Primordium Labs and found that one construct had a 719 bp duplication resulting in a frameshift with predicted absent TCR/CAR expression (tBTLA) and one plasmid had a mixed sequence of the expected WT sequence and a 34 bp duplication (IRF2). Individual pooled plasmid libraries were created by pooling single construct plasmids into respective libraries (transcription factors and related proteins, 100 members; surface receptor constructs, 129 members; controls, 2) or in one complete pool. The CD19 CAR plasmid pools were created in a pooled assembly fashion by amplifying constructs from the TCR plasmid pool as a DNA template. PCR amplification (Kapa Hot Start polymerase, Roche) produced a pooled library of amplicons with small overhangs homologous to a pUC19 plasmid containing the CD19 CAR HDR sequences. The amplicon pool was treated with DpnI restriction enzyme (New England Biolabs, NEB) to remove residual circular TCR plasmids, bead purified (Sera-Mag Speed-Beads), and eluted into H<sub>2</sub>O. We then used Gibson Assembly (NEB) to construct plasmid pools containing all 231 library members and knockin controls, plus the new CAR sequence. The CD19 CAR plasmid pools were bead-purified, transformed into Endura electrocompetent cells (Lucigen) and maxiprepped (Plasmid Plus Midi or Maxi Kit, Qiagen) for further use. The HA-GD2-28z CAR libraries were generated in a similar way. While the NY-ESO-1 TCR libraries were pooled at the plasmid stage (plasmids were synthesized individually), all other plasmid libraries in this project (CD19-BBz and -28z CAR, HA-GD2-28z CAR, combinatorial library) were generated by pooled Gibson assembly of the plasmids. The CD19 CAR consisted of an FMC63 scFv, a CD8 spacer and transmembrane domain and 4-1BB or CD28 co-stimulatory domains followed by a CD3z domain. A MYC-tag was included in between the spacer and the FMC63 domain to facilitate detection. The high-affinity GD2-28z CAR (HA-GD2-28z CAR) sequence was kindly provided by Crystal Mackall and Robbie Majzner, Stanford.<sup>28</sup> The HA-GD2-28z CAR consisted of a 14G2a scFv E101K with an IgG1 spacer, parts of CD28 extracellular, transmembrane and intracellular domains followed by CD3z. Primer sequences are listed in Table S1D. TCR and CAR sequences are listed in Table S1E.

### Generation of combinatorial libraries for pooled KI

The combinatorial HA-GD2-28z CAR plasmid libraries were generated by pooled Gibson assembly of an HA-GD2-28z CAR pUC19 backbone as well as TF insert 1 and TF insert 2. The backbone included the published HA-GD2-28z CAR sequence<sup>28</sup> with CD28 co-stimulation and mutations in the IgG1 CH2 region to increase tonic signaling<sup>73</sup> (kindly provided by Crystal Mackall and Robbie Majzner as described above). The inserts were PCR-amplified out of the pre-existing TF library using primers that removed the 5' barcode of the first insert and the 3' barcode of the second insert and added a constant linker in between the two combinatorial inserts. The HA-GD2-28z CAR backbone, the pools of insert 1 and the pools of insert 2 were assembled using NEBuilder HiFi DNA Assembly Master Mix (NEB). Thus, a DNA site was created which consisted of the 3' barcode of the TF in the 1<sup>st</sup> position, a constant linker (linker 2 – linker 1 junction) and the 5' barcode of the TF in the 2<sup>nd</sup> position, creating a unique combinatorial barcode for each TFxTF combination (Table S1C). The assembled product was bead-purified using Sera-Mag SpeedBeads (Thermo Fisher Scientific), transformed into Endura electrocompetent cells (Lucigen) and midi- or maxiprepped (Plasmid Plus Midi or Maxi Kit, Qiagen) for further use. Primer sequences are listed in Table S1D.

### Homology directed repair templates (HDRTs)

HDRTs were produced as previously described.<sup>37</sup> In brief, TCR or CAR plasmid pools were used as templates for PCR amplification (KAPA HiFi HotStart ReadyMix, Roche) to generate double-stranded DNA templates including truncated Cas9 target sequences.<sup>39</sup> Templates were bead-purified as described above and eluted into H<sub>2</sub>O. The concentrations of eluted HDRTs were normalized to 500–1,000 ng/μL. HDRT amplification was confirmed by gel electrophoresis in a 1.0% agarose gel. The templates for arrayed knockin of the different single constructs or combinations during the validation stage were generated in a similar way. Instead of libraries, single constructs served as templates for the PCRs. In all cases, primers were used that added a truncated Cas9 target sequence.<sup>39</sup>

### Cas9 RNP electroporation

Electroporation was done as previously described.<sup>37</sup> In brief, to produce ribonucleoproteins (RNPs), crRNA and tracrRNA (stock 160 μM, both Dharmacon) were mixed 1:1 by volume, and annealed by incubation at 37°C for 30 min to form an 80 μM guide RNA (gRNA) solution. Poly-L-glutamic acid (PGA, stock 125 mg/ml, Sigma) was mixed with gRNA at 0.8:1 volume ratio prior to complexing with Cas9-NLS (QB3 Macrolab) for final volume ratio gRNA:PGA:Cas9 of 1:0.8:1.<sup>39</sup> These were incubated at 37°C for 15 min to form a 14.3 μM RNP solution. RNPs and HDRTs were mixed with T cells before electroporation (3.5 μl of RNP with 500 ng - 1 μg=1 μL of HDRT). Bulk T cells were resuspended in electroporation buffer P3 (Lonza Bioscience) at 0.75e6 cells per 20 μl (per well) and transferred to a 96-well electroporation plate together with 4.5 μL of RNP/HDRT mix per well. Pulse code EH115 was used on a 4D-Nucleofector 96-well Unit (Lonza Bioscience). Cells were rescued in X-VIVO 15 without cytokines for 15 min and then cultured in X-VIVO 15 with 500 U/ml IL-2.

### Flow cytometry and FACS

For flow cytometric analysis, T cells were centrifuged at 300g for 5 min and resuspended in flow buffer (PBS/2%FBS) containing the respective antibody mix (see key resources table). For NY-ESO-1 TCR constructs, cells were stained for 12 min with Dextramer-HLA-A\*0201/SLLMWITQV-PE (ImmuDex) before adding surface antibodies. For HA-GD2-28z CAR constructs, cells were stained for 15 min at 4°C with Alexa Fluor 647 AffiniPure F(ab')2 Fragment Goat Anti-Mouse IgG, F(ab')2 fragment specific (Jackson ImmunoResearch), washed once with flow buffer (PBS with 2 mM EDTA), resuspended in 100μl 2% mouse serum in PBS, incubated for 10 min at 4°C, and washed again before surface stain antibodies were added. After another 10 min incubation, cells were washed again and resuspended in wash buffer, then analyzed on an Attune NxT Flow Cytometer (Thermo Fisher Scientific) or BD LSRFortessa (BD Biosciences). For CD19 CAR constructs, detection through the integrated MYC-tag was done according to the manufacturer's instructions (MYC-tag (9B11) Mouse mAb (Alexa Fluor 647 Conjugate), Cell Signaling Technology). Flow plots were analyzed using FlowJo software.

### Single stimulation screens

One day prior to set-up of the screen, 2.5e6 A375s were plated per T75 flask in cRPMI media assuming that they double within 24 h. One day later (= 7 days after electroporation), edited T cell pools were counted and washed once. 10e6 T cells were transferred to TRI Reagent (Sigma-Aldrich) representing the input population for amplicon sequencing. 10e6 T cells per screening condition were transferred to one T75 flask in 20 ml of X-VIVO 15 (Lonza Bioscience) supplemented with 5% FBS, beta-ME (Thermo Fisher Scientific), NAC (VWR) and 50 U/ml IL-2 (Proleukin). For A375 conditions, cRPMI was removed and flasks were filled up with 20 ml of X-VIVO 15 plus additives and 10e6 T cells. For Nalm-6 conditions, 5e6 Nalm-6 cells were added per T75 flask. In the stimulation conditions, T cells were stimulated with Dynabeads CD3/CD28 CTS (Thermo Fisher Scientific) at a 1:1 bead: cell ratio ("signal 1+2 stim") or a 5:1 ratio ("signal 1+2 excess stim"). For CD3 stimulation only ("signal 1 stim" condition), T cells were incubated with NY-ESO-1 specific dextramer (ImmuDex) for 12 min at RT (1:50 dilution), washed once and transferred to a T75 flasks. After 2 days, 10 ml of X-VIVO 15 were added to all conditions including supplements and 50 U/ml IL-2. Another 2 days later, cells were counted and 10e6 cells were transferred to TRI Reagent (Sigma-Aldrich) for RNA isolation and amplicon sequencing. The Nalm-6 cell line used in the TCR single stimulation screens had been previously modified to express the NY-ESO-1 antigen on HLA-A2 (in addition to GFP/Luc). All screening results can be found in Table S2.

**Repetitive and tonic stimulation screens**

One day prior to the start of the repetitive stimulation screen, A375 cells were counted and transferred to 24-well plates (50,000 cells per well in 1 ml of cRPMI media) assuming that they double within 24 h. One day later, edited T cell pools were counted and 10e6 cells were frozen in TRI Reagent (Sigma-Aldrich) for amplicon sequencing (input population). Media of the A375 cells was removed. 100,000 edited T cells (NY-ESO-1 multimer or CAR positive, ~1:1 effector:target ratio) were transferred to each well of the 24-well plate and co-cultured with the A375 cells in 2 ml of X-VIVO 15 containing supplements plus 50 U/ml IL-2. 24 h later, fresh A375 cells were plated as described above. One day later, media of the new A375 plate was removed and replaced by 1 ml of fresh X-VIVO 15 plus 1 ml of the T cell suspension from the first plate including 50 U/ml IL-2 calculated on the total volume per well. The rest of the T cells were counted and 10e6 cells were transferred to TRI Reagent (Sigma-Aldrich) for amplicon sequencing. The procedure was repeated every other day for a total number of five stimulations with target cells. Multiple wells of the 24-well plates were used per screen to reach cell coverage. For tonic signaling screens, the HA-GD2-28z CAR libraries were knocked into T cells. HA-GD2-28z CAR-T cells were not stimulated with target cells as the HA-GD2-28z CAR is known to drive tonic activation. Cells were harvested on day 4, 8, 12 and 16 after electroporation and transferred to TRI Reagent (Sigma-Aldrich). Combinatorial tonic signaling screens were performed in a similar way (harvest day 4 and day 16). When working with CD19 CARs in combination with A375 cells, we used CD19 overexpressing A375 cells (SFFV promoter knocked in upstream of endogenous CD19). All screening results can be found in [Table S2](#).

**FACS-based screen on IL2RA expression**

T cells were activated on day 0 and electroporated with the HA-GD2-28z CAR TF library 2 days later as described above. On day 8 after electroporation, T cells were stained for TCRab-BV711, Fab-AF647 (CAR detection) and CD25/IL2RA-BV421. For sorting, cells were gated on lymphocytes, singlets, TCRab-/CAR+ cells and then sorted based on the top and bottom ~20% of IL2RA expression. 500,000 cells per bin and donor were sorted. RNA was isolated and further processed for amplicon sequencing as described below. Log<sub>2</sub>FC of the construct representation in the IL2RA high vs low bin was calculated.

**Barcode/amplicon sequencing**

Genomic DNA (pilots) or RNA (unless otherwise noted) was isolated from input and output population. DNA isolation was performed with either Quick-DNA kits (Zymo Research) or conventional phenol chloroform extraction. Briefly, cells were resuspended in ChIP lysis buffer (1% SDS, 50 mM Tris, pH 8, 10 mM EDTA) and NaCl, then incubated overnight. After RNase A and proteinase K treatment, cells were mixed with Phenol:Chloroform:Isoamyl Alcohol (25:24:1, Sigma) and separated using gel phase lock tubes. The DNA was washed with isopropanol and ethanol. For RNA extraction, Direct-zol RNA kits were used (Zymo Research). RNA was reverse transcribed into cDNA using Maxima H Minus Reverse Transcriptase (Thermo Fisher Scientific). The sequencing library was generated by two PCRs. PCR1 was performed using KAPA HiFi HotStart ReadyMix (Roche) for 18 cycles. Amplicons from PCR1 were bead-purified. For PCR2, NEB Next Ultra II Q5 polymerase (NEB) was used for 10 cycles to append P5 and P7 Illumina sequencing adaptors. The PCR2 product was bead-purified, normalized libraries were pooled across samples and sequenced on a MiniSeq (MiniSeq High Output Kit) or NextSeq 500 (Mid or High Output Kit, all Illumina). Barcode distribution was analyzed and log<sub>2</sub> fold change of barcode representation in output vs input population was calculated to detect changes in abundance. Primer sequences are shown in [Table S1D](#). Primers were purchased from Integrated DNA Technologies (IDT). In our experience, PCR products (e.g., for HDR template generation of validation constructs) can easily contaminate NGS libraries for barcode sequencing. Therefore, we performed all ModPoKI screens using very strict pre/post PCR separation measures to minimize PCR contamination. However, we had to exclude and repeat some experiments and sequencing runs due to evidence of PCR contamination.

**Retrovirus generation and retroviral transduction**

Retroviral plasmids were amplified using NEB Stable Competent cells (NEB). To generate retrovirus for comparative analyses between CRISPR KI T cells and retrovirally transduced T cells, GP2-293 cells (Takara Bio) were cultured on poly-D-lysine-coated plates (BioCoat, Corning) and transfected with RD114 and the transfer plasmid (both kindly provided by Crystal Mackall and Robbie Majzner, Stanford) using Lipofectamine 3000 Transfection Reagent (Thermo Fisher Scientific). Opti-MEM (Thermo Fisher Scientific) media supplemented with 5% FBS, Pen/Strep, L-Glutamine, NEAA and Sodium Pyruvate was used during transfection and virus production. Media was replaced 24 h after transfection, viral supernatant was harvested 48 h and 72 h after transfection, centrifuged at 300g for 5 min to remove cell debris and frozen at -80°C until further use. T cells were activated as described above and transduced on Retronectin-coated plates (Takara) by spinfection 2 days later as previously described.<sup>28</sup> In brief, virus was centrifuged on Retronectin-coated plates at 3200 rpm for 2 h at 32°C. Supernatant was removed and T cells were added at 0.5e6/ml in X-VIVO 15 containing 5% FBS, beta-ME, NAC and 500 U/ml IL-2. Plate was spun at 1200 rpm for 2 min. T cells were washed 48 h after transduction.

**Competition assay**

For validations, after arrayed knockin of the different constructs (either derived from the original Twist Biosciences library, from *de novo* gene synthesis by GenScript or Integrated DNA Technologies (IDT) or cloned from existing DNA fragments/plasmids and amplified in Stbl3 Competent Cells (MacroLab)), T cells were sorted and a competition assay was set up on day 8–10 after electroporation. T cells were cultured at an ~50:50 ratio with control T cells in X-VIVO 15 containing 5% FBS, beta-ME, NAC and 50 U/ml

IL-2. The cell ratio was confirmed by flow analysis of the cell mixes and exact percentage of control T cells was determined at baseline level (NGFR expression). Changes in cell ratio were normalized based on percentages on day 0 of the assay.

### Activation marker and phenotype analysis

For HA-GD2-28z CAR validation assays, activation marker expression (4-1BB, IL2RA, CD69) was analyzed by flow cytometry on day 8 after electroporation. CD62L/CD45RA expression levels were analyzed by flow cytometry 14 days after electroporation.

### Proliferation analysis

For proliferation analyses with CD19-28z CAR-T cells as shown in [Figure S7I](#), T cells were sorted for CAR expression (MYC-tag) on day 6 after electroporation. Three days later, they were stained using CellTrace Violet Cell (CTV) Proliferation Kit (Thermo Fisher Scientific) according to the manufacturer's instructions and either cultured alone or co-cultured with CD19 KO Nalm-6 cells or CD19 positive Nalm-6 cells at a 1:1 E:T ratio in XVivo15 media with supplements and 50 U/ml IL-2. 72 h later, cells were stained with live/dead, CD4 and CD8 antibodies and T cells were analyzed by flow cytometry.

For proliferation analyses using the NY-ESO-1 TCR-, CD19-BBz and CD19-28z CAR-T cells as shown in [Figures S5C](#) and [S5D](#), T cells were not sorted for CAR/TCR expression since the different sorting strategies (multimer for TCR vs MYC-tag or recombinant CD19 for CARs) could influence the outcome of the assay. Ki rates were analyzed <24h before setting up the proliferation assay. 7 days after electroporation, T cells were stained using the CellTrace Violet Cell Proliferation Kit (Thermo Fisher Scientific) according to the manufacturer's instructions and co-cultured with CD19-expressing A375 cells at a 1:1 E:T ratio in XVivo15 media with supplements and 50 U/ml IL-2. 72 h later, cells were stained with live/dead, TCRab, CD4 and CD8 antibodies in addition to NY-ESO-1 multimer (TCR setting) or recombinant CD19 (CAR setting) and T cells were analyzed by flow cytometry. For staining with recombinant CD19, biotinylated CD19 (AcroBiosystems) was incubated for 1 h at RT, washed twice and then detected by addition of Streptavidin-PE (BD).

### RNA sequencing (bulk RNA-seq)

For control TCR vs CAR RNA-seq experiments ([Figures S3J–S3L](#)), a dataset from published work from our group was analyzed (GSE204862).<sup>23</sup> For HA-GD2-28z CAR vs CD19-28z CAR vs CD19-BBz CAR comparisons, edited T cells were sorted on day 6 and day 15 after electroporation (control constructs with tNGFR and the respective TCR/CAR), and stored in TRI Reagent (Sigma-Aldrich). RNA was isolated using Direct-zol RNA kits (Zymo Research). Library preparation and sequencing was performed by the QB3-Berkeley Genomics core labs. Total RNA quality as well as poly-dT enriched mRNA quality were assessed on an Agilent 2100 Bioanalyzer. Libraries were prepared using the KAPA RNA Hyper Prep kit (Roche KK8581). Truncated universal stub adapters were ligated to cDNA fragments, which were then extended via PCR using unique dual indexing primers into full length Illumina adapters. Library quality was checked on an AATI (now Agilent) Fragment Analyzer. Library molarity was measured via quantitative PCR with the KAPA Library Quantification Kit (Roche KK4824) on a BioRad CFX Connect thermal cycler. Libraries were then pooled by molarity and sequenced on an Illumina NovaSeq 6000 S4 flow cell for 2 x 150 cycles, targeting at least 25M reads per sample. Fastq files were generated and demultiplexed using Illumina BCL Convert, on a server running CentOS Linux 7. Kallisto was used to map the reads to the human reference transcriptome and genes with zero counts in more than 80% of samples were removed from the analysis. For HA-GD2-28z CAR validation experiments ([Figures 4H, S9G, S9H, and S10A–S10C](#)), edited cells were sorted for CAR+/TCR- expression on day 7 (single inserts) or on day 6 and day 14 (combo inserts) after electroporation. On day 14, one part of the sorted population was stored in TRI Reagent for RNA-seq (Sigma-Aldrich), the other part was stimulated with Nalm-6/GFP/Luc/GD2 cells at a 1:1 E:T ratio. After 24 h, the stimulated T cells were sorted again for CAR+/TCR- cells and stored in TRI Reagent (Sigma-Aldrich). RNA was isolated and sequenced as described above. DESeq2 R package was used for differential gene expression, fgsea package for gene set enrichment analysis (GSEA) with MSigDB v7.2 hallmark gene sets as reference gene lists.

For combined ATAC-/ChIP-/RNA-seq ([Figures 7, S11A, S11B, and S11E–S11I](#)), RNA was isolated from 2e5 sorted CAR-T cells by standard, TRIZol-based RNA precipitation method as follows. Cells were resuspended in 1 ml TRIZol (Ambion). Chloroform was added (200 µL) to this lysate and extensively vortexed to achieve a homogenous mixture; then, it was incubated for 3 min at room temperature before centrifugation at 14,000g at 4°C for 15 min. Aqueous layer was collected from the top and transferred into a new tube (~550 µL), 1 µL GlycoBlue (Ambion) was added, and the RNA was precipitated with equal volume of 2-propanol for 20 min at room temperature. RNA precipitates were centrifuged at 16,000g for 15 min at 4°C and supernatant was carefully discarded without disturbing the GlycoBlue-stained blue RNA pellet. RNA pellet was washed with 1 ml 75% EtOH and after the wash, dissolved in 30 µL nuclease-free water. RNA concentration was determined by nanodrop, and RNA quality was determined by Agilent Bioanalyzer. Approximately 50 ng RNA was reverse-transcribed to cDNA and second strand was synthesized by the Ovation RNA-seq System V2 (Tecan) according to the manufacturer's recommendations. Double-stranded DNA was subjected to isothermal amplification and was purified with Ampure XP beads. DNA was quantified by Qubit and 80 ng DNA was used for sequencing library construction with the Ovation Ultralow Library System V2 (Tecan) using 8 PCR cycles according to the manufacturer's recommendations. Libraries were sequenced with Illumina Novaseq 6000, using paired-end 75 bp read configuration. The sequencing data was processed using version 3.9 of the nf-core RNA-seq pipeline (<https://nf-co.re/rnaseq>). Fastq quality control was performed using FastQC, and filtered reads were trimmed with Trim Galore software. The resulting trimmed fastq files were aligned to the hg38 human genome using STAR, and Salmon was used to generate a gene-by-sample count matrix for downstream analysis. Differential

analysis of gene expression was performed using the DESeq2 package, with an absolute  $\log_2$  fold change of  $\geq 0.5$  and FDR  $< 0.05$ . Batch effects by donor were corrected with the removeBatchEffect function in the limma library. A heatmap was created by aggregating differential genes, standardizing expressions with z-scores across samples, and clustering them using the k-means clustering algorithm with Pearson correlation as the distance metric. Pathway analysis of the differential genes and grouped genes was performed using QIAGEN Ingenuity Pathway Analysis.

### ATAC sequencing

ATAC-seq was performed by using 1e5 sorted CAR-T cells from each condition. Nuclei were isolated with ATAC Lysis Buffer (10 mM Tris-HCl pH 7.4, 10 mM NaCl, 3 mM MgCl<sub>2</sub>, 0.1% IGEPAL). Nuclei were subjected to fragmentation using Nextera DNA Library Preparation Kit (Illumina). After fragmentation, DNA was purified with MinElute PCR Purification Kit (Qiagen). Fragmented DNA was then amplified with Phusion high-fidelity PCR master mix (NEB) using 14 PCR cycles. Amplified libraries were purified again with MinElute PCR Purification Kit. Fragment distribution of libraries was assessed with Agilent Bioanalyzer and libraries were sequenced on a Novaseq 6000 platform with 150 bp paired-end sequencing. The ATAC-seq libraries were processed using the pepatac pipeline (<http://pepatac.databio.org/>), with default options. The fastq files were first trimmed to remove adapter sequences, and then pre-aligned to the mitochondrial genome to exclude mitochondrial reads. Furthermore, multimapping reads aligning to repetitive regions of the genome were filtered out to ensure the accuracy of downstream analysis. After these initial steps, Bowtie2 was used to align the reads to the hg38 genome. Samtools was then employed to identify uniquely aligned reads, and Picard was used to remove the duplicate reads. The resulting deduplicated aligned BAM file was used for downstream analysis.

The identification of peaks in individual samples was performed using MACS2, and these peaks were compiled and resized into a standard non-overlapping 500 bp width consensus peak set. The peak-sample count matrix was generated using ChrAccR with the default parameters of the run\_atac function. Signal tracks for individual samples were then generated using the bamSitesToWig.py function in the pepatac pipeline. Finally, these tracks were merged by group using WiggleTools to produce a comprehensive view of the data across all the samples.

The peak-sample count matrix was analyzed with the DESeq2 package. Batch effects by donor were corrected with the removeBatchEffect function in the limma library. Differential peaks across different conditions were called using DESeq2 with an absolute  $\log_2$  fold change greater than 0.5 and an FDR less than 0.05. A heatmap was created by aggregating differential peaks across conditions, standardizing peak signals using z-score across samples, and clustering using k-means clustering algorithms. Motif enrichment analysis of TFAP4 in peaks of each group was performed with Fisher's exact test. Chromatin accessibility and TFAP4 ChIP binding signal histograms and heatmaps of group peaks were generated using signal tracks with featureAlignedDistribution in the ChIPseeker package, and the tornadoplot package with a 3 kb window around peaks.

### ChIP sequencing

ChIP-seq was performed as previously described with the following modifications.<sup>74</sup> Sorted CAR-T cells (5e6) were double cross-linked by 50 mM DSG (disuccinimidyl glutarate, ProteoChem) for 30 min followed by 10 min of 1% formaldehyde. Formaldehyde was quenched by the addition of glycine. Nuclei were isolated using ChIP lysis buffer (1% Triton x-100, 0.1% SDS, 150 mM NaCl, 1 mM EDTA, and 20 mM Tris, pH 8.0). Nuclei were sheared with Covaris sonicator using the following setup: Fill level – 10, Duty Cycle – 5, PIP – 140, Cycles/Burst – 200, Time – 4 min. Sheared chromatin was immunoprecipitated overnight with the following antibodies: BATF (brookwoodbiomedical – pab4003), TFAP4 (kind gift from Takeshi Egawa's group).<sup>75</sup> Antibody chromatin complexes were pulled down with Protein A magnetic beads and washed once in IP wash buffer I. (1% Triton, 0.1% SDS, 150 mM NaCl, 1 mM EDTA, 20 mM Tris, pH 8.0, and 0.1% NaDOC), twice in IP wash buffer II. (1% Triton, 0.1% SDS, 500 mM NaCl, 1 mM EDTA, 20 mM Tris, pH 8.0, and 0.1% NaDOC), once in IP wash buffer III. (0.25 M LiCl, 0.5% NP-40, 1mM EDTA, 20 mM Tris, pH 8.0, 0.5% NaDOC) and once in TE buffer (10 mM EDTA and 200 mM Tris, pH 8.0). DNA was eluted from the beads by vigorous shaking for 20 min in elution buffer (100 mM NaHCO<sub>3</sub>, 1% SDS). DNA was decrosslinked overnight at 65°C and purified with MinElute PCR purification kit (Qiagen). DNA was quantified by Qubit and 10 ng DNA was used for sequencing library construction with the Ovation Ultralow Library System V2 (Tecan) using 12 PCR cycles according to the manufacturer's recommendations. Libraries were sequenced with Illumina Nextseq 550, using paired-end 75 bp read configuration. Sequencing adapters were trimmed using Trimmomatic. The reads were aligned to the hg38 reference genome using Bowtie2 with the –very-sensitive option. The resulting BAM files were sorted by genomic coordinates using Samtools to remove PCR duplicates. Duplicates after alignment and sorting were marked and removed by Picard. Bed files were generated from bam files with bamToBed and intersected with the hg38 black-list. The bed files were used as input for genomeCoverageBed in the Bedtools package, and the output bedgraph files were normalized by total fragments and converted to bigwig files using bedGraphToBigWig in the UCSC tools. Peaks were called from the bed file using MACS2 with a false discovery threshold of 0.05 (-q 0.05). A non-overlapping consensus peak set was created by iteratively eliminating overlapping peaks with lower significance across all samples. A peak-by-sample matrix was created by counting overlaps of reads in each sample with the consensus peak set. Differential peak analysis was carried out on the peak-by-sample count matrix with an absolute  $\log_2$  fold change threshold of 0.5 and a p value threshold of 0.05. Motif enrichment of differential binding sites was performed with findMotifsGenome.pl using default parameters.

### Integrative analysis (RNA-, ATAC-, and ChIP-seq)

Chromatin accessibility and TFAP4 ChIP binding signal histograms and heatmaps around the TSS of differentially expressed genes were generated using featureAlignedDistribution in the ChIPseeker package and the tornadoplot package, respectively. A 3 kb window was used to aggregate ATAC and ChIP track signals at differentially accessible sites around the upstream and downstream 100 kb of the TSS. findMotifsGenome.pl in the Homer package was used to perform motif enrichment of the differentially accessible sites around the TSS.

### Modular pooled knockin sequencing (ModPoKI-seq)

PoKI-Seq was performed as previously published.<sup>37</sup> Briefly, since the knockin barcodes were closer to the 5' end of the transcript compared to the previous PoKI design, Chromium Single Cell 5' Reagent Kit, v1 chemistry (10x Genomics) was used according to the manufacturer's protocol. NY-ESO-1 TCR-positive cells were sorted by FACS, counted and resuspended at 1,000 cells/μL in PBS with 1% FBS. After GEM (Gel Bead-In Emulsions) recovery, the mRNA library was converted to cDNA, amplified for 11 cycles, and quantified with Agilent Bioanalyzer High Sensitivity. 75% of the amplified cDNA material was carried through for transcriptome library preparation according to the manufacturer's protocol. The remaining 25% of amplified cDNA was used for amplicon sequencing of the knockin barcodes. The cDNA was enriched for knockin barcodes using a nested PCR strategy with Kapa HiFi HotStart Ready Mix (Roche) for 8 cycles per round. For the first PCR, 0.5 μM each of ModPoKI\_Seq\_1\_forw primer and ModPoKI\_Seq\_1\_rev primer was used. Amplified products were purified with 0.8x SPRIselect Reagent Kit (Beckman Coulter) and eluted in 10 μL nuclease-free water. The libraries were further enriched with a second PCR using 0.5 μM each of ModPoKI\_Seq\_2\_forw primer and ModPoKI\_Seq\_2\_rev primer. Amplified products were purified with 0.8x SPRIselect Reagent Kit (Beckman Coulter) and eluted in 15 μL nuclease-free water. Lastly, index PCR was performed with Kapa HiFi HotStart Ready Mix (Roche) for 8 cycles with 2.5 μL each Nextera Chromium i7 Sample Indices N Set A (PN 3000262) and 0.5 μM ModPoKI\_Seq\_index primer. Amplified products were purified with 0.8x SPRIselect Reagent Kit (Beckman Coulter) and eluted in 45 μL nuclease-free water. Samples were pooled and sequenced on a NovaSeq S4 flow cell with 20% PhiX using read parameters 30x8x98. Fastq files were mapped to the human transcriptome (10x Genomics Cell Ranger, v5.0.0) and a custom knockin barcode reference and analyzed using Seurat (v4.1.1).<sup>76</sup> A small fraction (<0.4%) of A375 target cells forming a distinct cluster were removed from the dataset after manual inspection. All screening results can be found in [Table S2](#).

### Intracellular cytokine assay and Legendplex

T cells were stimulated with target cells at a 1:1 E:T ratio for 24 h. Cells were spun down and supernatant was frozen for Legendplex analysis (LEGENDplex Human CD8/NK Panel 13-plex, BioLegend, performed according to the manufacturer's information). 1x Brefeldin A (Thermo Fisher Scientific) was added to the culture for 4 h. Cells were stained for surface markers and intracellular cytokines (see [key resources table](#)) using the FIX & PERM Cell Fixation & Cell Permeabilization Kit (Thermo Fisher Scientific) according to the manufacturer's information. For HA-GD2-28z CAR assays, Nalm-6/GFP/Luc/GD2 were used as target cells (kind gift from the Mackall Lab, as described above). For CD19 CAR assays, A375s with CD19 (SFFV promoter knocked in upstream of endogenous CD19) and without CD19 expression (WT) or Nalm-6 cells with and without CD19 expression (CD19 knockout) were used.

### TOX stain

Intracellular TF stains were done using the eBioscience Foxp3/ Transcription Factor Staining Buffer Set (Thermo Fisher Scientific) according to the supplier's information. A list of flow antibodies is provided in the [key resources table](#).

### In vitro killing assay

For Incucyte assays with Nalm-6/GFP/Luc/GD2 (gift from the Mackall Lab, as described above), flat bottom 96-well plates were coated with 50 μl of 0.01% poly-L-ornithine (PLO) solution (Sigma) for 1 h. PLO was removed and plates were dried for 30–60 min. 10,000 Nalm-6/GFP/Luc/GD2 per well were mixed with sorted T cells in various effector:target (E:T) ratios. For Incucyte assays with A375 target cells (RFP+), 1,500 A375 cells were plated into flat bottom 96-well plates 24 h before start of the assay. T cells were added in various E:T ratios 1 day later (assuming that the A375 cells doubled within 24 h). The assay media consisted of X-VIVO 15 as described above, supplemented with 500 U/ml IL-2 and 1X Glucose Solution (Thermo Fisher Scientific). Cell counts were analyzed every 6 h using the Incucyte Live Cell Analysis System (Essen BioScience). When working with CD19 CARs in combination with A375 cells, we used CD19 overexpressing A375 cells (SFFV promoter knocked in upstream of endogenous CD19). When using 384-well plates instead of 96-well plates for Incucyte analysis, cell counts and volumes were scaled down accordingly (1,750 Nalm-6/GFP/Luc/GD2 cells or 260 A375/RFP cells per well).

### In vivo mouse model

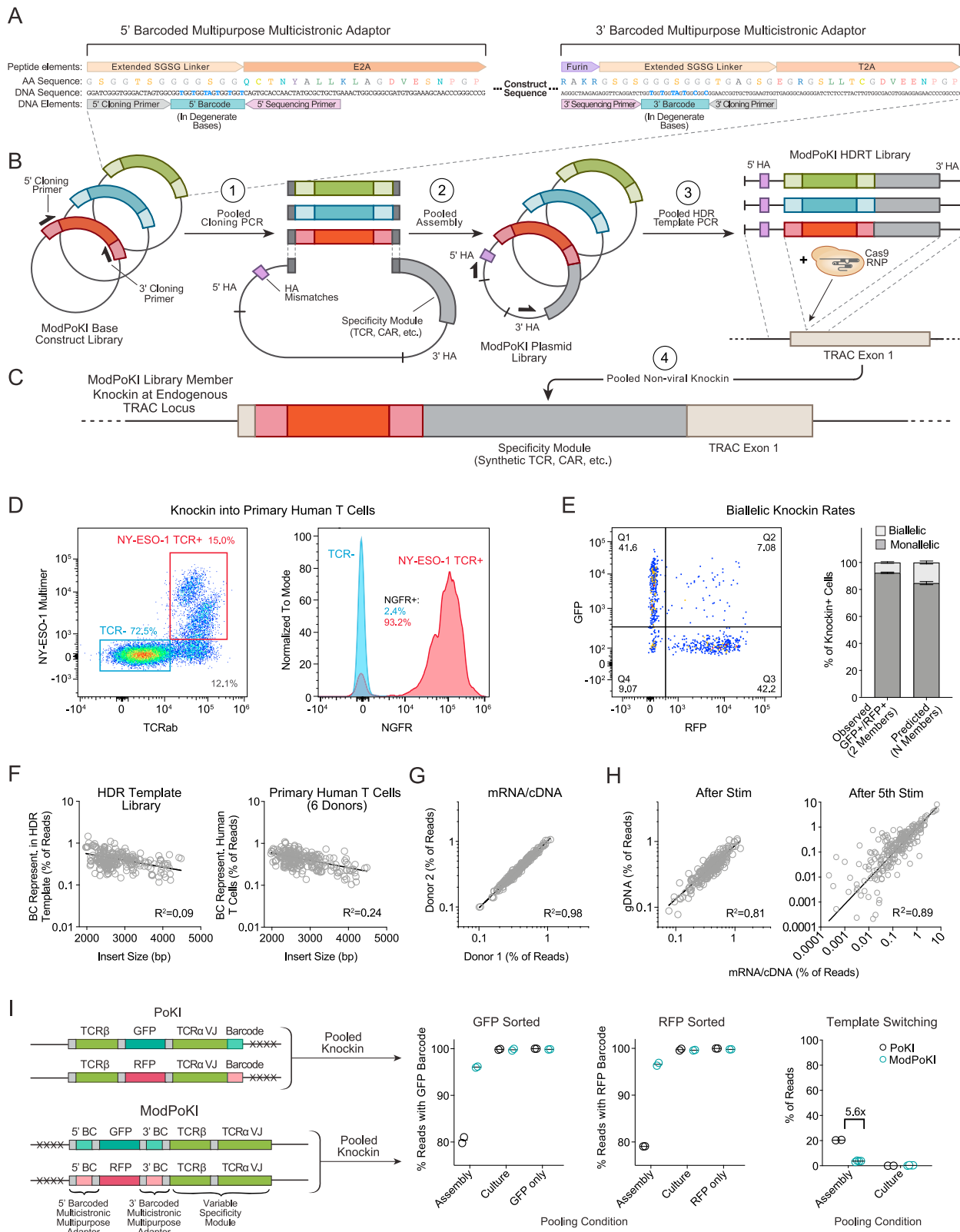
NSG mice were purchased from Jackson Laboratory. 8–12 weeks old female mice were used and mouse experiments were performed under an approved UCSF Institutional Animal Care and Use Committee protocol. For tumor control and survival analyses, mice were injected IV with Nalm-6/GFP/Luc/GD2 cells (gift from the Mackall Lab, as described above) on day 0. Three days later, edited human T cells were injected IV (T cell count was calculated based on CAR+ T cells). Nalm-6 and T cell doses are indicated in the Figure legends. As the GD2+ Nalm-6 CAR model is known for outgrowth of antigen-negative<sup>28</sup> and antigen-positive tumors

that can occur in body cavities especially after injection of low tumor/T cell numbers and complicate endpoint analysis, we used higher tumor/T cell doses for survival analyses to increase number of mice with clear clinical endpoint due to leukemia progression (hind limb paralysis) in contrast to solid tumor formation in body cavities that is challenging to detect and quantify. T cells were TCR-depleted 1 day before injection using EasySep Human TCR Alpha/Beta Depletion Kit (Stemcell) to avoid Graft-versus-Host disease in the mice by unedited cells. Knockin rates were adjusted between groups by adding TCR-negative T cells without CAR knockin right before injection. These cells were generated simultaneously with the therapeutic cells from the same donor and treated the same way except no HDR template was added during electroporation. For imaging, 200  $\mu$ L (3 mg) of D-Luciferin Potassium Salt (Gold BioTechnology) were injected IP and mice were imaged using an IVIS Spectrum *In Vivo* Imaging System (PerkinElmer) once/twice per week.

#### **QUANTIFICATION AND STATISTICAL ANALYSIS**

Statistical details for all experiments can be found in the figure legends. For Incucyte experiments, significance was calculated using 2-way ANOVA with multiple-testing correction (Holm-Sidak) across all timepoints (timeline plots) or across E:T ratios (plots depicting multiple E:T ratios) leading to differences in p values between the two plot types. Ns = not significant, \*  $<0.05$ , \*\* $<0.01$ , \*\*\* $<0.001$ , \*\*\*\* $<0.0001$ . Illustrations were done using Adobe Illustrator.

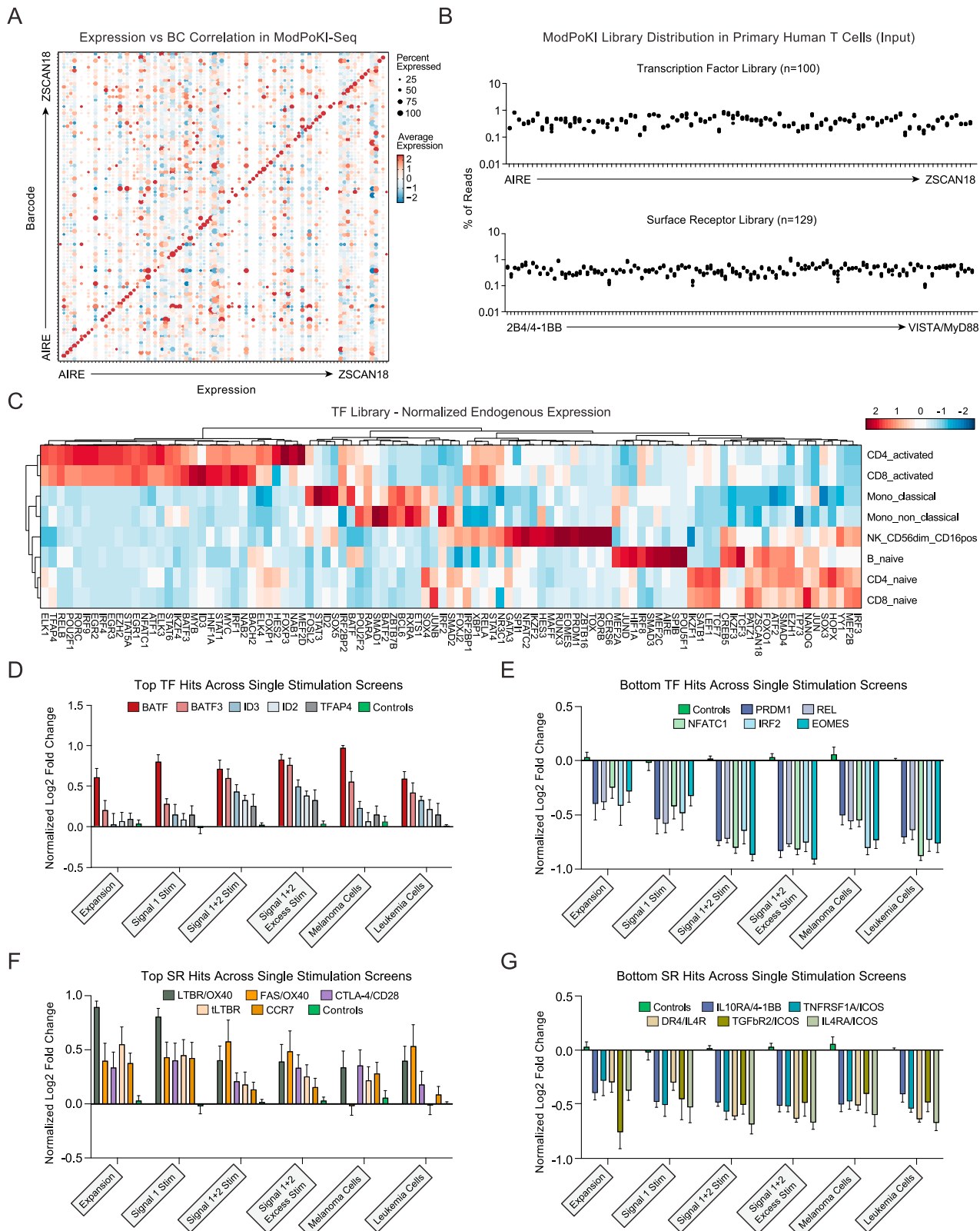
# Supplemental figures



*(legend on next page)*

**Figure S1. Design and quality control metrics of ModPoKI libraries, related to Figure 1**

- (A) To create flexible ModPoKI libraries of sequences that can be integrated into “a functional module” site in pooled knockin templates along with a replaceable antigen receptor in the “specificity module site,” we developed barcoded multicistronic multipurpose adaptors consisting of a 2A site in combination with a DNA barcode. Using degenerate bases, two barcodes per TF/SR member were hidden in the extended SGSG linker of both the 5' and 3' adaptor. The adaptors served as binding sites for the constant cloning primers during pooled library assembly and for the constant sequencing primers for barcode readout by amplicon sequencing. In contrast to the previous PoKI approach that had an ~600 bp distance between barcode and gene of interest,<sup>37</sup> barcodes of ModPoKI constructs were designed to be in close proximity to the gene insert (20–60 bp) to reduce template switching during PCR.<sup>42</sup>
- (B) We synthesized (Twist Bioscience) the initial two ModPoKI libraries, consisting of 100 TFs (and related proteins) and 129 SRs plus controls in combination with the NY-ESO-1 TCR. Using the 5' and 3' cloning primers (ModPoKI\_Cloning\_Insert\_forw/rev), the inserts were amplified in a pooled PCR reaction and then integrated by pooled Gibson assembly into the final plasmid backbone that contained the specificity module (e.g., CD19- or HA-GD2-28z CAR) as well as the homology arms (HAs). The 5' homology arm contained DNA mismatches to allow amplicon sequencing off the gDNA without sequencing the dsDNA template.<sup>37</sup> HDR templates were generated by pooled PCR resulting in double-stranded ModPoKI homology-directed repair template (HDRT) libraries.
- (C) The ModPoKI HDRT libraries were used for pooled non-viral knockin into exon 1 of the TRAC locus by ribonucleoprotein (RNP) electroporation of Cas9, a TRAC-targeting gRNA complex, and the templates. The readout of the screens was performed by either sequencing of gDNA, mRNA/cDNA or using commercially available scRNA reagents (see STAR Methods).
- (D) Exemplary flow cytometry assessment after knockin of an NY-ESO-1 TCR tNGFR construct including the barcoded multicistronic adaptor sequences into primary human T cells.
- (E) Biallelic knockin rates were calculated based on the observed percentage of GFP/RFP double positive cells after knockin of a 2-member GFP/RFP library. The predicted percentage of biallelic knockins was substantially lower than in the previous PoKI approach (15.3% in ModPoKI vs. 24.4% in the previous PoKI approach).<sup>37</sup> Predicted percentage of biallelic insertions = observed % double positive cells ×2. n = 2 donors.
- (F) A mild negative correlation between construct size and library representation was observed in the HDR template pool (mean of n = 4 replicates shown) and of knockin reads in six human donors (day 7 after electroporation, mean is shown). Insert size refers to the number of base pairs that gets inserted into the genomic DNA (without the constructs' homology arms). R<sup>2</sup> was calculated using nonlinear regression (semilog line model, GraphPad Prism). 100 TF and 129 SR library members shown.
- (G) Sequencing of the 3' BC from mRNA/cDNA was highly reproducible across biological replicates (day 7 after electroporation). n = 2 donors, one per axis. R<sup>2</sup> was calculated using nonlinear regression (log-log line model, GraphPad Prism).
- (H) Correlation between gDNA and mRNA/cDNA barcode sequencing strategies. 5' BCs sequenced off gDNA and 3' BCs sequenced off mRNA/cDNA from the same pooled knockin donor were well correlated after stimulation with CD3/CD28 beads for 4 days (days 7–11 after electroporation) and after a repetitive stimulation with target cells (A375 stimulation ×5 in the CD19-28z CAR model). One donor per screen is shown. Results from a second donor were also correlated (R<sup>2</sup> = 0.66 and 0.76, respectively). R<sup>2</sup> was calculated using nonlinear regression (log-log line model, GraphPad Prism). TF and SR libraries shown.
- (I) A pilot library of an NY-ESO-1-specific TCR plus GFP vs. RFP was pooled at the plasmid assembly stage or after separate electroporation. T cells were sorted for TCR knockin and GFP or RFP positivity and percentage of correctly assigned barcodes was determined by amplicon sequencing (3' barcode was sequenced off of mRNA/cDNA). Percent reads with correctly assigned barcodes in sorted populations was notably improved in the new version (ModPoKI) over PoKI<sup>37</sup> when pooling at the assembly state. Amount of template switching was calculated for the n = 2-member library and compared with the previous version of the pooled Ki platform.<sup>37</sup> The ModPoKI platform led to 5.6× decreased observed template switching in the n = 2-member library (extrapolated data for the n > 200-member library shown in Figure 1G). Bars represent mean. n = 2 donors.
- All primer sequences are listed in Table S1D.



(legend on next page)

---

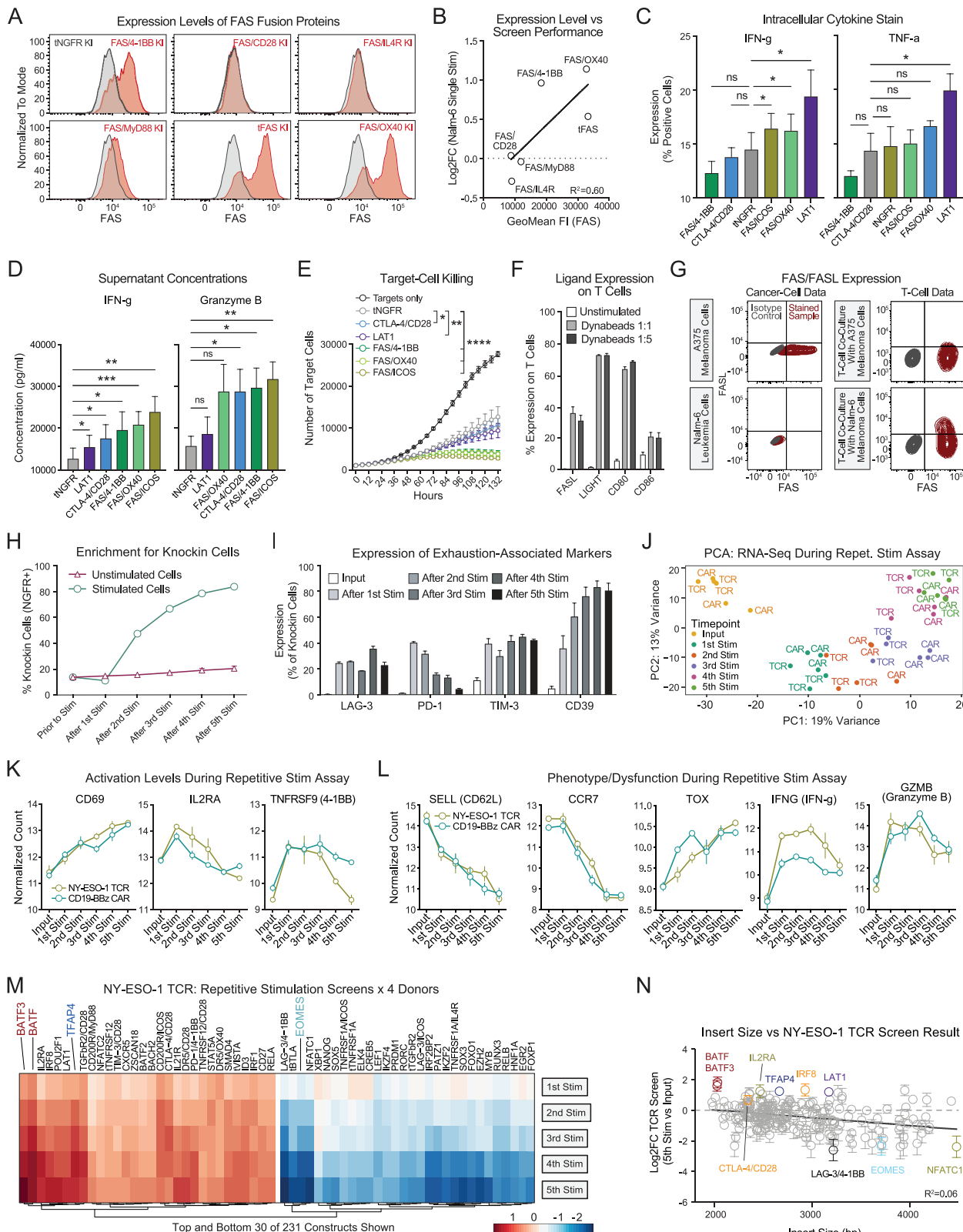
**Figure S2. Characterization of ModPoKI libraries and single stimulation ModPoKI screen hits, related to Figures 1 and 2**

(A) The TF library in combination with the NY-ESO-1 TCR specificity module was knocked into primary human T cells. Cells were sorted for NY-ESO-1 TCR expression and ModPoKI-seq (barcode sequencing and transcriptome sequencing) was performed. Cell identity (based on barcode sequencing) was well correlated with transcript expression of the knocked in TF confirming successful knockin and overexpression on RNA level. TF constructs that were codon optimized or showed no barcode/transcript expression were removed from the analysis. n = 2 donors.

(B) Percent of total reads of pooled knockin libraries in six human donors. TF and SR libraries were knocked in as one large library and subsequently computationally separated into individual libraries for analysis. Construct barcodes were consistently well represented with even library distribution.

(C) Endogenous expression of the TF library members based on published RNA-seq data (DICE dataset, <https://dice-database.org/>). Expression was scaled by column. SOX3 was excluded from the heatmap since it had no expression in the cell types shown according to the DICE database.

(D–G) Pooled knockin with constructs encoding the TF or SR library in combination with the NY-ESO-1 TCR was performed in primary human T cells. Resulting cells were subjected to the screens described in [Figure 2](#). Log<sub>2</sub> fold change in abundance for top and bottom hits (based on excessive stimulation) across single stimulation screens is shown (normalized to abundance of GFP and RFP controls and to fit on a scale from +1 to -1). n = 6 donors. Mean + SEM shown.

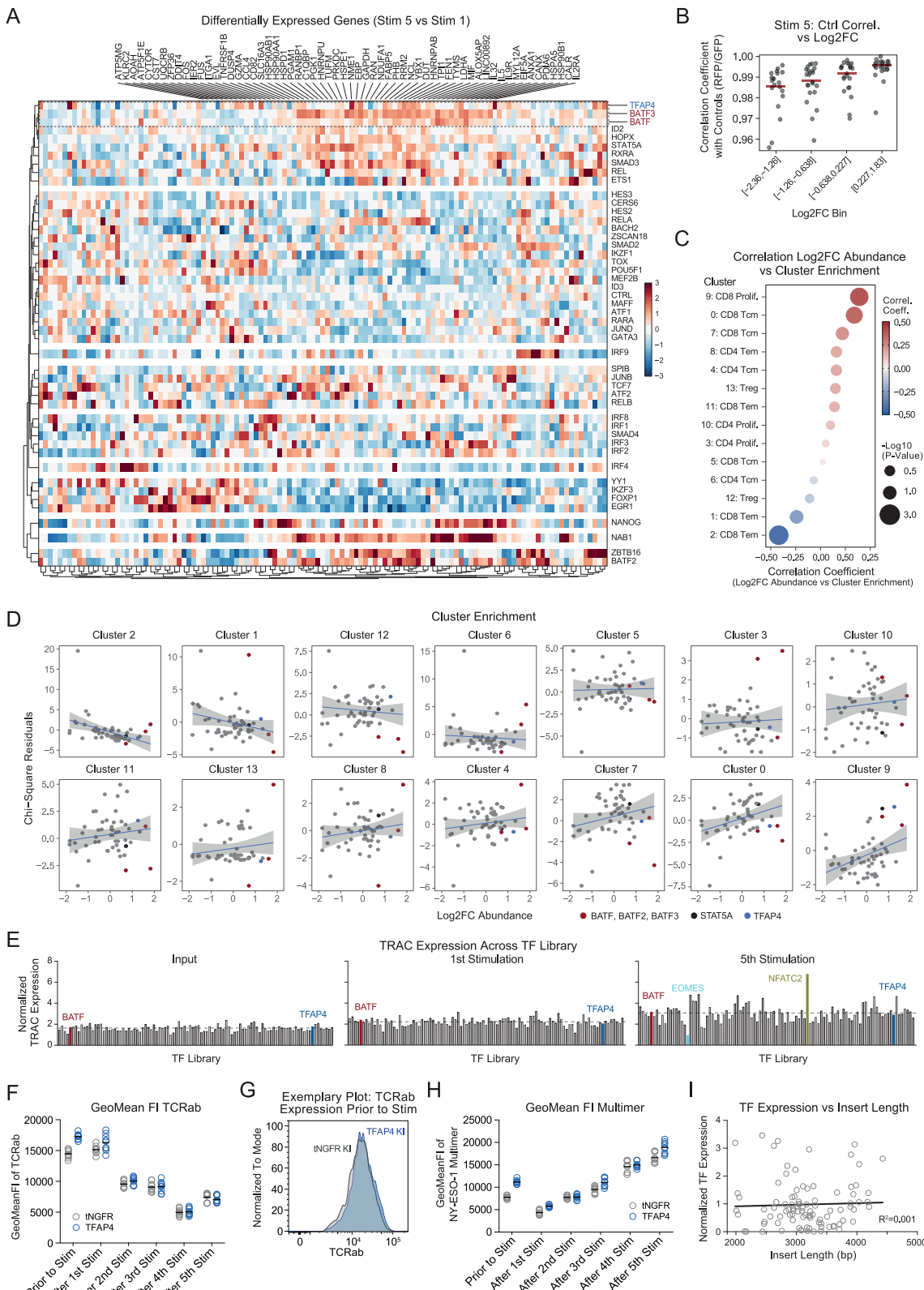


(legend on next page)

---

**Figure S3. FAS fusion protein validations and repetitive stimulation ModPoKI screens, related to Figures 2 and 3**

- (A) Constructs with NY-ESO-1 TCR in combination with different FAS-containing surface receptors were knocked into T cells. FAS surface expression levels detected by flow cytometry on day 7 after electroporation revealed a broad range of expression although all tested FAS proteins had the same FAS-derived extracellular and transmembrane domains and only differed in the intracellular domain. Results from one exemplary donor out of three donors are shown.
- (B) FAS fusion proteins with high expression on the cell surface tended to perform better in pooled knockin screens (NY-ESO-1 TCR single stimulation screen with Nalm-6 co-culture average  $\log_2 FC$  vs. average GeoMean FI (Geometric Mean Fluorescence Intensity) of FAS expression in flow cytometry is shown). Data of the six FAS proteins depicted in (A) are shown. n = 6 donors for screen data, n = 3 donors for flow data. Nonlinear regression (line model) was performed (GraphPad Prism).
- (C) SR constructs in combination with the NY-ESO-1 TCR were knocked into T cells. T cells were sorted and co-cultured with NY-ESO-1-expressing Nalm-6 target cells at a 1:1 E:T ratio for 24 h. Intracellular cytokine stain was performed 4 h after brefeldinA addition. n = 3 donors in technical duplicates. Mean + SEM is shown. RM one-way ANOVA (vs. tNGFR) with Geisser-Greenhouse correction and Holm-Sidak's test was performed (GraphPad Prism).
- (D) Interferon-gamma (IFN- $\gamma$ ) and granzyme B concentrations in co-culture supernatants derived from the co-cultures described in (C) were analyzed using LEGENDplex human CD8/NK panel. n = 3 donors in technical duplicates. Mean + SEM is shown. RM one-way ANOVA (vs. tNGFR) with Geisser-Greenhouse correction and with Holm-Sidak's test was performed (GraphPad Prism).
- (E) SR constructs in combination with the NY-ESO-1 TCR were knocked into T cells. T cells were sorted and co-cultured with RFP- and NY-ESO-1-expressing Nalm-6 target cells at a 1:4 E:T ratio. Killing was evaluated using Incucyte analysis. n = 3 donors in technical triplicates. Mean + SEM is shown. Significance at the last imaging time point is shown. Two-way ANOVA with Holm-Sidak's test was performed to determine statistical significance as described in the [STAR Methods](#).
- (F) The NY-ESO-1 TCR in combination with tNGFR was knocked into T cells. Surface expression of FASL, LIGHT (LTBR ligand), CD80 and CD86 (CD28 and CTLA-4 ligands) was evaluated on T cells with and without 24 h of CD3/CD28 stimulation (1:1 cells:bead ratio vs. 1:5 cells:bead ratio) using flow cytometry. n = 2 donors in technical duplicates. Mean + SEM is shown.
- (G) FAS (CD95) and FASL surface expression was analyzed on A375 melanoma and Nalm-6 leukemia cells (left panel) and on tNGFR NY-ESO-1 TCR KI T cells co-cultured with A375 melanoma cells or Nalm-6 leukemia cells for 24 h (right panel). Technical duplicates (left panel) and n = 3 donors in technical duplicates (right panel), one exemplary donor/measurement shown, respectively.
- (H) Control T cells (NY-ESO-1 TCR plus tNGFR) were subjected to the repetitive stimulation screen described in [Figure 3A](#). Knockin percentage (NGFR+) was determined by flow cytometry during the course of the assay and compared with T cells without restimulation. n = 2 donors in technical triplicates. Mean + SEM is shown.
- (I) Surface expression of inhibitory molecules LAG-3, PD-1, TIM-3, and CD39 was analyzed by flow cytometry through the course of the repetitive stimulation assay. n = 2 donors in technical triplicates for LAG-3, PD-1, and TIM-3. n = 4 donors in technical duplicates for CD39. Mean + SEM shown.
- (J) Control T cells (NY-ESO-1 TCR or CD19-BBz CAR plus tNGFR) were generated and bulk RNA-seq analysis was performed at every time point of the repetitive stimulation assay as previously reported (GSE204862).<sup>23</sup> Principal component analysis is shown. n = 3 donors.
- (K) Bulk RNA-seq (GSE204862)<sup>23</sup> revealed progressive induction of CD69 during the repetitive stimulation assay while *IL2RA* and *TNFRSF9* expression peaked relatively early and then decreased. n = 3 donors. Mean + SEM shown.
- (L) A variety of other transcript markers of T cell phenotype, effector function, and T cell dysfunction were analyzed in RNA-seq data and compared between CAR and TCR control T cells (GSE204862).<sup>23</sup> n = 3 donors. Mean + SEM shown.
- (M) The TF and SR libraries were knocked into primary human T cells in combination with the NY-ESO-1 TCR and subjected to the repetitive stimulation assay. Mean  $\log_2 FC$  (output vs. input) is shown. n = 4 donors. Top and bottom 30 of 231 constructs are shown.
- (N) Relationship between insert size and repetitive screening result ( $\log_2 FC$  of 5<sup>th</sup> stimulation vs. input abundance in NY-ESO-1 TCR repetitive stimulation screen). Indicated insert size does not include homology arms. Nonlinear regression (line model) was performed (GraphPad Prism). n = 4 donors.



*(legend on next page)*

---

**Figure S4. Repetitive stimulation ModPoKI-seq screening data, related to Figure 3**

(A) The 100-member TF library was knocked into primary human T cells from n = 2 donors in combination with the NY-ESO-1 TCR. ModPoKI-seq (single-cell transcriptome coupled with KI barcode sequencing) was performed. Heatmap shows differentially expressed genes (stimulation 5 vs. stimulation 1) of the different knockins (threshold >30 cells per knockin after 5 stimulations).

(B) Log<sub>2</sub>FC bins were generated based on abundance log<sub>2</sub>FC in the bulk NY-ESO-1 TCR repetitive stimulation fitness screen and compared with the correlation in gene expression with controls (RFP/GFP) in ModPoKI-seq. Best-performing knockins in fitness screens showed highest correlation coefficients with controls. n = 2 donors for ModPoKI-seq screen, n = 4 donors for bulk fitness screen.

(C) Correlation between cluster enrichment in ModPoKI-seq (threshold >30 cells per knockin after 5 stimulations) and abundance log<sub>2</sub>FC in bulk repetitive TCR stimulation fitness screens revealed highest correlation score for enrichment in the CD8 proliferating cluster 9. n = 2 donors for ModPoKI-seq screen, n = 4 donors for bulk fitness screen.

(D) Chi-square residuals for enrichment in cluster 0–13 (threshold >30 cells/knockin after 5 stimulations) were compared with abundance log<sub>2</sub>FC in the bulk screens. n = 2 donors for ModPoKI-seq screen, n = 4 donors for bulk abundance screen. Clusters are shown in order of correlation with abundance log<sub>2</sub>FC in bulk repetitive TCR stimulation fitness screens (see C).

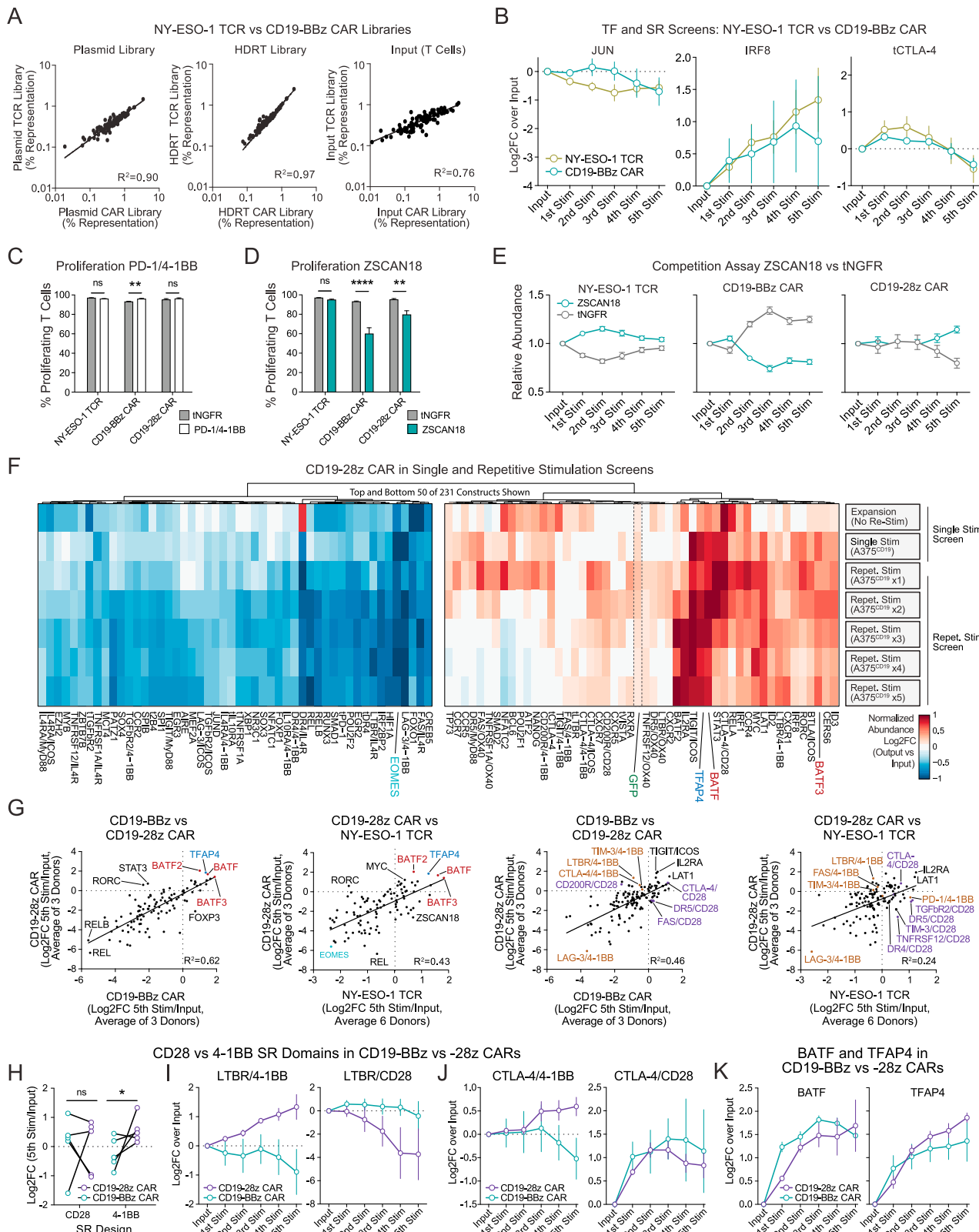
(E) TRAC expression levels were compared across the TF library using ModPoKI-seq screening data at input, after 1<sup>st</sup> stimulation and after 5<sup>th</sup> stimulation with target cells. Dotted line shows average TRAC expression at the respective time point. n = 2 donors.

(F) To validate TCR expression of key hit TFAP4 on protein level, TCRab expression of TFAP4 vs. tNGFR NY-ESO-1 TCR KIT T cells was analyzed by flow cytometry during the repetitive stimulation assay. Cells were gated on NY-ESO-1 multimer+/TCRab+ T cells. n = 3 donors in technical triplicates.

(G) Exemplary flow cytometry plot of the data prior to stimulation shown in (F) comparing TCRab protein expression of TFAP4 vs. tNGFR KIT T cells. Cells were gated on NY-ESO-1 multimer+/TCRab+ T cells.

(H) NY-ESO-1 multimer staining of TFAP4 vs. tNGFR NY-ESO-1 TCR KIT T cells was analyzed by flow cytometry during the repetitive stimulation assay. Cells were gated on NY-ESO-1 multimer+/TCRab+ T cells. n = 3 donors in technical triplicates.

(I) Average normalized TF expression (based on ModPoKI-seq data) vs. insert length is depicted and showed no correlation. n = 2 donors. Nonlinear regression (line model) was performed (GraphPad Prism).



(legend on next page)

**Figure S5. Construction of CD19 CAR libraries and construct performance in repetitive stimulation screens, related to Figure 3**

(A) To generate the CD19 CAR libraries, a CAR plasmid containing the *TRAC*-derived homology arms, the CD19-BBz CAR (FMC63) as well as constant linkers was generated and linearized by PCR. The TFs/SRs plus constant linkers were amplified from the TCR library by PCR. The CAR backbone plus TF/SR inserts were linked using pooled Gibson assembly. Representation of different library constructs was analyzed by amplicon sequencing of the plasmid pools, the HDR template libraries and the T cell pool 7 days after non-viral knockin (input population for the screens). Results from TF library are shown. n = 1 for CAR plasmid, n = 2 for TCR plasmid, n ≥ 3 for HDR templates and input population (individual donors). R<sup>2</sup> was calculated using nonlinear regression (log-log line model, GraphPad Prism).

(B) Log<sub>2</sub> fold changes in abundance were compared between the CAR and the TCR repetitive stimulation screen and showed comparable trends for most constructs. While IRF8 increased in abundance over time, JUN did not show a significant increase in abundance. Interestingly, control construct tCTLA-4 trended to increase after initial stimulations but dropped out later in the assay (in contrast to e.g., CTLA-4/CD28 fusion, see Figure 3J). n = 4 donors for TCR screens, n = 3 donors for CD19-BBz CAR screens. Mean + SEM shown.

(C) T cells were electroporated with PD-1/4-1BB or tNGFR in combination with either the NY-ESO-1 TCR, a CD19-BBz or a CD19-28z CAR. T cells were stained with CellTrace Violet (CTV) and co-cultured with CD19- and NY-ESO-1-expressing A375 melanoma cells at a 1:1 E:T ratio. Evaluation was performed 72 h later (gated on CAR+/TCRab- or NY-ESO-1 multimer+/TCRab+ T cells). n = 2 donors in technical duplicates. Statistical significance was calculated using two-way ANOVA with Holm-Sidak's test. Mean + SEM shown.

(D) T cells were electroporated with ZSCAN18 or tNGFR in combination with either the NY-ESO-1 TCR, a CD19-BBz or a CD19-28z CAR. T cells were stained with CTV and co-cultured with CD19- and NY-ESO-1-expressing A375 melanoma cells at a 1:1 E:T ratio. Evaluation was performed 72 h later. n = 2 donors in technical duplicates. Statistical significance was calculated using two-way ANOVA with Holm-Sidak's test. Mean + SEM shown.

(E) T cells were electroporated with ZSCAN18 or tNGFR in combination with either the NY-ESO-1 TCR, a CD19-BBz or a CD19-28z CAR. ZSCAN18 and tNGFR KI T cells were mixed at an ~50:50 ratio and co-cultured with CD19- and NY-ESO-1-expressing A375 melanoma cells in analogy to the repetitive stimulation protocols. %tNGFR positive cells was determined before and after every repetitive stimulation step. The divergent behavior of ZSCAN18 constructs in the CD19-BBz CAR vs. NY-ESO-1 TCR setting observed in the screens was confirmed in single knockin validation studies hinting at a context-dependent effect of ZSCAN18. Relative changes in abundance were calculated. n = 2 donors in technical duplicates. Mean + SEM shown.

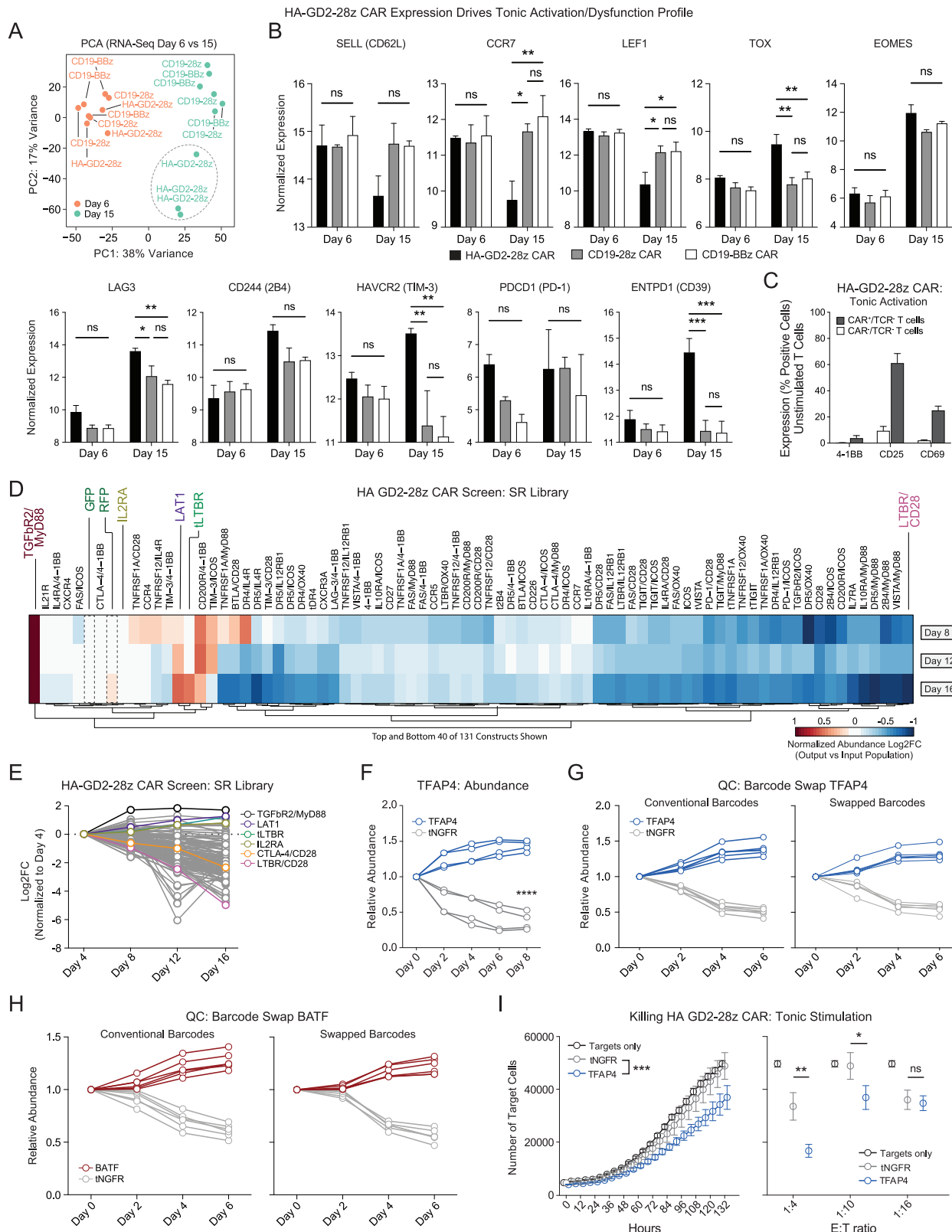
(F) TF and SR libraries were combined with a CD19 CAR with CD28 intracellular domain (CD19-28z CAR). Single stimulation and repetitive stimulation screens with CD19-expressing A375 melanoma cells were performed, similar to the screens with the CD19-BBz CAR. Log<sub>2</sub>FC of output vs. input was calculated and normalized based on controls GFP and RFP and to fit on a scale from -1 to +1. Top and bottom 50 of 231 constructs are shown. n = 3 donors for repetitive stimulation screens and n = 2 donors for single stimulation screens (due to insufficient coverage in the third donor).

(G) CD19-28z CAR repetitive stimulation screens were compared with CD19-BBz CAR and NY-ESO-1 TCR repetitive stimulation screens. TF and SR library results are shown separately. Unnormalized log<sub>2</sub>FC of representation in 5<sup>th</sup> stimulation vs. input population is shown. n = 3 donors for CAR screens and n = 4 donors for TCR screens. In the SR library plots (third and fourth plot), exemplary 4-1BB- or CD28-containing fusion proteins in the upper left or lower right quadrant are shown to highlight the divergent behavior of the different fusion proteins in CD19-BBz vs. CD19-28z models. Nonlinear regression (line model) was used to determine statistical significance (GraphPad Prism).

(H) Performance of CD28- and 4-1BB-based fusion receptors in CD19-28z and CD19-BBz CAR-T cell screens. Plot shows fusion proteins with a positive log<sub>2</sub>FC (5<sup>th</sup> stimulation vs. input population) in any or both of the two screens. 4-1BB-based fusion proteins tended to perform better in CD19-28z CARs compared with CD19-BBz CARs. Statistical significance was calculated using unpaired t test. n = 3 donors per screen, mean unnormalized log<sub>2</sub>FC is shown.

(I and J) Exemplary fusion proteins and their screen performance across five stimulations and both CAR models. Unnormalized log<sub>2</sub>FC mean + SEM shown, n = 3 donors per screen.

(K) Performance of BATF and TFAP4 KI constructs across five stimulations in the CD19-BBz and CD19-28z CAR screens. Unnormalized log<sub>2</sub>FC mean + SEM shown, n = 3 donors per screen.



(legend on next page)

**Figure S6. Characteristics of different CARs under *TRAC* promoter control and HA-GD2-28z SR screen with validations, related to Figure 4**

(A and B) RNA-seq was performed on HA-GD2-28z CAR-T cells, CD19-BBz CAR-T cells and CD19-28z CAR-T cells 6 and 15 days after electroporation. On day 15, HA-GD2-28z CAR-T cells showed decreased levels of early T cell differentiation/memory markers *CCR7* and *LEF1* and increased levels of dysfunction markers *TOX*, *LAG-3*, *HAVCR2* (TIM-3), and *ENTPD1* (CD39). n = 3 donors. Statistical significance in (B) was analyzed using two-way ANOVA with Holm-Sidak's test. Mean + SEM shown.

(C) Flow cytometric analysis of HA-GD2-28z CAR+ vs. bystander CAR- cells reveal elevated expression of activation markers 4-1BB, IL-2RA, and CD69 on CAR-T cells even in the absence of target cells 8 days after electroporation, consistent with tonic CAR signaling similar to what was previously described.<sup>28</sup> n = 2 donors in technical triplicates. Mean + SEM shown.

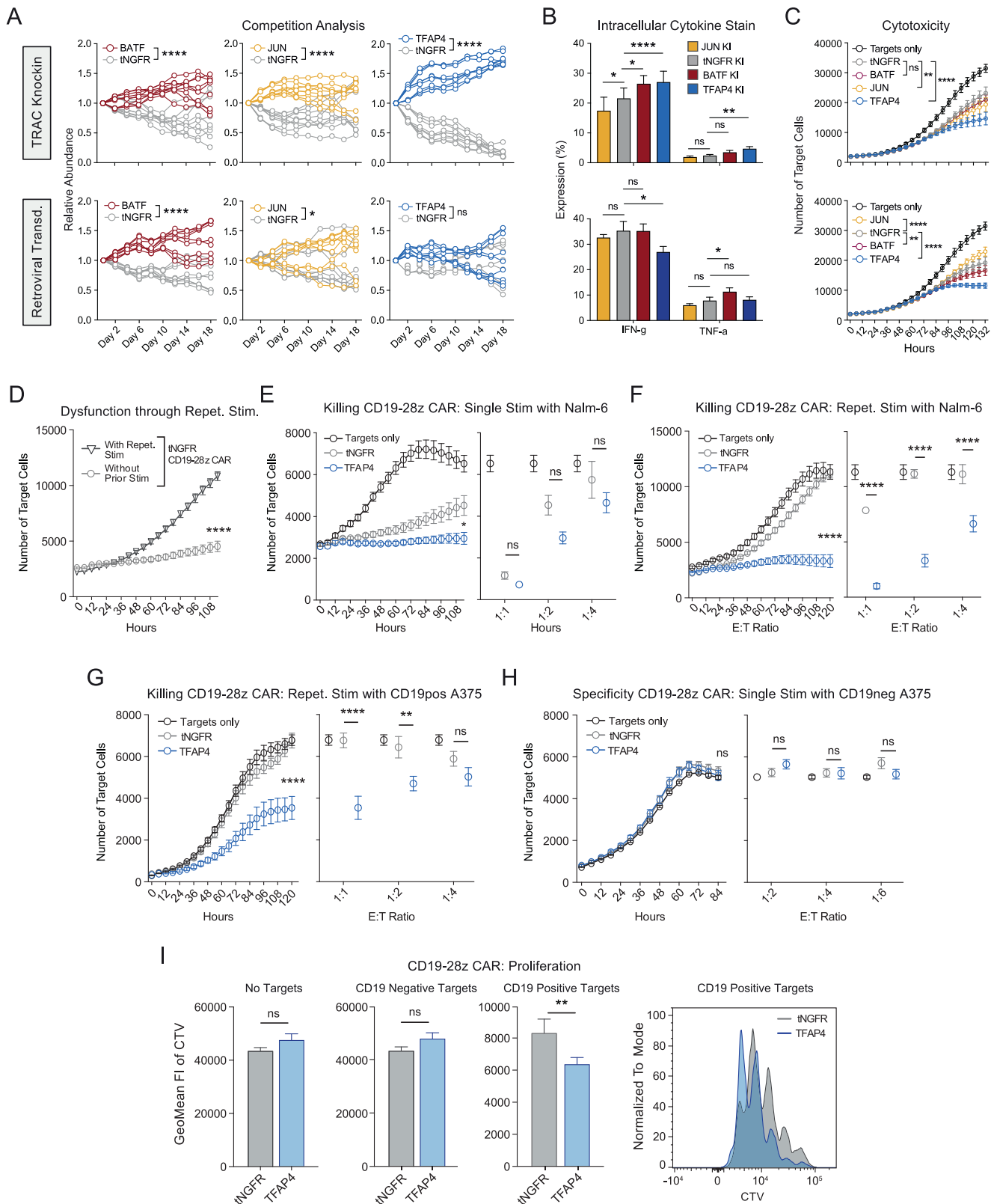
(D) A ModPoKI screen with the SR library was performed in HA-GD2-28z CAR-T cells. As the HA-GD2-28z CAR provides tonic stimulation, HA-GD2-28z CAR-T cells were cultured without addition of target cells. Log<sub>2</sub>FC in abundance is shown (compared with day 4 of culture). Heatmap was normalized based on controls (RFP/GFP) and to fit on a scale from +1 to -1. Top and bottom 40 out of 131 constructs are shown. n = 4 donors.

(E) Log<sub>2</sub> fold changes in the HA-GD2-28z CAR SR library screen are shown (no further normalization). Mean of n = 4 donors.

(F) The HA-GD2-28z CAR was knocked into human T cells in combination with either TFAP4 or a control construct (tNGFR). Cells were sorted for CAR+/TCR- cells and TFAP4 and tNGFR T cells were co-cultured at an ~50:50 ratio. Relative abundance of the NGFR+ cells was analyzed over time by flow cytometry. n = 2 donors in technical duplicates. Unpaired t test was used to calculate statistical significance on day 8.

(G and H) To exclude that cellular effects are dependent on specific barcodes linked to KI constructs, we swapped the TFAP4 and BATF barcodes with the tNGFR barcodes. T cells were electroporated with HA-GD2-28z CAR constructs and conventional TFAP4/tNGFR sequences or TFAP4/tNGFR sequences with swapped barcodes (G). Cells were sorted and TFAP4 and tNGFR KI cells were co-cultured at an ~50:50 ratio. Relative abundance over time (tNGFR positive vs. tNGFR negative cells) was analyzed and confirmed that the fitness effect of TFAP4 KI was not barcode-specific. The same analyses were done for BATF KI (H). n = 2 donors in technical triplicates.

(I) tNGFR or TFAP4 HA-GD2-28z CAR-T cells were co-cultured with GD2+ target cells (Nalm-6/GFP/Luc/GD2) at various effector:target (E:T) ratios. Number of remaining target cells was calculated using the Incucyte system. n = 2 donors in technical triplicates. Two-way ANOVA was used to calculate statistical significance including Holm-Sidak's test as described in the [STAR Methods](#). Significance at last time point (132 h) shown. Mean + SEM shown. Left panel shows 1:10 E:T ratio. Only significance between TFAP4 vs. tNGFR is shown.



(legend on next page)

**Figure S7. Comparison with retroviral system and extended TFAP4 validation data, related to Figure 4**

(A) The HA-GD2-28z CAR in combination with tNGFR, BATF, JUN, or TFAP4 was expressed using either the non-viral KI system or a retroviral transduction system. Cells were sorted on CAR expression and BATF, JUN, and TFAP4 overexpressing cells were co-cultured with tNGFR overexpressing cells at an ~50:50 ratio. Relative abundance (tNGFR positive vs. negative cells) was analyzed over the course of 18 days. TRAC knockin strategy is shown in the upper panel, retroviral transduction is shown in the lower panel. n = 3 donors in technical triplicates. Two-way ANOVA with Holm-Sidak's test was performed (GraphPad Prism).

(B) Cells were generated and sorted as described in (A) and co-cultured with GD2-expressing Nalm-6 cells for 24 h. TRAC knockin strategy is shown in the upper panel, retroviral transduction is shown in the lower panel. Intracellular cytokine expression was analyzed by flow cytometry. n = 3 donors in technical duplicates. One-way ANOVA (vs. tNGFR) with Holm-Sidak's test was performed (GraphPad Prism). Mean + SEM shown.

(C) Cells were generated and sorted as described in (A) and co-cultured with GD2-expressing Nalm-6 cells in an Incucyte analysis. TRAC knockin strategy is shown in the upper panel (E:T ratio 1:8), retroviral transduction is shown in the lower panel (E:T ratio 1:8). n = 3 donors in technical triplicates. Two-way ANOVA (vs. tNGFR) with Holm-Sidak's test was performed to analyze statistical significance as described in the [STAR Methods](#). Mean + SEM shown.

(D) tNGFR CD19-28z CAR-T cells were co-cultured with CD19+ target cells (Nalm-6) with or without prior 5x repetitive stimulation (CD19 positive A375s). Killing capacity of tNGFR CD19-28z CAR-T cells was markedly decreased after going through repetitive stimulation. n = 2 donors in technical quadruplicates. Multiple unpaired t test was performed to determine statistical significance including Holm-Sidak's test as described in the [STAR Methods](#). Significance at last time point (114 h) shown. E:T ratio = 1:2. Mean + SEM shown.

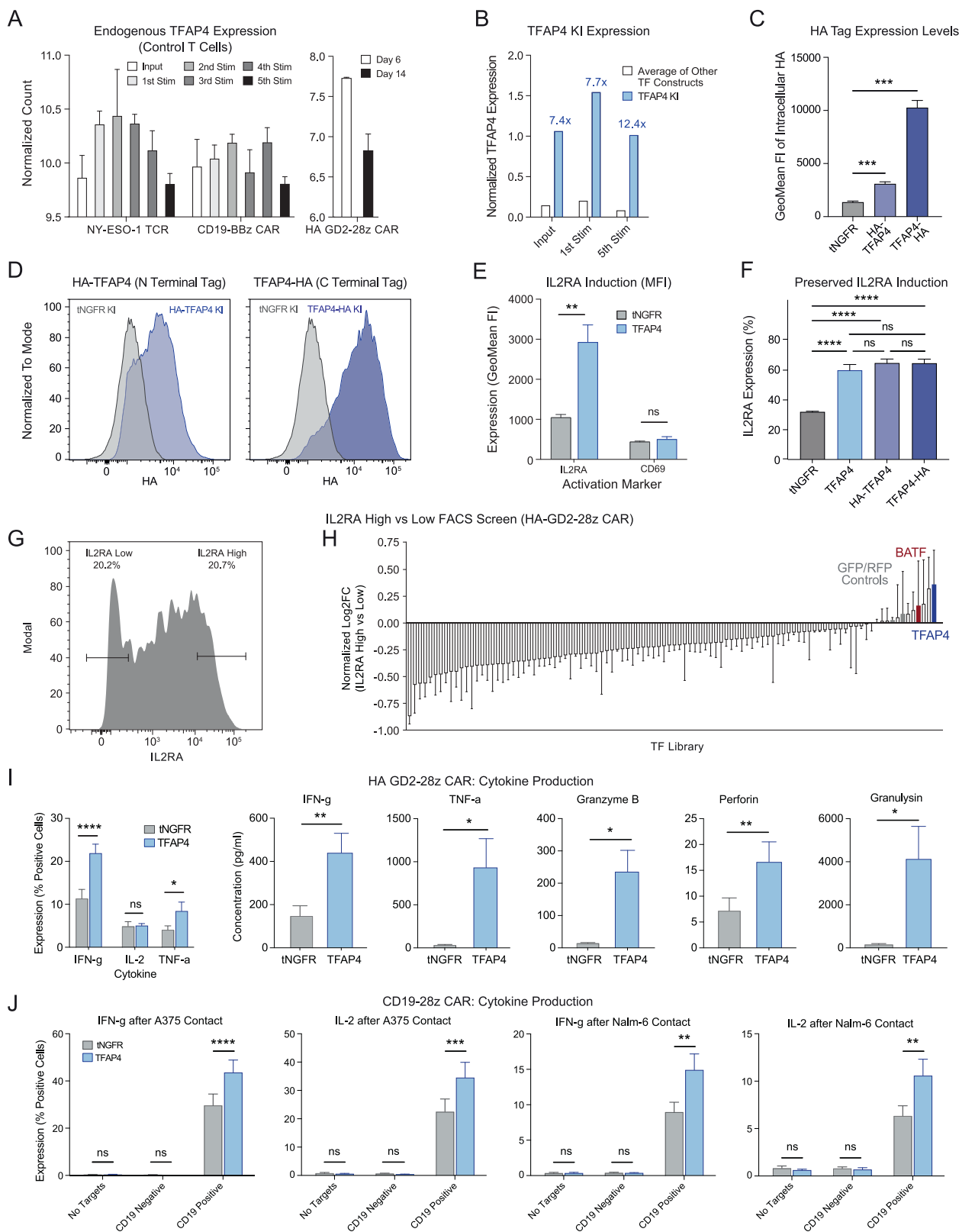
(E) The CD19-28z CAR in combination with tNGFR or TFAP4 was knocked into human T cells and co-cultured with CD19+ target cells (Nalm-6) at various E:T ratios. Number of remaining target cells/cancer cell killing was analyzed using the Incucyte system across various E:T ratios. n = 2 donors in technical quadruplicates. Two-way ANOVA was used to calculate statistical significance including Holm-Sidak's test as described in the [STAR Methods](#). Significance at last time point (114 h) shown. Mean + SEM shown. Left panel shows 1:2 E:T ratio.

(F) T cells were generated as described in (E), subjected to the repetitive stimulation assay (five stimulations with A375s) and then co-cultured with CD19+ target cells one more time (Nalm-6). Again, CD19-28z CAR-T cells with synthetic TFAP4 knockin were better able to control tumor cell growth. n = 2 donors in technical quadruplicates. Two-way ANOVA was used to calculate statistical significance including Holm-Sidak's test as described in the [STAR Methods](#). Significance at last time point (120 h) shown. Mean + SEM shown. Left plot shows 1:2 E:T ratio.

(G) T cells were generated as described in (E), subjected to the repetitive stimulation assay and then co-cultured with CD19+ target cells one more time (stimulations and final co-culture were with adherent cell line A375 that was modified to express CD19). Again, CD19-28z CAR-T cells with synthetic TFAP4 knockin were better able to control tumor cell growth. n = 2 donors in technical quadruplicates. Two-way ANOVA was used to calculate statistical significance including Holm-Sidak's test as described in the [STAR Methods](#). Significance at last time point (120 h) shown. Mean + SEM shown. Left plot shows 1:1 E:T ratio.

(H) tNGFR or TFAP4 CD19-28z CAR-T cells were co-cultured with CD19 negative target cells (A375). No elevated unspecific killing of the TFAP4 compared with the tNGFR construct was observed. Two-way ANOVA was used to calculate statistical significance including Holm-Sidak's test as described in the [STAR Methods](#). Significance at last time point (84 h) shown. Left plot shows 1:4 E:T ratio. n = 2 donors in technical triplicates. Mean + SEM shown.

(I) TFAP4 or tNGFR KI CD19-28z CAR-T cells were stained with CTV and either cultured without targets or co-cultured with CD19 negative or CD19 positive target cells (Nalm-6) for 72 h. Reduced CTV signal indicates increased proliferation of TFAP4 KI T cells after co-culture with CD19 positive targets, but not after co-culture with CD19 negative targets or after culturing them without target cells. n = 2 donors in ≥ 2 technical replicates. Paired t test was performed (GraphPad Prism). Mean + SEM shown. The histogram (right panel) shows exemplary CTV signal after co-culture with CD19 positive target cells for one out of two donors. Only significance between TFAP4 vs. tNGFR is shown in (E)–(H).



(legend on next page)

**Figure S8. Extended TFAP4 validation data and IL-2RA fluorescence-activated cell sorting (FACS)-sorted screen in HA-GD2-28z CAR-T cells, related to Figure 4**

(A) Endogenous *TFAP4* expression was analyzed by bulk RNA-seq throughout the repetitive stimulation assay using the NY-ESO-1 TCR or CD19-BBz CAR system and compared with endogenous *TFAP4* levels when culturing the HA-GD2-28z CAR (tonic activation). While *TFAP4* expression peaked after the 2<sup>nd</sup> stimulation in the TCR model, it was more heterogeneous in the CD19-BBz CAR model and decreased over time in the HA-GD2-28z CAR model. n = 3 donors for the NY-ESO-1 TCR and CD19-BBz CAR, n = 2 donors for the HA-GD2-28z CAR. Mean + SEM shown.

(B) *TFAP4* transcript overexpression resulting from *TFAP4* KI as determined by ModPoKI-seq (see Figure S2A, NY-ESO-1 TCR). Mean normalized *TFAP4* expression of *TFAP4* KI T cells vs. cells with KIs of the included other constructs is shown. n = 2 donors.

(C) To determine protein expression levels of *TFAP4* in *TFAP4* KI T cells, we generated *TFAP4* HA-GD2-28z CAR constructs with an N-terminal HA-tagged *TFAP4* and a C-terminal HA-tagged *TFAP4*. GeoMean FI of intracellular HA-tag expression is shown for conventional tNGFR HA-GD2-28z CAR KI cells vs. N-terminally tagged (HA-TFAP4) and C-terminally tagged (TFAP4-HA) *TFAP4* HA-GD2-28z CAR KI cells 10 days after electroporation. Mean + SEM shown. n = 2 donors in technical triplicates. Statistical significance was calculated using one-way ANOVA with Holm-Sidak's test.

(D) Exemplary flow cytometry data of the experiment described in (C) for one out of two donors 10 days after electroporation is shown (intracellular HA expression). Cells were gated on CAR+/TCRab- expression.

(E) GeoMean FI data of plot in Figure 4G is shown. IL-2RA and CD69 expression on HA-GD2-28z CAR-T cells were analyzed by flow cytometry on day 8 after electroporation; *TFAP4* KI led to increased IL-2RA surface expression. Multiple t test was performed to determine significance including Holm-Sidak's test. n = 2 donors in technical duplicates. Mean + SEM shown.

(F) Induction of IL-2RA (a key phenotype of *TFAP4* KI) was preserved after addition of an HA-tag to either the C or N terminus of the *TFAP4* KI construct. n = 3 donors in one to three technical replicates. Statistical significance was calculated using one-way ANOVA with Holm-Sidak's test.

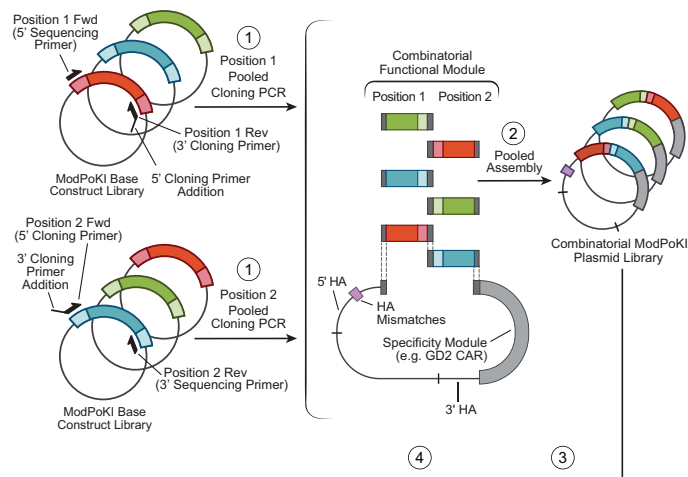
(G) A FACS-based ModPoKI screen was done to identify TFs that can affect IL-2RA expression. ModPoKI was performed with the HA-GD2-28z CAR in combination with the TF library. Cells were FACS-sorted on day 8 after electroporation into top and bottom ~20% IL-2RA expression bins. RNA was isolated and barcode amplicon sequencing performed. n = 3 donors. Sorting strategy is shown for one exemplary donor.

(H) The IL-2RA FACS-sorted screen was performed as described in (G). Log<sub>2</sub>FC of construct representation in IL-2RA high vs. low bin was calculated and dataset was normalized based on GFP/RFP controls and to fit on a scale from -1 to 1. n = 3 donors, mean + SEM shown.

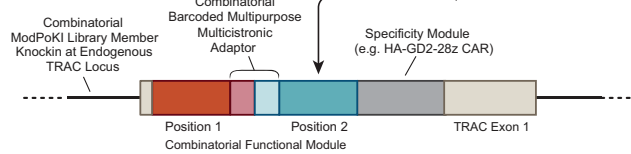
(I) Cytokine production and secretion of *TFAP4* KI vs. tNGFR KI HA-GD2-28z CAR-T cells were analyzed after 24 h co-culture with GD2+ target cells by intracellular cytokine stain (left panel) and LEGENDplex analysis of the supernatant (right panels). n = 2 donors in ≥2 technical replicates. Multiple paired t test was performed to determine statistical significance. Mean + SEM shown.

(J) *TFAP4* or tNGFR KI CD19-28z CAR-T cells were co-cultured with either CD19 negative or CD19 positive target cells (A375 and Nalm-6). IFN-g and IL-2 production was evaluated by intracellular cytokine stain and confirmed elevated cytokine levels only in the presence of CD19 positive target cells. In the presence of CD19 negative target cells or in absence of target cells, *TFAP4* KI CD19-28z CAR-T cells did not release increased amounts of IFN-g and IL-2 compared with the control. Multiple paired t test was performed to determine statistical significance. n = 2 donors in technical triplicates. Mean + SEM shown.

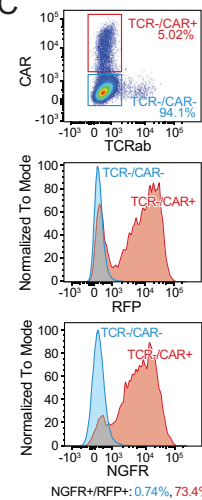
A



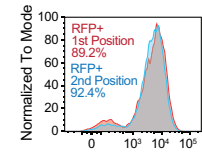
B



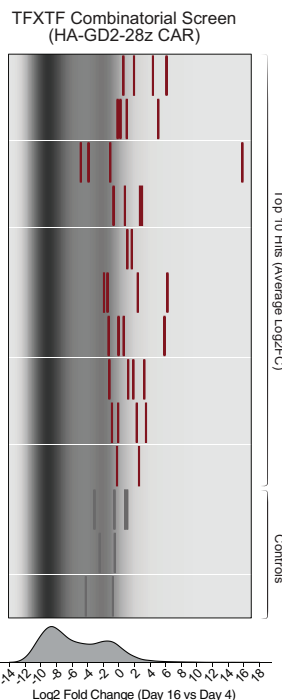
C



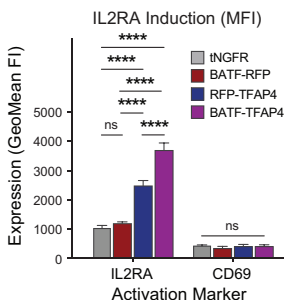
D



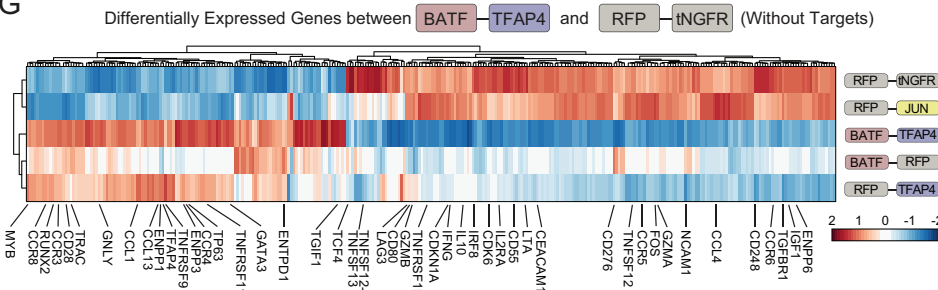
E



F



G



H

Log2FC Correlation Analyses of **BATF** **TFAP4** with Other Combinations (Without Targets)

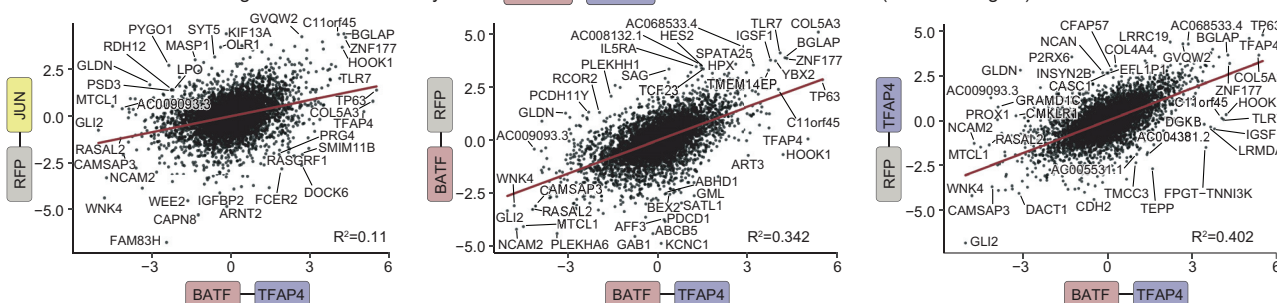


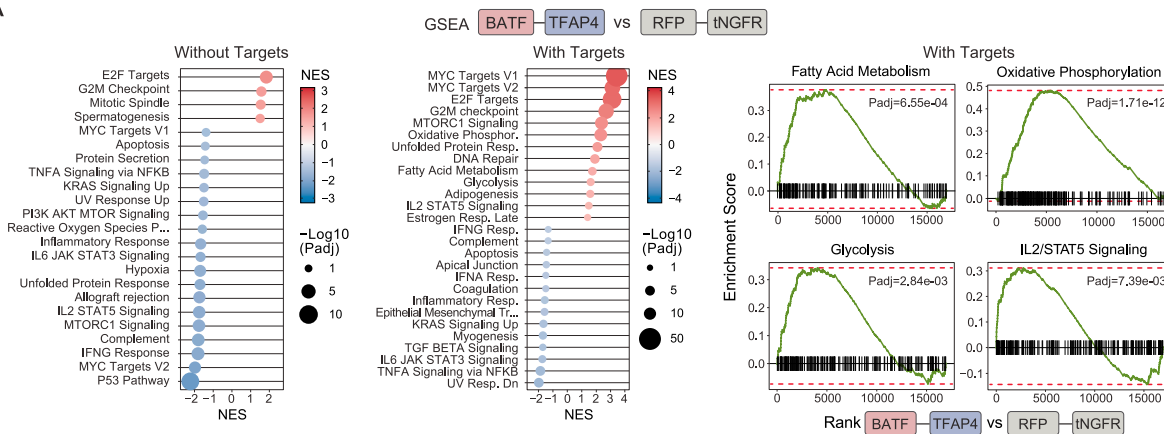
**Figure S9. Combinatorial knockin strategy and BATF-TFAP4 validation analyses, related to Figures 5 and 6**

(A and B) Schematic illustration showing the pooled assembly approach used to generate a combinatorial library of the tonic signaling HA-GD2-28z CAR plus 100 TFs  $\times$  100 TFs resulting in an  $\sim$ 10,000-member library. The inserts for TF position 1 and 2 were separately generated by pooled PCRs off of the existing TF library. The backbone (consisting of the HA-GD2-28z CAR plus homology arms) and the two inserts were assembled in a pooled Hifi DNA assembly reaction resulting in the combinatorial ModPoKI plasmid library. Double-stranded HDR template was generated by pooled PCR followed by non-viral pooled knockin into primary human T cells. The resulting sequences between the two TFs (combinatorial barcoded multicistronic adaptor) can be used to read out the identity of the constructs (see STAR Methods).

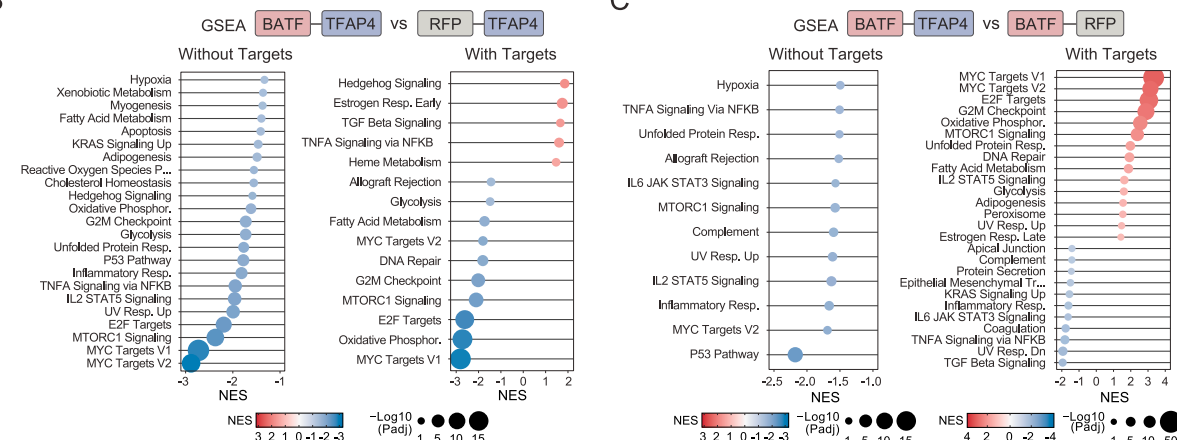
(legend continued on next page)

- (C) Exemplary knockin of a control construct containing the HA-GD2-28z CAR with tNGFR and RFP including the combinatorial barcoded multicistronic adaptor sequences into primary human T cells.
- (D) To assess if the direction of the knockin influences expression levels, HA-GD2-28z CAR constructs including RFP-tNGFR (RFP in 1<sup>st</sup> position) and tNGFR-RFP (RFP in 2<sup>nd</sup> position) were generated and RFP expression was analyzed by flow cytometry on day 4 after electroporation. Exemplary flow cytometry plot from one donor out of two donors is shown, cells were gated on CAR+/TCRab- T cells.
- (E) The TF×TF combinatorial ModPoKI library was knocked into primary human T cells. As the HA-GD2-28z CAR provides tonic signaling, T cells were cultured without addition of target cells. Cells were sorted on day 4 and day 16 after electroporation and the log<sub>2</sub>FC over time was calculated (day 16/day 4). Log<sub>2</sub>FC for the top 10 combinatorial TF×TF constructs is shown and compared with controls. n = 2 donors. Panel shows data for various KI combinations (with barcodes for constructs with both orientations included as bars × two donors).
- (F) Data from [Figure 6B](#) shown as GeoMean FI instead of percent positive. The data from the single knockin tNGFR HA-GD2-28z CAR construct were added to illustrate that the BATF-TFAP4 KI construct increases levels of IL-2RA surface expression beyond baseline. Mean + SEM shown. Two-way ANOVA with Holm-Sidak's test was performed to analyze statistical significance. n = 2 donors in technical duplicates.
- (G) Different combinatorial validation constructs were knocked into primary human T cells as described in [Figure 6](#). Bulk RNA-seq was performed 14 days after electroporation. Differentially expressed genes between BATF-TFAP4 KI and RFP-tNGFR KI HA-GD2-28z CAR-T cells are plotted. n = 2 donors.
- (H) Log<sub>2</sub> fold changes in gene expression between the tested KI condition and control KI (RFP-tNGFR) were compared between BATF-TFAP4 KI and the other constructs. Correlation analyses indicated that BATF-TFAP4 KIs were most similar in gene expression changes with RFP-TFAP4 and BATF-RFP, while the correlation between BATF-TFAP4 KI cells and RFP-JUN KI cells was lower. n = 2 donors. Statistics were done using linear regression (lm function in RStudio).

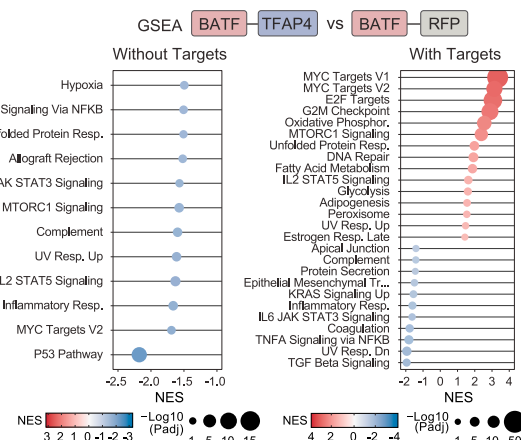
A



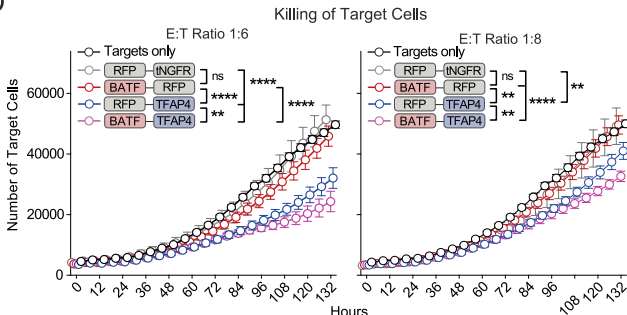
B



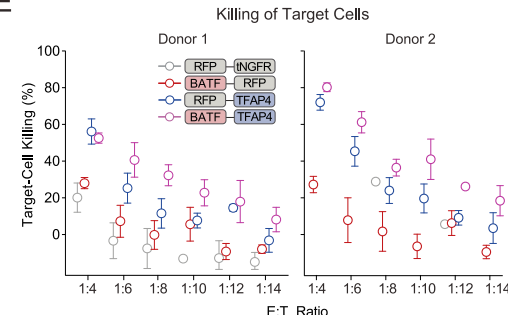
C



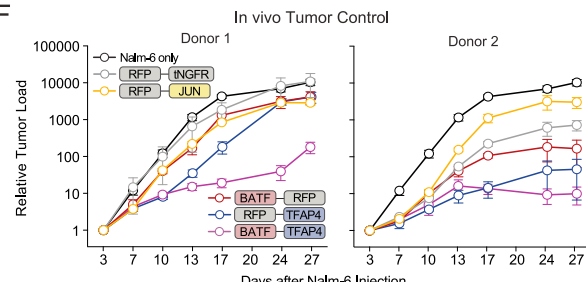
D



E



F



(legend on next page)

---

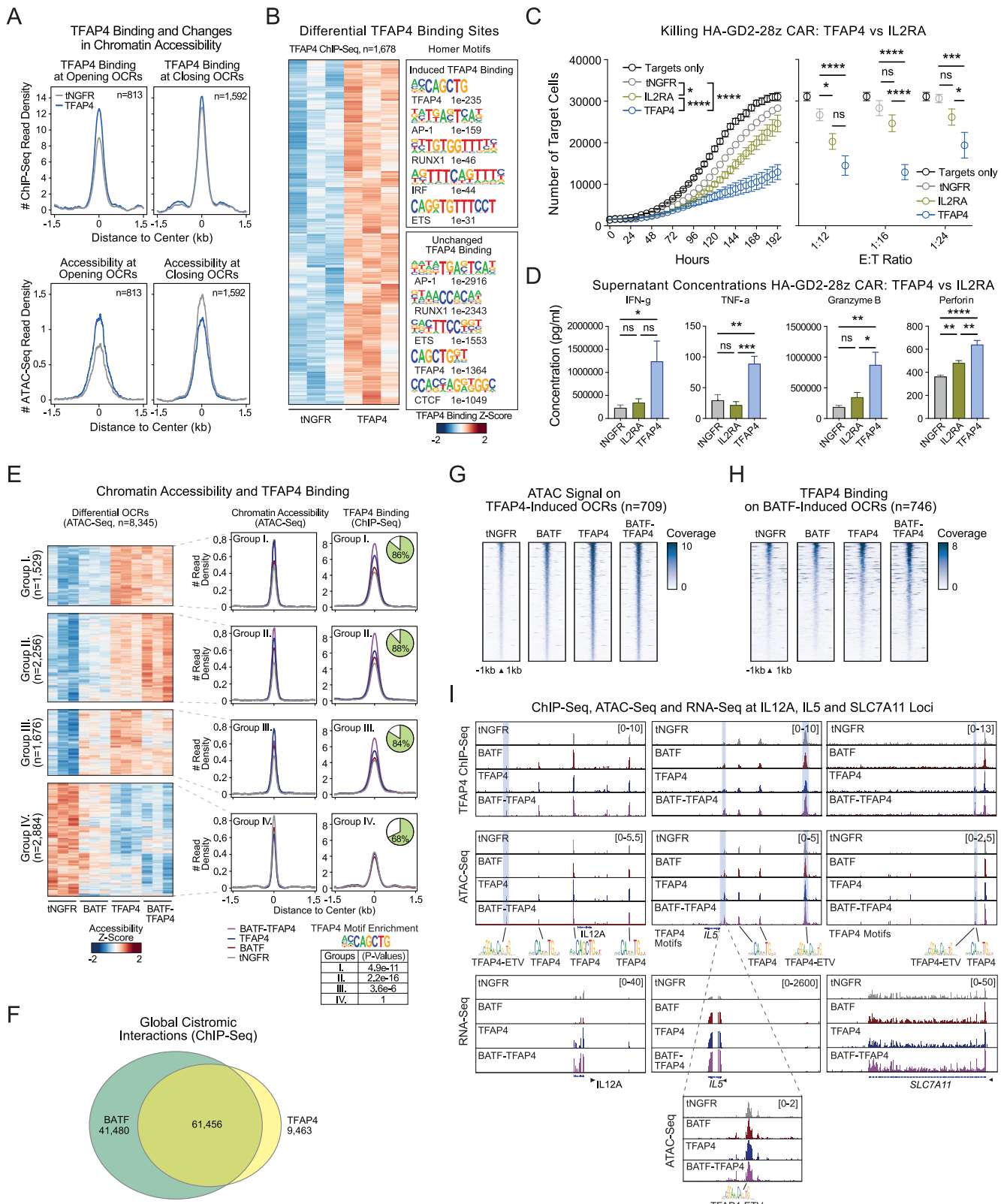
**Figure S10. Extended BATF-TFAP4 validation data, related to Figure 6**

(A–C) Gene set enrichment analyses of the BATF-TFAP4 combinatorial construct compared with RFP-tNGFR (A), RFP-TFAP4 (B), or BATF-RFP (C) without and with addition of GD2+ target cells for 24 h is shown (day 14 vs. day 15 after electroporation, respectively). Notably, after stimulation with target cells, the gene sets involved in fatty acid metabolism, glycolysis, oxidative phosphorylation and IL-2/STAT5 signaling were enriched in genes differentially expressed between BATF-TFAP4 cells compared with RFP-tNGFR cells. n = 2 donors.

(D) Combinatorial KI HA-GD2-28z CAR-T cells were co-cultured with Nalm-6/GFP/Luc/GD2 target cells and target-cell killing was analyzed via Incucyte. BATF-TFAP4 combinatorial KI HA-GD2-28z CAR-T cells trended toward improved performance relative to other combinatorial KI HA-GD2-28z CAR-T cells in terms of *in vitro* killing capacity. n = 2 donors in technical triplicates. Reduced number of replicates for the RFP-tNGFR condition was due to low cell counts (see E). Two-way ANOVA with Holm-Sidak's test was performed to analyze significance as described in the [STAR Methods](#). Significance at the last imaging time point is shown; mean + SEM shown.

(E) Data from [Figure 6F](#) divided by donors and with more E:T ratios. n = 3 for all conditions in donor 1. n = 3 for BATF-TFAP4, RFP-TFAP4, and BATF-RFP condition in donor 2. Due to low cell counts, RFP-tNGFR only has one datapoint in E:T ratios 1:8 and 1:12 and no datapoint in the other E:T ratios for donor 2. Mean + SEM shown in all conditions with n > 1.

(F) Data from [Figure 6G](#) divided by donors. Mean + SEM shown.



(legend on next page)

**Figure S11. BATF facilitates TFAP4-mediated increases in T cell fitness, related to Figure 7**

- (A) HA-GD2-28z CAR-T cells with single or combinatorial knockin of BATF and/or TFAP4 vs. controls were generated, sorted for CAR+/TCR<sup>ab-</sup> T cells and subjected to RNA-seq, ATAC-seq and TFAP4 and BATF ChIP-seq 14 days after electroporation. Metagene plot of normalized (#) TFAP4 ChIP-seq signal intensity (top) and ATAC-seq signal intensity (bottom) at TFAP4 KI-regulated chromatin regions (opening or closing) in the indicated conditions. FDR < 0.05, log<sub>2</sub>FC ≥ 0.5.
- (B) Heatmap shows differential TFAP4 binding sites in tNGFR vs. TFAP4 HA-GD2-28z KI CAR-T cells. n = 3 donors; FDR < 0.05, log<sub>2</sub>FC ≥ 0.5. De novo TF motif analysis by Homer at induced and unchanged TFAP4-bound genomic regions is shown.
- (C) tNGFR, TFAP4, or IL2RA HA-GD2-28z KI CAR-T cells were co-cultured with GD2-expressing Nalm-6 cells. TFAP4 KI significantly increased cytotoxic capacity compared with IL2RA KI. Two-way ANOVA was used to determine statistical significance including Holm-Sidak's test as described in the [STAR Methods](#). Significance at the last time point (192 h) is shown. n = 3 donors in technical triplicates. Mean + SEM shown. Left plot shows 1:16 E:T ratio. Only significance between TFAP4 vs. IL2RA, IL2RA vs. tNGFR and TFAP4 vs. tNGFR is shown.
- (D) tNGFR, TFAP4, or IL2RA HA-GD2-28z KI CAR-T cells were co-cultured with GD2-expressing Nalm-6 cells at a 1:1 E:T ratio. Cytokine concentrations in co-culture supernatants were analyzed using LEGENDplex human CD8/NK panel. n = 3 donors in technical triplicates. Mean + SEM is shown. One-way ANOVA was used to calculate statistical significance between TFAP4, IL2RA, and tNGFR KIs including Holm-Sidak's test.
- (E) Heatmap representation of differentially accessible open chromatin regions (OCRs) in the indicated conditions (left). OCR groups were defined by k-means clustering and describe distinct chromatin accessibility patterns, as follows: group I. Accessibility is induced by TFAP4 KI and not affected by BATF KI; group II. Accessibility is induced by TFAP4 KI and further increased by BATF-TFAP4 combination KI; group III. Accessibility is induced by TFAP4 KI, but decreased by BATF-TFAP4 combination KI; and group IV. Accessibility is reduced in all conditions compared with tNGFR control KI. n = 3 donors; FDR < 0.05, log<sub>2</sub>FC ≥ 0.5. Metagene plot of normalized (#) ATAC-seq (middle) and TFAP4 ChIP-seq (right) signal intensity in the four groups of OCRs in the indicated conditions. Pie charts represent the percentage of OCRs bound by TFAP4. Targeted TFAP4 motif analysis in the four OCR groups is shown (bottom table; p values were calculated by Fisher's exact test).
- (F) Venn diagram depicts the global cistromic interactions between BATF and TFAP4 in KI T cells across all conditions (tNGFR, TFAP4, BATF, BATF-TFAP4). Cistrome comprises all detected genome sites bound by BATF and/or TFAP4 as assessed by ChIP-seq. FDR < 0.05, log<sub>2</sub>FC ≥ 0.5.
- (G) Tornado plots depict ATAC-seq read distribution at TFAP4 KI-induced OCRs in a ±1 kb window around the summits of ATAC-seq peaks in the indicated conditions (related to metagene plot in [Figure 7K](#)).
- (H) Tornado plots depict TFAP4 ChIP-seq read distribution at BATF KI-induced OCRs in a ±1 kb window around the summits of ATAC-seq peaks in the indicated conditions (related to metagene plot in [Figure 7L](#)).
- (I) Genome browser examples with ChIP-seq, ATAC-seq, and RNA-seq tracks at genomic loci where TFAP4 KI and BATF KI induce gene expression and chromatin accessibility (in the highlighted genomic regions—light blue), and BATF KI facilitates the binding of TFAP4. Gene examples (*IL12A*, *IL5*, and *SLC7A11*) are derived from group II genes from [Figure 7F](#).
- (A) and (B) include data on TFAP4 vs. tNGFR single KI HA-GD2-28z CARs. (F) summarizes data from all ChIP-seq conditions (TFAP4, BATF, tNGFR HA-GD2-28z CAR single KIs and BATF-TFAP4 HA-GD2-28z CAR combinatorial KIs). (E), (G), and (I) include RNA-seq and/or ATAC-seq from RFP-tNGFR (labeled as tNGFR), BATF-RFP (labeled as BATF), RFP-TFAP4 (labeled as TFAP4), and BATF-TFAP4 HA-GD2-28z CARs. (H) shows ChIP-seq data from TFAP4, BATF and tNGFR single KI HA-GD2-28z CARs and BATF-TFAP4 combinatorial KI HA-GD2-28z CARs.